Title
Self-Assembly and Crystallization of Conjugated Block Copolymers

Author
Davidson, Emily Catherine

Publication Date
2016

Peer reviewed|Thesis/dissertation

Self-Assembly and Crystallization of Conjugated Block Copolymers

By

Emily Catherine Davidson

A dissertation submitted in partial satisfaction of the

requirements for the degree in

Doctor of Philosophy

in

Chemical Engineering

in the

Graduate Division

of the

University of California, Berkeley

Committee in Charge:

Professor Rachel A. Segalman, Co-Chair
Professor Nitash P. Balsara, Co-Chair
Professor Bryan McCloskey
Professor Andrew Minor

Fall 2016

Self-Assembly and Crystallization of Conjugated Block Copolymers

by Emily Catherine Davidson

Abstract

Self-Assembly and Crystallization of Conjugated Block Copolymers

by

Emily Catherine Davidson

Doctor of Philosophy in Chemical Engineering

University of California, Berkeley

Professor Rachel A. Segalman, Co-Chair
Professor Nitash P. Balsara, Co-Chair

Conjugated polymers are class of electrically conductive polymers used in applications including organic photovoltaics, organic light emitting diodes, and organic field effect transistors. Incorporating this class of materials into block copolymer architectures offers the opportunity to combine the optoelectronic properties of conjugated polymers with precise, long-range nanopatterning via block copolymer self-assembly. Importantly, conjugated polymer crystallinity is essential for determining the charge transport properties of the material. Achieving high performing materials in block copolymer geometries requires that conjugated polymer crystallinity be both confined and optimized. Furthermore, while crystallinity in conjugated polymers is essential for excellent performance, many aspects of conjugated polymer crystallinity are still poorly understood. Block copolymers offer an opportunity to study conjugated polymer crystallization in highly-defined geometries with controlled chain tethering at the interfaces, allowing a precise level of control over the crystallization conditions.

This dissertation demonstrates the utility of molecular design in conjugated polymers to create diblock copolymers that robustly self-assemble in the melt and confine crystallization upon cooling. This work leverages the model conjugated polymer poly(3-(2′-ethyl)hexylthiophene) (P3EHT), which features a branched side chain, resulting in a dramatically reduced melting temperature (T_m ~80°C) relative to the widely-studied poly(3-hexylthiophene) (P3HT) (T_m ~200°C). This reduced melting temperature permits an accessible melt phase, without requiring that the segregation strength (χN) be dramatically increased. Thus, diblock copolymers containing P3EHT demonstrate robust diblock copolymer self-assembly in the melt over a range of compositions and morphologies. Furthermore, confined crystallization in the case of both glassy (polystyrene (PS) matrix block) and soft (polymethylacrylate (PMA) matrix block) confinement is studied, with the finding that even in soft confinement, crystallization is constrained within the diblock microdomains. This success demonstrates the strategy of leveraging molecular design to decrease the driving force for crystallization as a means to achieving robust self-assembly and confined crystallization in conjugated block copolymers.

Importantly, despite the relatively flexible nature of P3EHT in the melt, the diblock copolymer phase behavior appears to be significantly impacted by the stiffness (persistence length of ~3 nm) of the P3EHT chain compared to the coupled amorphous blocks (persistence length ~0.7 nm). In particular, it is shown that the synthesized morphologies are dominated by a very large composition window for lamellar geometries (favored at high P3EHT volume fractions); cylindrical geometries are favored when P3EHT is the minority fraction. This asymmetry of the composition window is attributed to impact of conformational asymmetry (the difference in chain stiffness, as opposed to shape) between conjugated and amorphous blocks. These results emphasize that targeting curved morphologies with majority conjugated polymer – even when the conjugated polymer is fairly flexible, as is the case with P3EHT – will continue to be an important challenge.

The detailed balance between the unique properties of conjugated polymer crystallization and diblock copolymer self-assembly in these materials is illuminated by examining the crystallite orientation and the response of microdomains to crystallization. A critical parameter is found to be the P3EHT drive for extended-chain crystals. It is found that under all probed conditions in lamellar P3EHT-*b*-PMA, P3EHT chains crystallize with their chains perpendicular to the diblock interface. Further, in P3EHT-*b*-PMA with a deformable amorphous block, P3EHT drives domain expansion during crystallization despite increasing P3EHT density. This expansion corresponds to the formation of extended-chain crystallites. This resulting conformation is not necessarily expected to be favorable, given that it induces a stretching penalty in the coupled amorphous block. However, this expansion appears to be not only preferred but necessary: crystallization in lamellar confinement with a glassy PS matrix suppresses not only domain extension but also P3EHT crystallization. Interestingly, in cylindrical confinement, it is shown that this drive for extended chain crystals results in local deformation of the cylindrical domains themselves.

Finally, the relationship between the detailed crystallization process and the diblock structure is examined. The degree of crystalline perfection of P3EHT can be controlled in confinement by controlling the crystallization temperature (T_c) or, alternatively, via re-crystallization at temperatures below the melting temperature. Surprisingly, in P3EHT-*b*-PMA increasing the crystallization temperature both improves the crystalline perfection and results in less domain extension. By tracking the changes in domain structure during melting, three distinct melting regimes are identified. A structural model of the conjugated block melting process is proposed, consisting of (I) excluded-chain relaxation followed by (II) chain inter-digitation during melt-recrystallization, and finally (III) complete melting independent of the initial crystallization conditions. These detailed studies of the impact of processing conditions suggest that crystallization processes coupled to temperature-dependent diffusion and nucleation are critical for determining the final crystalline state in confinement. They also suggest that, surprisingly, improvement in conjugated polymer crystallinity may correspond to a more compact structure along the chain dimension.

Throughout this dissertation, we consider how key parameters governing structure formation impact self-assembly and crystallization. In particular, we consider the driving forces

for crystallization versus microphase separation, the impact of conformational asymmetry, the drive for extended chain crystallites, and finally the role of detailed crystallization processes. The findings presented here demonstrate the biases introduced by conjugated polymers for the self-assembly and crystallization of such systems, and suggest design rules for the targeted creation of block copolymers containing high-performing conjugated polymers.

Table of Contents

List of Figures

List of Tables

Acknowledgements

First of all, I would like to thank my advisor Rachel Segalman for the extraordinary combination of encouragement, freedom, and support you have given me. Thank you for your constant confidence in me, and for always pushing me to start and explore new things (and to finish old ones). I also would like to thank all of the other members of the Segalman lab, past and present. In particular, thank you to Victor Ho for your work on this project stretching back years before I joined, and for teaching me both how to do polymer synthesis and the basic physics of conjugated polymers. Thank you also to Bryan Beckingham for pushing me in the right directions as I learned about polymer physics and polymer crystallization during my first two years in the group. What I learned from Victor and Bryan is the foundation of the knowledge and work that went into this dissertation. Thanks to Boris Russ for teaching me how to prepare for and image samples by TEM, and Jacob Thelan from Nitash Balsara's group at Berkeley for teaching me how to do X-ray scattering. I also particularly want to thank George Rizis, Anastasia Patterson, and Scott Danielsen, who were the first people to join the new Segalman lab in Santa Barbara: you were all instrumental in forming the team that got us off the ground here. The work that you put into getting everything working, building new systems, and establishing a strong culture in our new group was so important and appreciated. For the most recent members, especially Alex, Elayne, Rubayn and Sam: I am constantly inspired by your curiosity, questions, and your willingness to learn and to work hard. For everyone in the group, I am so excited about the research you are working on, the teamwork I see between you, and for the future – I am excited to see you use (and eventually pass on) all that you have learned.

I am also especially grateful for the hard work of staff at both UC Berkeley and UCSB (in particular Carlet Altamirano and Laura Crownover) who enabled me to finish my research in the Segalman Lab's new home at UCSB but complete my degree where I began with UC Berkeley. A number of instrument scientists have been incredibly important in helping me with my research; I especially need to thank Rachel Behrens who never fails to brighten my day and who has also moved boulders helping to get instruments together and running experiments for me and so many other students at UCSB. Thank you also to the members of my qualifying and dissertation committees (Nitash Balsara, Teresa Head-Gordon, Andy Minor, Bryan McCloskey, and Jeff Reimer) for discussion and their support. Thanks to my family for your support and patience as I seem to have gotten stuck on the West coast in the last six years. An especially huge thank you to the friends who have kept these last several years in both Berkeley and Santa Barbara full of joy alongside the hard work of graduate school, in particular the residents of the Continental for helping a new city become home so quickly. Most recently, Kathryn O'Hara has been a constant source of encouragement during this last month of writing. And finally thank you to Eric for always keeping me laughing and calm and inspired all these years, even from the opposite side of the country.

Chapter 1. Introduction

1.1 Conjugated Polymers as Functional Materials

Conjugated polymers are polymers characterized by stabilized planar configurations and long-range electron delocalization via π-conjugation between hybridized carbon atoms. While classical polymers behave as insulators, the existence of π-conjugation creates band-like electronic structure and allows conjugated polymers to behave as semiconductors capable of charge transport. As a result, conjugated polymers are promising materials for lightweight, scalable organic electronic materials for applications including field effect transistors (FETs), light emitting diodes (LEDs), organic photovoltaics (OPVs), and organic thermoelectrics. Conjugated polymers vary widely in molecular design, resulting in a diversity of bandgaps, air stabilities, solubilities in processing solvents, absorption and emission spectras, abilities to form well-ordered structures, and ultimately in their performances.[1, 2]

Charge transport in conjugated polymer materials depends crucially on hierarchical structuring across a wide range of length scales.[3, 4] These length scales range from the very local scale, defined by the extent of electron delocalization or 'conjugation length' on a single chain (on the order of several nanometers), up to long-range percolation between many crystallites (spanning over microns or even millimeters).[1, 2, 5-14] At very local length scales, the distance of electron delocalization also structurally corresponds to the distance over which a chain maintains planarity before encountering a kink or defect in the backbone. This stabilized planarity causes chains to be quite rigid, which can lead to semiflexible chain conformations and liquid crystalline interactions between chains.[15] On the mesoscale, rigid chains can be electronically coupled through aligned π-stacks; this feature is critical because interchain transport is ultimately limiting in a real device composed of many distinct chains. This difference in electronic coupling within a single chain versus between distinct chains emphasizes that transport in conjugated polymer materials is inherently anisotropic. At intermediate length scales, the electronic coupling along versus between chains is moderated by the local crystal packing structure. Changes in processing or molecular design that alter this crystal structure therefore impact the effective transport properties in the material. Furthermore, charge must transfer from crystallite to crystallite, so ultimately the degree of chains that are both locally ordered and that participate in an effectively percolated pathway for charge transport will contribute to the material's ultimate mobility.[8, 10-13] Experimental work across a wide range of conjugated polymer chemistries has demonstrated that increasing the degree of crystallinity, inducing orientation of crystallites, and increasing the size of crystallites all impact the effective percolation pathway and contribute to improving the resulting charge transport properties.[12, 14-18]

Significant interest exists in creating block copolymers containing functional components such as conjugated polymers. While coil-coil block copolymer phase behavior in the melt has been deeply explored,[19, 20] functional materials often adopt non-ideal chain shapes,[21-24] exhibit liquid crystallinity or crystallinity,[23, 25, 26] or must adopt specific structures in order to be effectively functional; these changes can impact the resulting phase behavior in the melt and self-assembly. In this dissertation, I will specifically examine how the polymer crystallization essential to the behavior of conjugated polymers is impacted by confinement in block copolymer

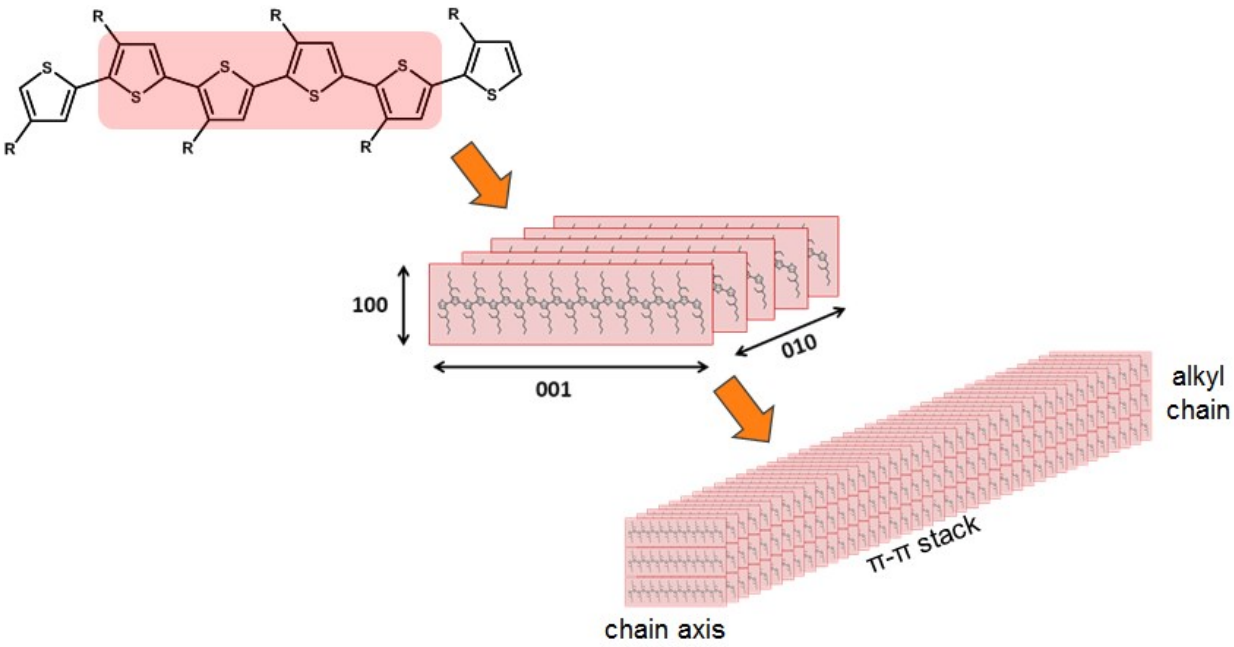

Figure 1.1 Conjugated polymer crystallization

In many systems, conjugated polymer crystallization is influenced by stabilized planar configurations and strong π-π interactions (left; example poly(3-alkylthiophene)) that drive fast growth along the π-stacking ordering direction (middle). The favored ordering along the π-stack leads to fibrillar nanostructures with the π-stack oriented along the long axis of the fibril (right).

microdomains, in order to develop design and processing rules for future materials. Furthermore, with the block copolymer architecture, we can control block copolymer crystallinity through confinement within microdomains of controlled geometry and induce tethering of chains at the microdomain interfaces.

1.2 Conjugated Polymer Crystallization

Polymer crystallization is a highly hierarchical process which is classically important for defining the mechanical and optical properties of polymer materials. Importantly, in classical systems, at the local length scale polymer chains fold into lamellae with a thickness that is determined by the temperature of crystallization; adding chains to the primary nucleus can be described as a secondary nucleation process, where the thickness of the lamellae is essentially determined by the stability of this secondary nucleus.[27-29] The initial lamella emanates from a single nucleation event; lamellae branch off of this initial point to form spherulitic structures composed of both amorphous and crystalline regions, causing polymer crystallization to result in a semicrystalline material.[27] These spherulitic structures then grow to be several microns in size, with growth eventually limited by impingement upon neighboring spherulites. The size and bridging of chains between spherulites in addition to the lamellar thickness can be varied by changing the crystallization temperature as well as by seeding nucleation with heterogenous nucleation agents.[27-33] While conjugated polymer crystallization is also hierarchical in nature, it differs from classical polymer crystallization in the driving mechanisms for crystallization, rate of chain diffusion, resulting crystallite morphologies. Conjugated polymers characteristically form crystals demonstrating a fibrillar (as opposed to lamellar) morphology; this is especially clear at relatively low molecular weights.[18, 26, 34-36] Furthermore, crystallites typically are limited to individual fibrils (as opposed to extended spherulites), indicating that each crystallite corresponds to a single nucleation event; this may be due to the very large degrees of undercooling and relatively slow chain diffusion in these stiffer polymers. Poly(3-hexylthiophene) (P3HT) is the most ubiquitous model conjugated polymer. Crystals of P3HT are characterized by three primary stacking directions: (1) packing along the chain (monomer to monomer) direction, (2) packing along the π-π stack, and (3) packing along the alkyl-chain stacking direction. Selected area diffraction of aligned P3HT fibrils has demonstrated that the π-π stack is aligned along the fibril axis,[37] while the chain direction and the alkyl-chain stacking directions compose the short axes (Figure 1.1).

In addition, while classical polymers chain fold readily, several studies of P3HT indicate that extended chain crystals persist up to modestly large molecular weights; this is attributed to the relatively rigid nature of P3HT chains.[38] It is also not well understood why the π-stacking direction apparently grows over much longer distances than the alkyl chain direction.[39] In addition, the nature of crystal interfaces which may be composed of tie chains, loops, and/or a 'rigid amorphous fraction,' the impact of processing on the development of these features, and their role in determining the final crystal size and morphology remain poorly understood.[12, 13, 40-43] A number of modern donor-acceptor polymers with increasingly stiff backbones have demonstrated deviations from these rules, for example by growing crystalline fibrils with the chain backbone parallel to the long axis of the fibril.[6, 7, 10] These materials display promise for

creating materials with excellent long-range charge percolation, but raise new questions about crystallinity in this class of materials. In particular, while in poly(3-alkylthiophene)s, excellent coherence along the π-π stack seems critical to charge transport, major questions remain concerning the role of tie chains between crystallites. Furthermore, the importance of the degree of crystallinity, crystallite size, and crystallite coherence along the different ordering directions in new donor-acceptor polymers remain important questions.

1.2.1 Conjugated Polymer Crystallization in Confinement

Confinement of polymer crystals offers an opportunity to examine crystallinity at controlled length scales and chain orientation, and is particularly relevant to applications such as thin film transistors (TFT) that rely crucially on the orientation and crystallinity of the monolayer at the top or bottom of the film (depending on the geometry of the contacts). Studies of conjugated polymer crystallization in thin films highlight the importance of considering surface energies and nucleation mechanisms in controlling the structure and ultimately charge transport of the system. For example, when confined in thin films, P3HT shows preferential alignment of crystallites relative to the substrate in either 'face on' or 'edge on' orientations in which polymer chains are parallel to the substrate, with improved charge mobility in the highly oriented 'edge on' orientations.[15, 16] In addition, the substrate effectively behaves as a nucleation site for crystallites. Significant effort has been expended to control orientation and crystal size in these thin films via processing including off-centered spin-coating, blade-coating, or wire-bar coating.[7, 44] Further, studies of P3EHT confined to thin films on a silicon substrate allowed the initial model development of the crystallization mechanism of P3EHT.[12] Similarly, when P3HT is confined in the pores of anodized alumina pores (AAO), crystallite orientation relies crucially on crystallization temperature and pore size, reflecting a balance of surface versus bulk dominated nucleation.[45, 46] These confinement geometries reveal the importance of considering surface energies and nucleation effects in controlling system behavior. However, they do not permit control of the precise location of chain ends, and also restrict the suite of techniques available to study conjugated polymer crystallization. In particular, in thin film confinement the primary techniques available to study order include grazing-incidence X-ray scattering (GIXS) and UV-vis spectroscopic studies. However thin films preclude thermal analysis; calorimetry of may be accomplished only carefully by transferring a thin film onto specialized and sensitive Flash DSCs, and even then this is only an emerging technique. A much more robust approach technique is in thermal analysis to study the melting behavior of polymer crystals in the bulk. As many conjugated polymers demonstrate complex melting behavior with peaks at multiple temperatures, thermal analysis reveals a wealth of information. In some cases, these peaks may be attributed to melting of different polymorphs or melting of side chains (as opposed to main chain crystals).[5, 47-49] Studies of the impact of confinement on conjugated polymer crystallization that are incapable of leveraging thermal analysis are therefore limited in their ability to probe the structural transitions in these materials.

1.3 Self-Assembly and Confined Crystallization of Block Copolymers

Block copolymers self-assemble into nanometer scale domains and can effectively confine conjugated polymers while maintaining a bulk format. Block copolymers are formed

from covalently linked blocks consisting of immiscible polymers that self-assemble into nanoscale patterns including cylinders, spheres, lamellae, and bicontinuous phases based on the balance of the blocks attempting to separate but suffering an entropic chain stretching penalty. The strength of segregation of the blocks is parametrized by χN, where χ is the Flory-Huggins interaction parameter which describes the free energy cost of contacts between immiscible polymers, and N describes the number of volumetric units along the chain. At sufficiently large temperatures, entropic gains overcome enthalpic penalties, resulting in the block copolymer transitioning to a homogenous, disordered state; this critical temperature is termed the order-disorder transition temperature (T_{ODT}).[19, 20, 50] Block copolymers permit confined crystallization, while permitting bulk calorimetry measurements to understand detailed properties of the confined crystallites.

1.3.1 Requirements for Achieving Confined Crystallization

In order to successfully achieve confined crystallization in block copolymer microdomains, it is essential that a number of conditions be met. First, it is critical that crystallization of the crystallizable block proceeds from the microphase separated melt; if crystallization proceeds from the homogenous melt, the resulting morphology will be unconfined and crystallization-driven (Figure 1.2). To accomplish this requires judicious choice of system; essentially, it is critical that the polymer's crystallization temperature (T_C) be lower than the diblock copolymer's order-disorder transition temperature (T_{ODT}).[51] In conjugated polymer systems, this requirement can be especially challenging to accomplish; the crystallization temperatures of conjugated polymers are typically extremely high (in excess of 200°C), making an extremely large χN required for an accessible melt phase to be microphase separated. Furthermore, even when these large χN values are attained, ordering kinetics are typically very slow, requiring long annealing times at elevated temperatures to achieve ordered microphase separation; this may either prevent the development of well-ordered phases or be chemically detrimental to conjugated polymers which require high degrees of purity for transport. In addition, it is not sufficient to simply have crystallization develop from the microphase separated melt. If the driving force for crystallization is strong relative to the ability of the conjugated polymer to confine it, the result will be still be crystallization-driven structure that destroys the order imposed by the diblock (Figure 1.3). This final case is termed 'breakout' and can be prevented by either having a second block that is vitreous at the crystallization temperature ('hard confinement') or by having a χN at the crystallization temperature that is sufficiently larger than the driving force for crystallization (termed 'soft confinement').

1.3.2 Melt Self-Assembly in Conjugated-Amorphous Block Copolymers

Classical diblock copolymers follow Gaussian chain statistics with identical statistical segment lengths in each block. The resulting morphology represents a tradeoff between the enthalpic cost of contact at interfaces and the entropic cost of chain stretching. However, conjugated block copolymers are universally stiffer than their classical analogues which impacts the phase diagram even in the limit of small lp/Lc (persistence length to block contour length) where chains still follow the statistics of Gaussian chains.52-55 As molecular weight decreases

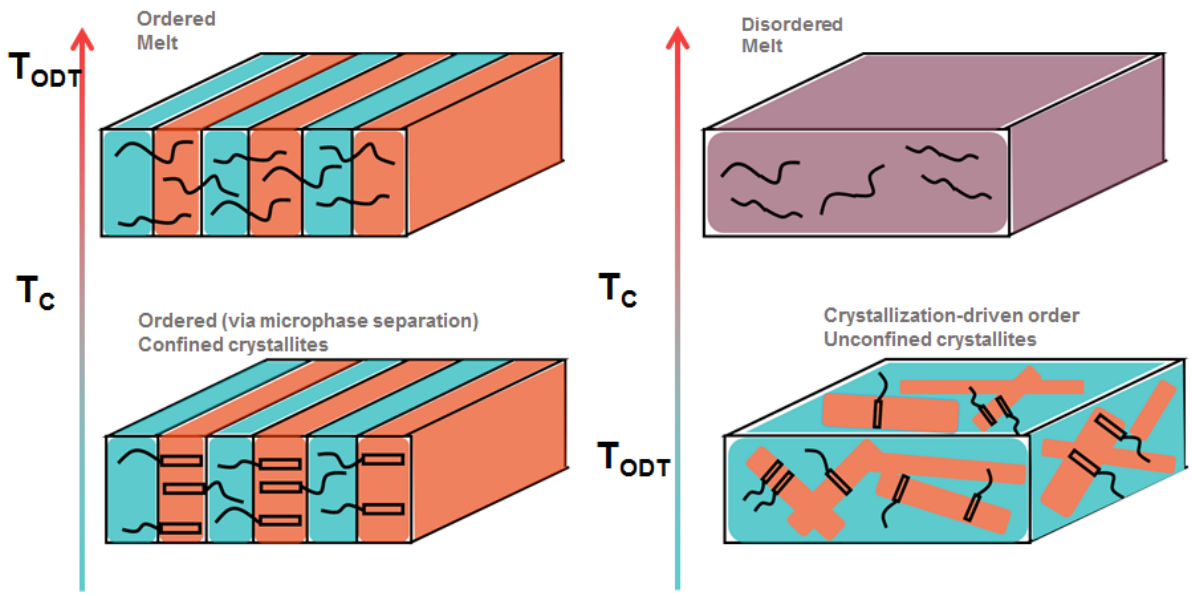

Figure 1.2 Crystallization temperature requirements for confined crystallization

To achieve confined crystallization, the material must have an accessible ordered melt with $T_{ODT} > T_c$. For large T_c, the result may be either an inaccessible melt phase, or a disordered melt. Crystallization from the ordered melt (left) may result in confined crystallites, while crystallization from the disordered melt (right) will result in crystallization-driven order.

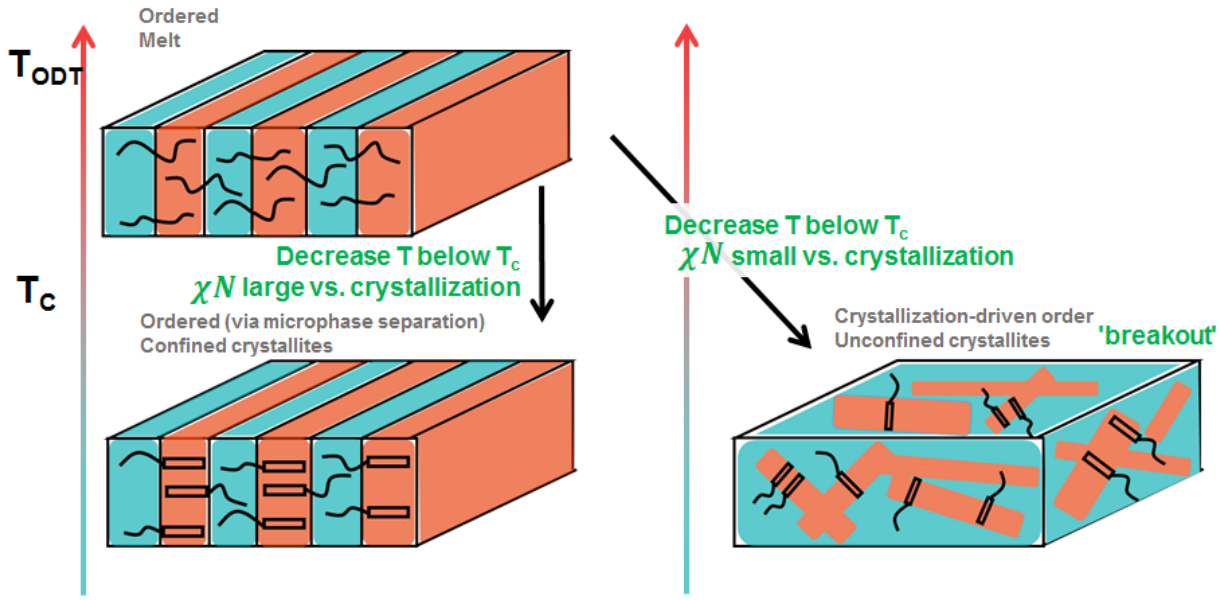

Figure 1.3 χN requirements for confined crystallization

Even if T_{ODT} is greater than T_c, if χN is not sufficiently large relative to the driving force for crystallization, crystallization from the ordered melt can destroy block copolymer microdomain order.

or as persistence lengths increase, when L_c becomes less than $10*l_p$, the chain shape is no longer well-described by Gaussian statistics. Here, the chain shape enters the semiflexible regime; eventually, as L_c becomes much greater than l_p, the chain shape enters a rod-like regime. With this change in chain shape (as opposed to just stiffness), additional impacts on phase behavior emerge, especially as chain-chain liquid crystalline behavior influences the assembly of the conjugated block in the melt.[56-58] Ultimately for templating diblocks of distinct morphologies including crystalline components, conjugated polymers present a more complex phase behavior than their flexible cousins. Importantly, different regions of this phase behavior will tend to favor some morphologies (generally lamellar phases, especially with high conjugated content) and disfavor others (phases with curved interfaces, especially with high conjugated content) compared to coil-coil materials, which significantly influences the molecular design, and may limit which conjugated polymers can be incorporated to achieve certain morphologies.

1.3.3 Self-Assembly of Crystalline-Amorphous Block Copolymers

Prior work on crystalline-amorphous block copolymers have focused on not only the requirements to achieve confined crystallization, but also the impacts of confinement on crystallization. In flexible materials, crystalline-*b*-rubbery-*b*-crystalline triblocks were originally of considerable interest for their potential use as an alternative to thermoplastic elastomers that utilize glassy hard blocks that form physical crosslinks between rubbery domains; the goal was to achieve improved mechanical properties via incorporation of crystalline blocks. This goal inspired studies to understand the processing conditions necessary to achieve the crystallinity in these domains required for form physical crosslinks. In particular, the crystallization kinetics as a function of the degree of confinement were studied; in less-confined geometries (lamellae or cylinders where the majority phase is the crystalline material), the crystallization kinetics are relatively unaffected relative to the constituent homopolymer.[59-61] However, as the degree of confinement increases – in particular in the confined spherical or cylindrical geometries useful in thermoplastic elastomers – crystallites experience a change in nucleation mechanism, requiring significantly longer time-scales or degrees of undercooling to achieve crystallinity, and the observation that crystallization rates follow first-order kinetics indicated that domains crystallize independently of each other. Significant work also went into examining whether materials exhibit cavitation or other deformation due to the significant change in density upon crystallization; interestingly, in polyethylene synthesized via hydrogenation of polybutadiene, this did not have any apparent significant impact. Importantly, the change in nucleation mechanism and accommodation of density changes has important implications for the processing considerations and final stresses experienced following crystallization.

In addition, following a theoretical treatment predicting an equilibrium degree of chain folding, significant interest arose in crystalline-amorphous lamellar diblocks as a system to study equilibrium effects in polymer crystallization arose.[62, 63] Prior work on the crystalline lamellar thickness of semicrystalline polymers had inspired significant debate over the ability of block copolymers to have an equilibrium degree of chain folding of the crystalline block due to a balance between stretching of the amorphous material and bending penalties in the crystalline material. Numerous experimental studies examined the resulting scaling relationships of a range

of model systems. Interestingly, while some materials clearly demonstrated a step function like change in the integer number of folds as amorphous block length was changed,[64] other materials instead accommodated these by apparently reorienting crystallites within the microdomains by ninety degrees.[65-69] Importantly, these studies demonstrate that tethered confinement within block copolymer microdomains induces a number of additional constraints that are not present within the crystalline homopolymers in the bulk or in untethered confinement. The results of these studies begin to illustrate the critical parameters we expect to impact conjugated polymer crystallization in confinement.

1.4 Motivation and Dissertation Outline

In this dissertation, the model conjugated polymer P3EHT is leveraged within nanopatterned block copolymers to understand the balance between conjugated polymer crystallization and the structure of the block copolymer itself. Block copolymers are an ideal platform to study conjugated polymer crystallization under highly controlled conditions: the geometry of confinement is determined by microphase separation, and the boundary conditions are set by chain tethering at the interface. In addition, block copolymers containing conjugated material are an opportunity to develop materials that combine nanopatterning with the optoelectronic properties of conjugated polymers. Given that the crystallinity of conjugated polymers is closely tied to performance, this work aims to develop both design and processing rules for developing materials with optimized performance. Importantly, a number of parameters are essential to controlling the final self-assembly and crystallization. First, achieving confined crystallization requires a system with an accessible microphase separated melt phase. To control the nanopatterning of the resulting confined crystallites also requires control over phase behavior in the melt, since the melt phase templates the nanostructure of the crystalline block copolymer. Achieving this phase control is challenging; in these block copolymers, the stiffness of the conjugated block means the phase behavior deviates significantly from that of an ideal coil-coil block copolymer with identical statistical segment lengths. Finally, the performance of the confined conjugated polymer will depend strongly on its crystallinity. This crystallinity depends not only on the morphology in confinement, but also the thermal conditions under which it is crystallized and the coupling of conjugated polymer chains to the second block. This dissertation not only explores the fundamentals of how to achieve crystallization of conjugated polymers confined within block copolymer microdomains, but also aims to understand how that crystallization is impacted by factors including morphology, the mechanical properties of the second block, and thermal processing. Ultimately, the goal is to provide design and processing rules to create nanostructured, crystalline, high performance materials from conjugated block copolymers.

Chapter 2 demonstrates the lamellar confinement of model conjugated polymer with a depressed melting temperature of ~80°C, poly(3-(2′-ethyl)hexylthiophene) (P3EHT), and shows that the preference for extended-chain crystals in conjugated polymers is essential in templating the orientation of the crystallites. In addition, it shows that to achieve highly crystalline conjugated polymers in confinement, chains must be able to extend as they crystallize. Chapter 3 studies the crystallization of P3EHT in cylindrical confinement, finding that cylinders induce an

unexpected orientation of P3EHT crystallites, and demonstrating thermal pathways to high quality P3EHT crystallites. Chapter 4 studies the detailed impacts of the crystallization process on crystallinity and self-assembly. It shows how careful thermal processing manipulate both crystalline perfection and domain structure, and develops a refined model of melt-recrystallization in P3EHT. Chapter 4 also demonstrates the utility of using conjugated diblocks for fundamental studies of crystallization. Since changes in crystalline structure are reflected in the structure of the entire domain, in-situ SAXS studies of these diblocks allows detailed studies of structural changes in crystallinity that would be inaccessible via tools such as TEM or AFM. Finally, Chapter 5 summarizes the major conclusions of this work and provides insight into the future challenges and opportunities in the field.

1.5 References

1. Heeger, A. J., Semiconducting and metallic polymers: The fourth generation of polymeric materials. J Phys Chem B 2001, 105 (36), 8475-8491.

2. Heeger, A. J., Semiconducting polymers: the Third Generation. Chem Soc Rev 2010, 39 (7), 2354-2371.

3. Nguyen, T. Q.; Doan, V.; Schwartz, B. J., Conjugated polymer aggregates in solution: Control of interchain interactions. J Chem Phys 1999, 110 (8), 4068-4078.

4. Spano, F. C.; Silva, C., H- and J-Aggregate Behavior in Polymeric Semiconductors. Annual Review of Physical Chemistry, Vol 65 2014, 65, 477-500.

5. Prosa, T. J.; Moulton, J.; Heeger, A. J.; Winokur, M. J., Diffraction line-shape analysis of poly(3-dodecylthiophene): A study of layer disorder through the liquid crystalline polymer transition. Macromolecules 1999, 32 (12), 4000-4009.

6. Tseng, H. R.; Phan, H.; Luo, C.; Wang, M.; Perez, L. A.; Patel, S. N.; Ying, L.; Kramer, E. J.; Nguyen, T. Q.; Bazan, G. C.; Heeger, A. J., High-Mobility Field-Effect Transistors Fabricated with Macroscopic Aligned Semiconducting Polymers. Adv Mater 2014, 26 (19), 2993-2998.

7. Patel, S. N.; Su, G. M.; Luo, C.; Wang, M.; Perez, L. A.; Fischer, D. A.; Prendergast, D.; Bazan, G. C.; Heeger, A. J.; Chabinyc, M. L.; Kramer, E. J., NEXAFS Spectroscopy Reveals the Molecular Orientation in Blade-Coated Pyridal[2,1,3]thiadiazole-Containing Conjugated Polymer Thin Films. Macromolecules 2015, 48 (18), 6606-6616.

8. Salleo, A., Charge transport in polymeric transistors. Mater Today 2007, 10 (3), 38-45.

9. Himmelberger, S.; Salleo, A., Engineering semiconducting polymers for efficient charge transport. Mrs Commun 2015, 5 (3), 383-395.

10. Wang, S. H.; Fabiano, S.; Himmelberger, S.; Puzinas, S.; Crispin, X.; Salleo, A.; Berggren, M., Experimental evidence that short-range intermolecular aggregation is sufficient for efficient charge transport in conjugated polymers. P Natl Acad Sci USA 2015, 112 (34), 10599-10604.

11. Noriega, R.; Rivnay, J.; Vandewal, K.; Koch, F. P. V.; Stingelin, N.; Smith, P.; Toney, M. F.; Salleo, A., A general relationship between disorder, aggregation and charge transport in conjugated polymers. Nat Mater 2013, 12 (11), 1037-1043.

12. Duong, D. T.; Ho, V.; Shang, Z. R.; Mollinger, S.; Mannsfeld, S. C. B.; Dacuna, J.; Toney, M. F.; Segalman, R.; Salleo, A., Mechanism of Crystallization and Implications for Charge Transport in Poly(3-ethylhexylthiophene) Thin Films. Adv Funct Mater 2014, 24 (28), 4515-4521.

13. Mollinger, S. A.; Krajina, B. A.; Noriega, R.; Salleo, A.; Spakowitz, A. J., Percolation, Tie-Molecules, and the Microstructural Determinants of Charge Transport in Semicrystalline Conjugated Polymers. Acs Macro Lett 2015, 4 (7), 708-712.

14. Boudouris, B. W.; Ho, V.; Jimison, L. H.; Toney, M. F.; Salleo, A.; Segalman, R. A., Real-Time Observation of Poly(3-alkylthiophene) Crystallization and Correlation with Transient Optoelectronic Properties. Macromolecules 2011, 44 (17), 6653-6658.

15. Kline, R. J.; Mcgehee, M. D.; Toney, M. F., Highly oriented crystals at the buried interface in polythiophene thin-film transistors. Nat Mater 2006, 5 (3), 222-228.

16. Jimison, L. H.; Himmelberger, S.; Duong, D. T.; Rivnay, J.; Toney, M. F.; Salleo, A., Vertical Confinement and Interface Effects on the Microstructure and Charge Transport of P3HT Thin Films. J Polym Sci Pol Phys 2013, 51 (7), 611-620.

17. Marsh, H. S.; Reid, O. G.; Barnes, G.; Heeney, M.; Stingelin, N.; Rumbles, G., Control of Polythiophene Film Microstructure and Charge Carrier Dynamics Through Crystallization Temperature. J Polym Sci Pol Phys 2014, 52 (10), 700-707.

18. Kline, R. J.; McGehee, M. D.; Kadnikova, E. N.; Liu, J. S.; Frechet, J. M. J., Controlling the field-effect mobility of regioregular polythiophene by changing the molecular weight. Adv Mater 2003, 15 (18), 1519-+.

19. Bates, F. S.; Fredrickson, G. H., Block Copolymer Thermodynamics - Theory and Experiment. Annu Rev Phys Chem 1990, 41, 525-557.

20. Cochran, E. W.; Garcia-Cervera, C. J.; Fredrickson, G. H., Stability of the gyroid phase in diblock copolymers at strong segregation. Macromolecules 2006, 39 (7), 2449-2451.

21. McCulloch, B.; Ho, V.; Hoarfrost, M.; Stanley, C.; Do, C.; Heller, W. T.; Segalman, R. A., Polymer Chain Shape of Poly(3-alkylthiophenes) in Solution Using Small-Angle Neutron Scattering. Macromolecules 2013, 46 (5), 1899-1907.

22. Zhang, W. L.; Gomez, E. D.; Milner, S. T., Predicting Chain Dimensions of Semiflexible Polymers from Dihedral Potentials. Macromolecules 2014, 47 (18), 6453-6461.

23. Zhang, W. L.; Gomez, E. D.; Milnert, S. T., Predicting Nematic Phases of Semiflexible Polymers. Macromolecules 2015, 48 (5), 1454-1462.

24. Zhang, W. L.; Gomez, E. D.; Milner, S. T., Surface-Induced Chain Alignment of Semiflexible Polymers. Macromolecules 2016, 49 (3), 963-971.

25. Baklar, M.; Barard, S.; Sparrowe, D.; Wilson, R. M.; McCulloch, I.; Heeney, M.; Kreouzis, T.; Stingelin, N., Bulk charge transport in liquid-crystalline polymer semiconductors based on poly(2,5-bis(3-alkylthiophen-2-yl)thieno[3,2-b]thiophene). Polym Chem-Uk 2010, 1 (9), 1448-1452.

26. DeLongchamp, D. M.; Kline, R. J.; Jung, Y.; Lin, E. K.; Fischer, D. A.; Gundlach, D. J.; Cotts, S. K.; Moad, A. J.; Richter, L. J.; Toney, M. F.; Heeney, M.; McCulloch, I., Molecular basis of mesophase ordering in a thiophene-based copolymer. Macromolecules 2008, 41 (15), 5709-5715.

27. Hoffman, J. D.; Lauritzen, J. I., Crystallization of Bulk Polymers with Chain Folding - Theory of Growth of Lamellar Spherulites. J Res Nat Bur Stand 1961, A 65 (4), 297-+.

28. Lauritzen, J. I.; Hoffman, J. D., Extension of Theory of Growth of Chain-Folded Polymer Crystals to Large Undercoolings. J Appl Phys 1973, 44 (10), 4340-4352.

29. Hoffman, J. D.; Weeks, J. J., X-Ray Study of Isothermal Thickening of Lamellae in Bulk Polyethylene at Crystallization Temperature. J Chem Phys 1965, 42 (12), 4301-&.

30. Hoffman, J. D.; Frolen, L. J.; Ross, G. S.; Lauritzen, J. I., Growth-Rate of Spherulites and Axialites from Melt in Polyethylene Fractions - Regime-1 and Regime-2 Crystallization. J Res Nbs a Phys Ch 1975, 79 (6), 671-699.

31. Hoffman, J. D.; Lauritze.Ji; Passagli.E; Ross, G. S.; Frolen, L. J.; Weeks, J. J., Kinetics of Polymer Crystallization from Solution and Melt. Kolloid Z Z Polym 1969, 231 (1-2), 564-&.

32. Hoffman, J. D.; Weeks, J. J., Melting Process and Equilibrium Melting Temperature of Polychlorotrifluoroethylene. J Res Nbs a Phys Ch 1962, 66 (Jan-F), 13-+.

33. Hoffman, J. D.; Weeks, J. J., Rate of Spherulitic Crystallization with Chain Folds in Polychlorotrifluoroethylene. J Chem Phys 1962, 37 (8), 1723-&.

34. Snyder, C. R.; Kline, R. J.; DeLongchamp, D. M.; Nieuwendaal, R. C.; Richter, L. J.; Heeney, M.; McCulloch, I., Classification of Semiconducting Polymeric Mesophases to Optimize Device Postprocessing. J Polym Sci Pol Phys 2015, 53 (23), 1641-1653.

35. Kline, R. J.; McGehee, M. D.; Kadnikova, E. N.; Liu, J. S.; Frechet, J. M. J.; Toney, M. F., Dependence of regioregular poly(3-hexylthiophene) film morphology and field-effect mobility on molecular weight. Macromolecules 2005, 38 (8), 3312-3319.

36. Kline, R. J.; McGehee, M. D., Morphology and Charge Transport in Conjugated Polymers. Journal of Macromolecular Science, Part C 2006, 46 (1), 27-45.

37. Liu, J. H.; Arif, M.; Zou, J. H.; Khondaker, S. I.; Zhai, L., Controlling Poly(3-hexylthiophene) Crystal Dimension: Nanowhiskers and Nanoribbons. Macromolecules 2009, 42 (24), 9390-9393.

38. Zhang, R.; Li, B.; Iovu, M. C.; Jeffries-EL, M.; Sauve, G.; Cooper, J.; Jia, S. J.; Tristram-Nagle, S.; Smilgies, D. M.; Lambeth, D. N.; McCullough, R. D.; Kowalewski, T., Nanostructure dependence of field-effect mobility in regioregular poly(3-hexylthiophene) thin film field effect transistors. J Am Chem Soc 2006, 128 (11), 3480-3481.

39. Lim, J. A.; Liu, F.; Ferdous, S.; Muthukumar, M.; Briseno, A. L., Polymer semiconductor crystals. Mater Today 2010, 13 (5), 14-24.

40. Beckingham, B. S.; Ho, V.; Segalman, R. A., Formation of a Rigid Amorphous Fraction in Poly(3-(2 '-ethyl)hexylthiophene). Acs Macro Lett 2014, 3 (7), 684-688.

41. Hu, H. L.; Zhao, K.; Fernandes, N.; Boufflet, P.; Bannock, J. H.; Yu, L. Y.; de Mello, J. C.; Stingelin, N.; Heeney, M.; Giannelise, E. P.; Amassian, A., Entanglements in marginal solutions: a means of tuning pre-aggregation of conjugated polymers with positive implications for charge transport. J Mater Chem C 2015, 3 (28), 7394-7404.

42. Nieuwendaal, R. C.; Snyder, C. R.; DeLongchamp, D. M., Measuring Order in Regioregular Poly(3-hexylthiophene) with Solid-State C-13 CPMAS NMR. Acs Macro Lett 2014, 3 (2), 130-135.

43. Snyder, C. R.; Nieuwendaal, R. C.; DeLongchamp, D. M.; Luscombe, C. K.; Sista, P.; Boyd, S. D., Quantifying Crystallinity in High Molar Mass Poly(3-hexylthiophene). Macromolecules 2014, 47 (12), 3942-3950.

44. Murphy, C. E.; Yang, L.; Ray, S.; Yu, L. Y.; Knox, S.; Stingelin, N., Wire-bar coating of semiconducting polythiophene/insulating polyethylene blend thin films for organic transistors. J Appl Phys 2011, 110 (9).

45. Martin, J.; Campoy-Quiles, M.; Nogales, A.; Garriga, M.; Alonso, M. I.; Goni, A. R.; Martin-Gonzalez, M., Poly(3-hexylthiophene) nanowires in porous alumina: internal structure under confinement. Soft Matter 2014, 10 (18), 3335-3346.

46. Martin, J.; Nogales, A.; Martin-Gonzalez, M., The Smectic-Isotropic Transition of P3HT Determines the Formation of Nanowires or Nanotubes into Porous Templates. Macromolecules 2013, 46 (4), 1477-1483.

47. Koch, F. P. V.; Heeney, M.; Smith, P., Thermal and Structural Characteristics of Oligo(3-hexylthiophene)s (3HT)(n), n=4-36. J Am Chem Soc 2013, 135 (37), 13699-13709.

48. Prosa, T. J.; Winokur, M. J.; Moulton, J.; Smith, P.; Heeger, A. J., X-Ray Structural Studies of Poly(3-Alkylthiophenes) - an Example of an Inverse Comb. Macromolecules 1992, 25 (17), 4364-4372.

49. Beckingham, B. S.; Ho, V.; Segalman, R. A., Melting Behavior of Poly(3-(2 '-ethyl)hexylthiophene). Macromolecules 2014, 47 (23), 8305-8310.

50. Bates, F. S.; Fredrickson, G. H., Block copolymers - Designer soft materials. Phys Today 1999, 52 (2), 32-38.

51. Loo, Y. L.; Register, R. A.; Ryan, A. J., Modes of crystallization in block copolymer microdomains: Breakout, templated, and confined. Macromolecules 2002, 35 (6), 2365-2374.

52. Bates, F. S.; Fredrickson, G. H., Conformational Asymmetry and Polymer-Polymer Thermodynamics. Macromolecules 1994, 27 (4), 1065-1067.

53. Matsen, M. W.; Bates, F. S., Conformationally asymmetric block copolymers. J Polym Sci Pol Phys 1997, 35 (6), 945-952.

54. Bates, F. S.; Schulz, M. F.; Rosedale, J. H.; Almdal, K., Correlation of Binary Polyolefin Phase-Behavior with Statistical Segment Length Asymmetry. Macromolecules 1992, 25 (20), 5547-5550.

55. Bates, F. S.; Schulz, M. F.; Khandpur, A. K.; Forster, S.; Rosedale, J. H.; Almdal, K.; Mortensen, K., Fluctuations, Conformational Asymmetry and Block-Copolymer Phase-Behavior. Faraday Discuss 1994, 98, 7-18.

56. Olsen, B. D.; Gu, X.; Hexemer, A.; Gann, E.; Segalman, R. A., Liquid Crystalline Orientation of Rod Blocks within Lamellar Nanostructures from Rod Coil Diblock Copolymers. Macromolecules 2010, 43 (16), 6531-6534.

57. Olsen, B. D.; Segalman, R. A., Structure and thermodynamics of weakly segregated rod-coil block copolymers. Macromolecules 2005, 38 (24), 10127-10137.

58. Olsen, B. D.; Shah, M.; Ganesan, V.; Segalman, R. A., Universalization of the phase diagram for a model rod-coil diblock copolymer. Macromolecules 2008, 41 (18), 6809-6817.

59. Loo, Y. L.; Register, R. A.; Adamson, D. H., Direct imaging of polyethylene crystallites within block copolymer microdomains. J Polym Sci Pol Phys 2000, 38 (19), 2564-2570.

60. Loo, Y. L.; Register, R. A.; Ryan, A. J.; Dee, G. T., Polymer crystallization confined in one, two, or three dimensions. Macromolecules 2001, 34 (26), 8968-8977.

61. Loo, Y. L.; Register, R. A.; Ryan, A. J., Polymer crystallization in 25-nm spheres. Phys Rev Lett 2000, 84 (18), 4120-4123.

62. Douzinas, K. C.; Cohen, R. E.; Halasa, A. F., Evaluation of Domain Spacing Scaling Laws for Semicrystalline Diblock Copolymers. Macromolecules 1991, 24 (15), 4457-4459.

63. Whitmore, M. D.; Noolandi, J., Theory of Crystallizable Block Copolymers. Makromol Chem-M Symp 1988, 16, 235-249.

64. Lee, L. B. W.; Register, R. A., Equilibrium control of crystal thickness and melting point through block copolymerization. Macromolecules 2004, 37 (19), 7278-7284.

65. Nandan, B.; Hsu, J. Y.; Chen, H. L., Crystallization behavior of crystalline-amorphous diblock copolymers consisting of a rubbery amorphous block. Polym Rev 2006, 46 (2), 143-172.

66. Hamley, I. W.; Fairclough, J. P. A.; Ryan, A. J.; Bates, F. S.; TownsAndrews, E., Crystallization of nanoscale-confined diblock copolymer chains. Polymer 1996, 37 (19), 4425-4429.

67. Zhu, L.; Cheng, S. Z. D.; Calhoun, B. H.; Ge, Q.; Quirk, R. P.; Thomas, E. L.; Hsiao, B. S.; Yeh, F. J.; Lotz, B., Crystallization temperature-dependent crystal orientations within nanoscale confined lamellae of a self-assembled crystalline-amorphous diblock copolymer. J Am Chem Soc 2000, 122 (25), 5957-5967.

68. Hamley, I. W.; Fairclough, J. P. A.; Bates, F. S.; Ryan, A. J., Crystallization thermodynamics and kinetics in semicrystalline diblock copolymers. Polymer 1998, 39 (6-7), 1429-1437.

69. Zhu, L.; Cheng, S. Z. D.; Calhoun, B. H.; Ge, Q.; Quirk, R. P.; Thomas, E. L.; Hsiao, B. S.; Yeh, F.; Lotz, B., Phase structures and morphologies determined by self-organization, vitrification, and crystallization: confined crystallization in an ordered lamellar phase of PEO-b-PS diblock copolymer. Polymer 2001, 42 (13), 5829-5839.

Chapter 2. Confined Crystallization in Lamellae Forming Poly(3-(2′-ethyl)hexylthiophene (P3EHT) Block Copolymers

Reproduced with permission from Emily Davidson, Victor Ho, Bryan Beckingham, and Rachel Segalman. *Reproduced by permission of John Wiley and Sons*. (http://onlinelibrary.wiley.com/doi/10.1002/polb.23904/full)

Charge transport in poly(3-alkylthiophene)s (P3AT)s is closely linked to the nanoscale organization of crystallites. Block copolymer morphologies provide an ideal platform to study crystallization as the chain ends are tethered at a known interface in a well-defined geometry. The impact of soft versus hard confinement on P3EHT crystallization is studied using poly(3-(2′-ethyl)hexylthiophene) (P3EHT) containing diblocks with both rubbery poly(methyl acrylate) (PMA) and glassy polystyrene (PS) blocks. Here, P3EHT's lower melting point relative to the commonly studied P3HT facilitates its confined crystallization and makes it an ideal model system. While TEM and SAXS reveal well-ordered lamellar morphologies both in the melt and post-crystallization for both sets of diblocks, the glassy blocks inhibit confined crystallization of P3EHT relative to rubbery matrix blocks. Analysis of aligned diblocks by both SAXS and WAXS reveals that the P3EHT chain axis aligns perpendicular to domain interfaces, allowing preferential growth of the alkyl-chain and π-π stacking directions parallel to lamellae. Finally, we show that following diblock self-assembly in the melt, crystallite growth drives expansion of microdomains to match the P3EHT contour length. We conclude that P3EHT chains adopt an extended conformation within confined crystallites due to the rigid nature of polythiophenes relative to flexible chain crystalline polymers.

2.1 Introduction

Polythiophenes with solubilizing alkyl side-chains – namely poly(3-hexylthiophene) (P3HT) – have been especially well-studied, reporting high FET mobilities[1] and good solar cell performance.[2] Polythiophene charge mobility is highly dependent on subtle variations in crystallinity as influenced by casting solvent, casting temperature, post-deposition annealing, thin-film confinement, and surface treatment.[3,4] In addition, studies have investigated hierarchical structures built from block copolymers containing one or more conjugated blocks. However, the achievement of well-ordered conjugated block copolymer morphologies has proven difficult: microphase separation in these systems is typically driven by P3HT crystallization, resulting in fibrillar morphologies displaying varied degrees of modulation relative to polythiophene homopolymers.[5,6,7,8] It is important to note that many fundamental studies of polymer crystallization in both the homopolymer and confined within block copolymer microdomains require an accessible melt phase. Unfortunately, melt studies in P3HT homopolymer and block copolymers have been generally precluded by P3HT's high melting temperature (approaching degradation) and by both large segregation strengths (kinetically trapping block copolymer structures) and large degrees of undercooling (encouraging crystallization-driven self-assembly).[5,6,7]

Prior work in the Segalman group examined a polythiophene with a side chain variant, poly(3-(2′-ethyl)hexylthiophene) (P3EHT) which displays a depressed melting transition (~85ºC)

relative to P3HT (>200ºC at similar molecular weights).[9] The P3EHT homopolymer develops fibrillar crystals with the π-π stack aligned along the fibril axis similar to P3HT. However, the reduced melting transition has allowed detailed studies of homopolymer crystallization as a function of isothermal crystallization temperature, showing that crystallite size/perfection is tunable via the degree of undercooling.[10] This depressed melting temperature also permitted the observation that P3EHT both displays a melt-recrystallization mechanism during melting[10] and develops a rigid amorphous fraction (RAF).[11] In addition, the accessible kinetics relative to P3HT allowed examination of both the charge mobility as a function of relative degree of crystallinity[12] as well as the crystallization mechanism as a function of thin film confinement.[13] Importantly, this reduced crystalline driving force in P3EHT relative to P3HT also allows P3EHT-containing block copolymers to robustly form classical block copolymer microstructures.[14,15] While classically well-ordered poly(3-hexylthiophene) (P3HT) and poly(3-dodecylthiophene) P3DDT-containing diblocks have been achieved, they have been limited to low molecular weights and characterized by poor ordering kinetics requiring either extended solvent or high-temperature. Thus, due to the relatively limited ability to manipulate P3HT and P3DDT crystallization within confined domains, studies have largely examined the formation of these diblocks and not the hierarchical ordering of the crystallites within these systems.[16] Notably, in these hierarchical systems, P3EHT chains are tethered to their respective coil blocks at lamellar block copolymer interfaces. This tethering is expected to have a significant impact on confinement effects, differentiating crystallization within microdomains from crystallization in thin film confinement. For example, when flexible chain polymers are crystallized within microdomains the combination of chain tethering effects and preferential crystal growth directions results in preferred crystallite and chain orientations.[17,18] Further, while poly(3-alkylthiophenes) display significantly stiffer backbones than classically flexible polymers, both experiment[19] and simulation[19,20] find that their persistence lengths in solution are merely 1.5-3.3 nm, significantly more flexible than other conjugated polymers which are treated as rigid rods.[21]

When studying confined crystallization, the mechanical modulus of the confining material is critical. In the hard confinement case a glassy (high T_g) matrix block is well-known to suppress domain deformation following crystallization.[22] However, for confined crystallization studies in classical flexible polymers such as polyethylene (PE) and polyethylene oxide (PEO) a glassy interface does not usually impede confined crystallization.[17,23] A rubbery matrix, on the other hand, explicitly allows deformation. Thus, the degree to which the final structure following crystallization reflects that of the melt is determined by the relative driving forces for interblock segregation-driven microphase separation versus crystallization.[22] These relative driving forces fall into three modes of crystallization corresponding to increasing ratios of χN (segregation strength) at the crystallization temperature versus χN at which the system disorders.[22] When blocks are insufficiently segregated during crystallization, crystallites may exhibit breakout – in which crystallization dominates structure formation, effectively destroying the melt structure. At intermediate segregations, the melt structure merely 'templates' crystallization, allowing significant deformation of domains or crystallites spanning between domains. Finally, above a critical segregation strength, the melt structure is able to truly 'confine' crystallites. Clearly, the critical χN at the boundaries of these regimes varies by the crystallizing polymer. It is also important to consider that in diblocks containing relatively rigid blocks (such as the conjugated

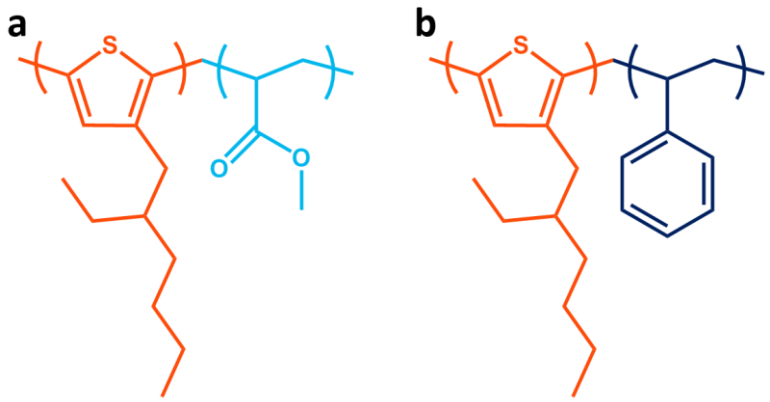

Figure 2.1 P3EHT-*b*-PMA and P3EHT-*b*-PS chemical structures

Structures of (a) P3EHT-*b*-PMA, a polythiophene with a rubbery second block and (b) P3EHT-*b*-PS, with a glassy second block.

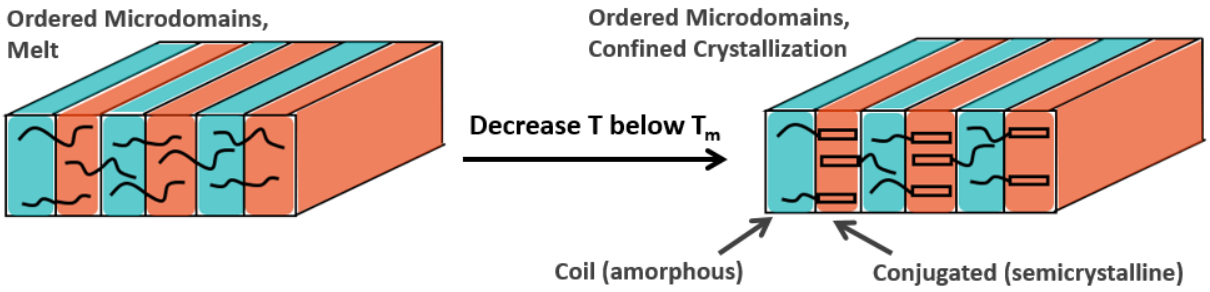

Figure 2.2 Cartoon of confined crystallization in a diblock copolymer

Cartoon of P3EHT-*b*-PMA (or P3EHT-*b*-PS) microphase separated structure in the melt (left) and post-crystallization (right). Blue domains represent coil blocks (PMA, PS) and orange represents conjugated blocks (P3EHT). To achieve crystallization confined by microdomains (as opposed to crystallization driven microphase separation), it is essential that diblocks access a microphase separated morphology in the melt which is maintained upon crystallization. Crystallized chains are depicted here as rectangles for simplicity. Notably, crystallized chains are tethered at interfaces during confined crystallization in diblock copolymer microdomains.

polymers examined here), we can expect interfacial effects to propagate more strongly into the domain center. Thus, the glassy versus rubbery systems directly contrast the degree to which polymer chains are pinned versus allowed to reorganize at this interface.

Microphase separated domain structures have been known to induce preferential orientation and growth habits in crystallites of polyethylene (PE) and polyethylene oxide (PEO) over a range of geometries and conditions.[17,18, 24,25,26,23, 27,28] Interestingly, despite chain tethering at domain interfaces, PE is typically observed to fold such that it forms short lamellae spanning crystalline domains. This behavior has been attributed to the system attempting to prevent a free energy penalty: i.e this folding behavior minimizes the decrease in interfacial area per chain and resultant increase in domain spacing.[26] In P3AT containing block copolymers, a structure with a crystalline chain axis perpendicular to the microdomain interfaces may instead be favored – despite the penalty in interfacial area – due to P3EHT chain rigidity.

Here, the impact of both hard and soft confinement on the resulting crystallite population is examined, focusing on the system's ability to crystallize and the impact on properties previously studied in homopolymer P3EHT.[11,10] The controlled microstructures achieved by self-assembly of P3EHT containing block copolymers (both P3EHT-*b*-PMA and P3EHT-*b*-PS, Figure 2.1) are leveraged to examine the impact of controlled 2-D confinement on the polythiophene crystallization (as depicted in Figure 2.2). These studies utilize a combination of differential scanning calorimetry and WAXS on melting to interpret the changes in crystallite population as a function of confinement and thermal processing. In addition, to understand how the tethering of polythiophene chains to block copolymer interfaces templates the local crystallite orientation within these lamellar microdomains, lamellar diblock structures are aligned in the melt via a channel-flow die[29] and then isothermally crystallized. The relative orientation of the block copolymer domains versus crystalline material is thus determined from a combination of small-angle X-ray scattering and wide-angle X-ray scattering of aligned material. Finally, changes in the P3EHT chain conformation (and thus the degree of chain folding in the resultant confined P3EHT crystals) is inferred via small-angle X-ray scattering of the diblock structure over the course of P3EHT melting.

2.2 Experimental

2.2.1 Synthesis

Reagents and solvents were used as received from Sigma-Aldrich unless otherwise noted. THF used for the GRIM polymerization was dried and degassed by freeze-pump-thawing three times and stirring over CaH_2 overnight. 2,5-dibromo-3-(2′-ethyl)-hexylthiophene was synthesized as previously described.[9] Regioregular poly(3-(2′-ethyl)hexylthiophene (P3EHT) with a low dispersity was synthesized via the Grignard Metathesis (GRIM) procedure.[30,31] 2,5-dibromo-3-(2′-ethyl)-hexylthiophene was added to an oven dried three-neck flask, and vacuum was pulled for ten minutes before backfilling with nitrogen and adding THF and 2.0 M *tert*-butylMgCl in diethyl ether. After refluxing for 90 minutes and cooling to room temperature, $Ni(dppp)Cl_2$ was added and allowed to react for 45 minutes. Molecular weight was controlled by varying the concentration of $Ni(dppp)Cl_2$ initiator in each reaction mixture. P3EHT was end

functionalized by injecting 14 mLs of 0.5 M ethynyl MgCl in THF to quench the reaction mixture and allowing to react for two minutes prior to precipitation into methanol.[32] The ethynl-P3EHT was then separated by centrifugation, and extraction with hexanes. The final ethynyl-P3EHT product was separated by precipitating into methanol and drying under vacuum, yielding a dark red powder, and stored in a freezer until ready for use.

Poly(methyl acrylate) (PMA) and polystyrene (PS) were synthesized by atom transfer radical polymerization (ATRP).[33] Inhibitor was removed by running methyl acrylate or styrene monomer through basic alumina. Methyl acrylate or styrene monomer, ethyl bromo isobutyrate (EBiB), CuBr, and PMDTA were added (typical ratio of 350:1:0.5:0.5) to a schlenk flask. The reaction mixture was subjected to three freeze/pump/thaw cycles, and reacted for between one and ten hours. Molecular weight was controlled by varying both the initiator concentration and the time duration of the polymerization. Polymers grown by ATRP were purified by diluting in chloroform and running through basic alumina to remove copper followed by precipitation into a 2:1(v/v) 0ºC methanol and water mixture (PMA) and methanol (PS). Azide functionality was conferred to PS and PMA blocks by stirring for 24 hours with 1.5 molar excess NaN_3 in DMF. Polymer was passed through silica, re-precipitated and dried under vacuum to yield a clear rubbery substance and a white powder for PMA and PS respectively.

Block copolymers were synthesized by combining 20% excess ethynyl-P3EHT with N_3-PMA or N_3-PS with 0.5 molar equivalents CuBr and PMDTA in THF, submitting to three freeze-pump-thaw cycles to prevent parasitic Glaser coupling between ethynyl-P3EHT blocks[34] and allowed to stir at room temperature for 24 hours. Block copolymers were run through basic alumina to remove CuBr, precipitated in petroleum ether (in which excess P3EHT homopolymer is selectively soluble for both systems), filtered, and dried under vacuum to yield a bright orange to deep red block copolymer.

2.2.2 Molecular Characterization

Gel permeation chromatography (GPC) was performed on a Waters instrument using a refractive index detector and Agilent PLgel 5μm MiniMIX-D column. THF at 25ºC was used as the mobile phase with a flow rate of 0.3 mL/min. Traces in Figure 2.14. Reported dispersity values ($Đ$) are according to their polystyrene equivalents as calibrated with narrow polystyrene standards (Agilent). ^{1}H NMR spectra were collected on a Bruker AV-500 spectrometer using deuterated chloroform (Cambridge) as the solvent with ~1 wt% polymer. Reported molecular weights are by end group analysis. Densities of amorphous (via rapid quench to 25ºC; measured prior to the onset of crystallization) and semicrystalline P3EHT homopolymer measured via gas pycnometry in the TEMPO lab of UCSB's MRL. Molecular characteristics are in Table 2.1.

2.2.3 Small and Wide-Angle X-Ray Scattering

Isotropic samples for X-ray scattering were prepared by melt pressing sample into 1 mm thick aluminum washers at 150ºC. Aligned samples for X-ray scattering were prepared by creating aligned strips with a channel flow die.[29] Samples were isothermally crystallized for one week within temperature-controlled ovens prior to data collection. SAXS and WAXS patterns

Table 2.1 Molecular characterization of lamellar P3EHT diblocks

P3EHT-*b*-PMA	P3EHT M_n[a]	PMA M_n[a]	$Đ$[c]	Morphology	$f_{melt,\ P3EHT}$[d]
11.1/6.0k	11.1	6.0	1.14	LAM	0.67
11.1/8.1k	11.1	8.1	1.15	LAM	0.61
8.3/9.8k	8.3	9.8	1.20	LAM	0.48
8.3/8.8k	8.3	8.8	1.15	LAM	0.51
7.6/9.5k	7.6	9.5	1.16	LAM	0.47
P3EHT-*b*-PS	**P3EHT M_n**	**PS M_n[b]**	**$Đ$**	**Morphology**	**$f_{melt,\ P3EHT}$**
8.3/6.0k	8.3	6.0	1.21	LAM	0.59
8.3/4.6k	8.3	4.6	1.14	LAM	0.65

[a] PMA and P3EHT M_n values calculated via homopolymer ^{1}H NMR

[b] PS M_n via narrow PS standard calibrated GPC

[c] Reported dispersities ($Đ$) via PS equivalent GPC values. See Figure 2.14 for diblock GPC traces.

[d] P3EHT density via gas pycnometry of P3EHT rapidly quenched from the melt ($\rho_{amorphous}$= 0.97 g/cm^3); temperature dependent PMA and PS densities from Brunacci et al.[35], and Richardson et al.[36], respectively. See appendix for details.

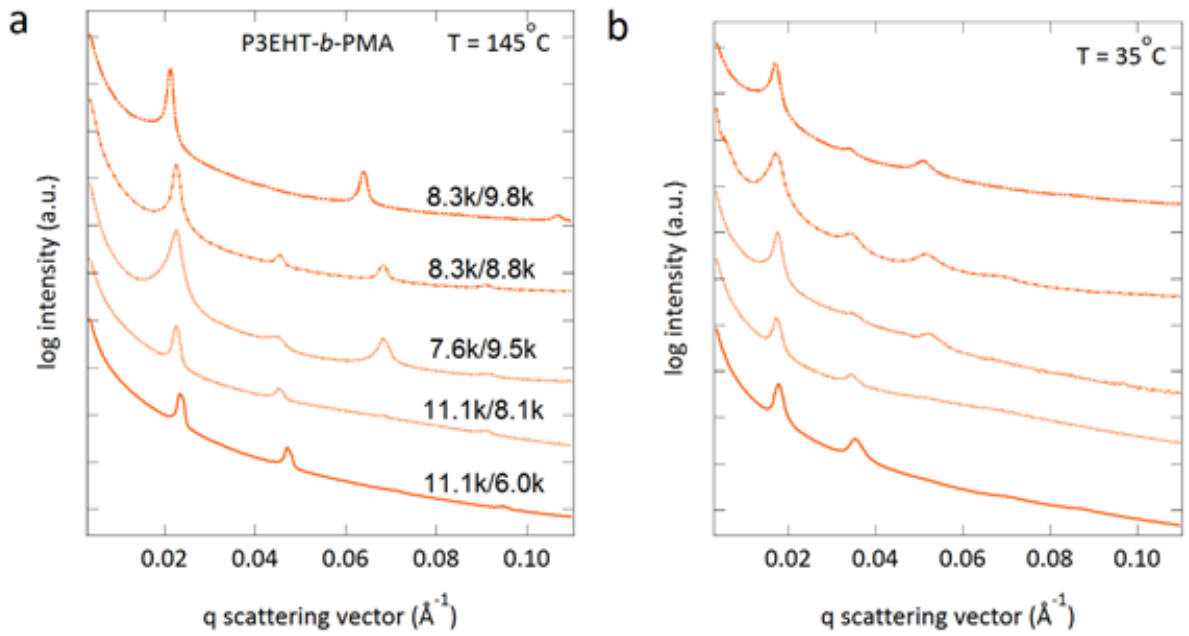

Figure 2.3 Transmission SAXS of P3EHT-*b*-PMA diblock copolymers

(a) Transmission SAXS of P3EHT-*b*-PMA diblocks in the melt at 145°C (b) post-crystallization at 35°C. Multiple higher order peaks in both cases emphasizes that diblocks are highly ordered in the melt and maintain that order post-crystallization. Order of traces is the same for both plots.

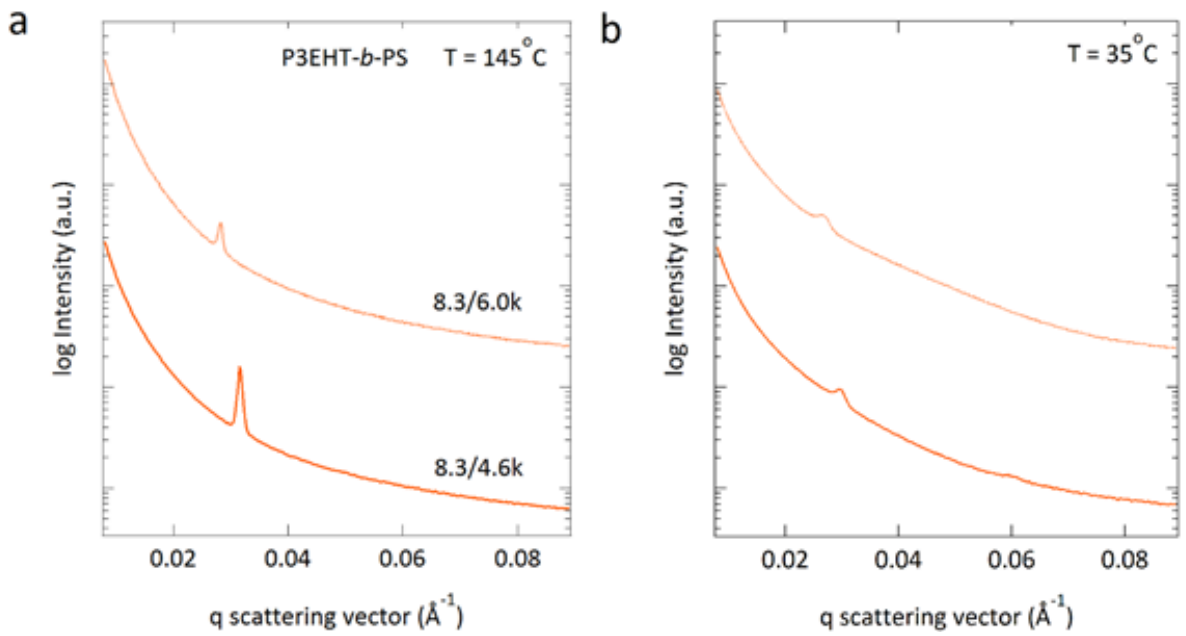

Figure 2.4 Transmission SAXS of P3EHT-*b*-PS diblock copolymers

(a) Transmission SAXS of P3EHT-*b*-PS diblocks in the melt at 145°C (b) after isothermal 'crystallization'; 35°C. Sharp scattering peak in conjunction with TEM (Figure 2.5 a,b) emphasizes that the system is highly ordered in both melt and post-crystallization, despite poor scattering contrast. Order of traces is the same for both plots.

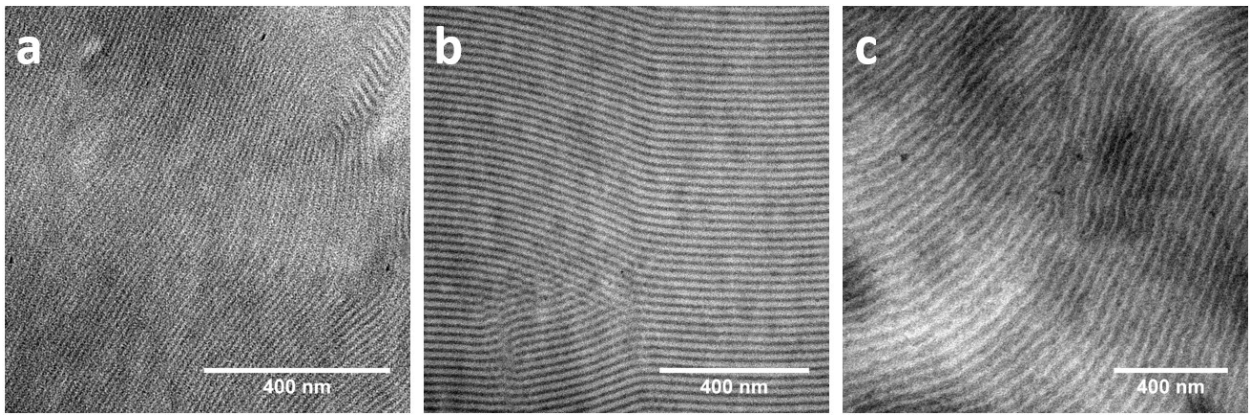

Figure 2.5 Bright field TEM of lamellar P3EHT-*b*-PMA and P3EHT-*b*-PS

Bright field TEM of microtomed bulk unaligned lamellar P3EHT-containing block copolymers shows highly ordered domains. P3EHT domains stained dark by RuO_4. (a) P3EHT-*b*-PS 8.3/4.6k (b) P3EHT-*b*-PS 8.3/6.0k (c) P3EHT-*b*-PMA 11.1/6.0k.

were collected at both beamline 7.3.3 of Lawrence Berkeley National Lab's Advanced Light Source (ALS) and at beamlines 1-4 and 11-3 of the Stanford Synchrotron Radiation Laboratory (SSRL). Scattering angles were calibrated using a silver behenate (AgBe) standard.[37] Intensities are plotted versus the momentum transfer vector $q = (4\pi/\lambda) \sin \theta$. Data was reduced using the Nika[38] package for Igor and WxDiff.

2.2.4 Thermal Characterization

Differential scanning calorimetry (DSC) measurements were performed using a TA Q2000 calorimeter. Each ~10 mg sample was hermetically sealed inside a TZero aluminum pan. Samples in pans were heated to 145°C offline and held for ten minutes to clear their thermal histories, then allowed to isothermally crystallize in temperature controlled ovens for one week prior to performing melting scans to 130°C at 10°C/min.

2.2.5 Transmission Electron Microscopy

Samples for TEM were prepared by melt pressing polymer at 150°C between two sheets of Kapton followed by isothermal crystallization in temperature controlled ovens for one week. 100 nm thick thin sections for TEM were sliced from these samples using a Leica Ultracut UCT microtome and diamond knife. P3EHT-*b*-PS samples were microtomed at room temperature, while P3EHT-*b*-PMA samples were cryomicrotomed at -25°C. Thin sections were placed on CF300 amorphous carbon coated Cu grids from Electron Microscopy Sciences prior to staining by exposure to RuO_4 (2% aqueous RuO_4 solution, Electron Microscopy Sciences) vapors for 20 minutes. Imaging was performed using an FEI Tecnai G2 Sphera microscope operating at 200 kV.

2.2.6 Results and Discussion

To investigate the impact of both hard and soft confinement on polythiophene crystallization within controlled lamellar block copolymer microdomains, a family of low dispersity P3EHT-*b*-PMA (Figure 2.1 a) and P3EHT-*b*-PS (Figure 2.1 b) serve as a model system. Microphase separated structures were observed both in the melt and maintained upon crystallization (Figure 2.3, Figure 2.4) via small-angle X-ray scattering (SAXS), emphasizing that crystallization is truly confined. DSC studies of both systems indicates that the glassy PS in the hard confinement case significantly suppresses P3EHT crystallization, while the rubbery PMA permits crystallization. DSC studies of P3EHT-*b*-PMA crystallites revealed a rigid-amorphous fraction stable to higher temperatures than the constituent homopolymer. In addition, similar to P3EHT homopolymer, P3EHT crystallites in lamellar confinement demonstrate melt-recrystallization behavior and tunable crystal size/perfection.[10] Examination of aligned P3EHT-*b*-PMA via SAXS/WAXS reveals that microdomains preferentially orient P3EHT chains perpendicular to the lamellar interfaces. Finally, it is observed that P3EHT crystallization drives domain expansion, and that P3EHT adopts a fully extended structure when crystallized in soft confinement.

2.3 Formation of Well-Ordered Semiflexible-*b*-Flexible Lamellar Block Copolymer Structures

To study the confined crystallization of a conjugated polymer within block copolymer microdomains, it is essential that diblocks reach a well-ordered microphase separated structure in the melt and maintain that structure following crystallization. Here, P3EHT-*b*-PMA samples in the melt display well-ordered lamellar morphologies by SAXS (Figure 2.3 a). Interestingly, P3EHT-*b*-PS samples show only a single, sharp scattering peak independent of temperature (Figure 2.4 a,b). The sharp nature of this peak (FWHM of 0.00093 $Å^{-1}$ for P3EHT-*b*-PS 8.3/4.6k compared to FWHM of 0.0011 $Å^{-1}$ for P3EHT-*b*-PMA 11.1/6.0k in the melt, and FWHM~0.0020 $Å^{-1}$ for both at 35ºC) suggests that it is not merely a correlation hole of a disordered structure. In addition, transmission electron microscopy on thin sections cut from bulk P3EHT-*b*-PS (Figure 2.5 a,b) reveals well-ordered lamellar structures, so the lack of well-defined higher reflections in the X-ray scattering is attributed to poor scattering contrast for this system. Clearly, both systems ordered strongly in the melt state. In addition, our consideration of these materials as semiflexible-*b*-flexible diblocks is supported by the fact that the P3EHT-*b*-PMA diblocks examined here does not deviate strongly from the phase diagram expected of strongly segregated diblocks.[39] Lamellar morphologies are observed in the melt for φ_{P3EHT} ranging from 0.46 to 0.66 (the primary focus of this study); in addition, for φ_{P3EHT} ~0.35 a hexagonally perforated lamellar structure is assigned, and from φ_{P3EHT} ~0.10 to 0.21 hexagonally packed cylinders are observed.

The glassy PS matrix, as expected, prevented deformation of the structure by crystallization and maintained the lamellar P3EHT-*b*-PS structure. In the rubbery P3EHT-*b*-PMA system, the soft confinement created a higher risk of crystallization destroying the domain architecture created in the melt. However, small angle X-ray scattering post-crystallization (Figure 2.3, b) clearly shows that a lamellar structure is maintained - emphasizing that P3EHT does not exhibit breakout behavior.[22] No accessible order-disorder transition was found (ODT > 190˚C). In addition, TEM confirms that crystallites are fully contained within microdomains: P3EHT-*b*-PMA post-crystallization (Figure 2.4 c) shows only continuous PMA (light) domains surrounding P3EHT (dark; RuO_4 stained) domains. Overall, this behavior is in contrast to the many published accounts of P3HT diblock copolymer self-assembly in which crystallization drives structure formation.[5-7] The successful confinement of P3EHT crystallization in a PMA matrix highlights the importance of careful design strategy: while increasing χN for a given crystalline block reduces the possibility of breakout, it simultaneously slows the ordering kinetics and limits well-ordered structures to relatively low molecular weight materials. Since the breakout condition is determined by a balance of χN with the driving force for crystallization, reducing the latter quantity is an effective strategy to robustly achieve confined crystallization within well-ordered structures.

2.4 Impact of Lamellar Confinement on Net Crystallinity, Rigid Amorphous Fraction, and Melt-Recrystallization Mechanism

The glassy versus rubbery nature of the coil block has a dramatic influence on the melting behavior of the P3EHT block. Essentially, stringent pinning of the semiflexible P3EHT

chain end at the interface strongly suppresses the resulting crystallinity, while loose pinning permits crystallization behavior very similar to the parent homopolymers. Here, the parent P3EHT homopolymers display the expected behavior on heating by DSC (Figure 2.6, red) corresponding to a rigid-amorphous fraction (T_a) and a melt-recrystallization mechanism (T_{m1}, T_{m2}).[11,10] The melting traces of the rubbery P3EHT-*b*-PMA (Figure 2.6, dark blue) immediately reveal that the material is semicrystalline and displays the trimodal melting behavior characteristic of the P3EHT homopolymer. By contrast, P3EHT-*b*-PS diblocks synthesized from the same parent homopolymer display significantly less crystallinity by DSC (Figure 2.6, light blue); the most distinct feature upon heating is a PS T_g at ~90ºC.

One explanation for the reduced crystallinity in P3EHT-*b*-PS is that pinning P3EHT chain ends into the glassy PS matrix prevents P3EHT reorganization into crystallites. Meanwhile, the rubbery PMA matrix permits the necessary reorganization, allowing P3EHT to form crystallites. Alternatively, the glassy PS matrix could prevent P3EHT densification during crystallization. However, this is not an impediment to crystallization of flexible polymers,[17, 23] so suppressed crystallinity of P3EHT in confinement cannot be attributed to space-filling constraints alone. Instead, the relatively semiflexible nature of P3EHT must permit increased propagation of pinning effects that suppress crystallinity. Given this simplistic model, one would expect that as P3EHT molecular weight increases, the chain behavior will become increasingly decoupled from the interface, and crystallinity in the P3EHT-*b*-PS system will improve.

The melting behavior of lamellar P3EHT-*b*-PMA is remarkably similar to that of the parent homopolymers (Table 2.2). In this case, the rubbery PMA matrix permits limited deformation and local pinning effects are relaxed. Like P3EHT homopolymer, the lowest melting peak (T_a) is attributed to the presence of a rigid amorphous fraction (RAF). However, the T_a observed for confined P3EHT is elevated by 5-11ºC relative to the homopolymers. The simplest explanation is that within lamellar confinement the rigid amorphous regions are nested between crystallites and tethered PMA domains (thereby decreasing the entropic gain the transition achieves relative to RAF in the homopolymer). Meanwhile, the profile of the dual-peak melting shows peaks within 1-2ºC of those observed in P3EHT homopolymer. Since both crystallite size and surface energy are tied to melting temperature, the similar melting temperature loosely implies that crystallite sizes are similar in the homopolymer and in lamellar confinement. However, it is critical to consider the role of crystallite surfaces and shape in determining melting point. In classical crystallizing block copolymer systems (polyethylene, PEO etc.), flexible chains form lamellae with a thickness directly correlated to the crystallization temperature. By contrast, poly(3-alkylthiophene) homopolymers form fibrillar structures with a long axis aligned with the π-π stack. The near-identical melting peak positions between homopolymer and confined P3EHT suggests that P3EHT forms crystallites over the same length scales in both cases.

However, the possibility remains that the form factor of P3EHT crystallites may shift from fibrils to extended lamellar or ribbon-like crystallites, as has been observed under certain conditions.[40] This change would reduce the surface area to volume of crystallites, increasing

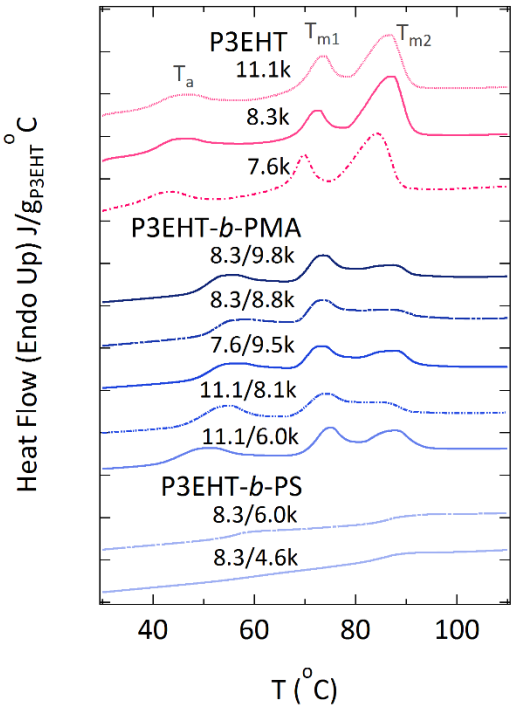

Figure 2.6 DSC endotherms of P3EHT homopolymer and P3EHT-*b*-PMA and P3EHT-*b*-PS

DSC endotherms taken upon heating of (top, red) P3EHT homopolymers, (middle, dark blue) lamellae-forming P3EHT-*b*-PMA and (bottom, light blue) lamellae-forming P3EHT-*b*-PS diblocks. Trimodal melting behavior corresponding to a rigid amorphous fraction and melt-recrystallization in the homopolymer is maintained in confinement with a rubbery matrix, but suppressed with a glassy matrix. Samples crystallized at 25°C; traces normalized by P3EHT content.

Table 2.2 Melting characteristics of P3EHT-*b*-PMA diblocks and component P3EHT homopolymer

Sample	T_a (°C)	T_{m1} (°C)	T_{m2} (°C)
P3EHT-b-PMA			
11.1k/6.0k	49.5	74.7	86.9
11.1k/8.1k	54.1	73.0	87.0
8.3k/9.8k	55.2	72.0	[a]
8.3k/8.8k	53.8	73.2	86.1
7.6k/9.5k	54.5	73.0	87.0
P3EHT			
11.1k	44.9	73.1	86.1
8.3k	44.2	71.7	86.4
7.6k	42.9	69.9	84.4

[a]Distinct melting peak not clearly distinguishable

their apparent size. Additionally, surface energies will be affected by the changed chemical composition within confinement[41].

Due to tethering effects, confinement is also expected to reduce the entropic gain of P3EHT upon melting, resulting in an increase in T_{m2}. The uncertainty in these confinement-induced effects on crystallite stability prevents using melting point and melting enthalpy measurements to yield a quantitative analysis of crystallite size or degree of crystallinity in confinement.

The existence of tunable size/perfection of crystals in confinement via thermal processing and of a melt-recrystallization mechanism in these P3EHT-*b*-PMA diblocks is studied in more depth via WAXS. To investigate the degree to which the size/perfection of crystals in confinement are tunable, P3EHT-*b*-PMA diblocks are crystallized at several increasing isothermal crystallization temperatures (T_c) between 25°C and 55°C. Following these controlled thermal treatments, reduced 1-D WAXS (Figure 2.7) shows increasing peak intensity and decreased peak breadth of the 110 reflection and higher order peaks with increasing T_c corresponding to preferential improvement in the π-π stacking direction. Thus, we conclude that (similar to P3EHT homopolymer), crystallite size/perfection in confinement may be tuned via controlled thermal processing.

In addition, the existence of a melt-recrystallization mechanism is observed by collecting *in-situ* WAXS traces of P3EHT-*b*-PMA during melting. For P3EHT-*b*-PMA crystallized with T_c = 25°C, while the 110 reflection sharpens and increases in magnitude prior to melting, for T_c=55°C no change is observed prior to melting. In other words, crystals which are small/poorly ordered in the π-π stacking direction (T_c = 25°C) reorganize to form more perfect crystals when given the energy to do so, while large/well-ordered crystals (T_c = 55°C) do not. This behavior is clear evidence that the melt-recrystallization mechanism is active for P3EHT-*b*-PMA. By contrast, the reflection corresponding to the alkyl chain stacking direction (the 100), is negligibly affected by varying T_c. Indeed, the 100 is invariant until reaching the temperature corresponding to final melting of the polymer, emphasizing that thermal processing does not appear to significantly impact ordering in the alkyl chain stacking direction. The melt-recrystallization process does apparently display slower kinetics in the diblock system than in the homopolymer: the two DSC melting peaks tend to be broader in the diblock system, with the T_{m1} peak generally larger than the T_{m2} peak while the opposite is observed for the parent P3EHT homopolymer. In other words, for a given melting rate, the slower the system's reorganization kinetics are, the fewer of the crystals we expect to reorganize into the larger/more perfect (T_{m2}) state. Similar behavior is observed in P3EHT homopolymer with increasing molecular weight.[10] In summary, control over the isothermal crystallization temperature grants tunability over P3EHT crystallite size/perfection within confined P3EHT-*b*-PMA lamellae (comparable to the behavior in the homopolymer). In addition, P3EHT in confinement displays melt-recrystallization behavior that is mechanistically analogous (although kinetically hindered) relative to that observed for P3EHT homopolymers.[10]

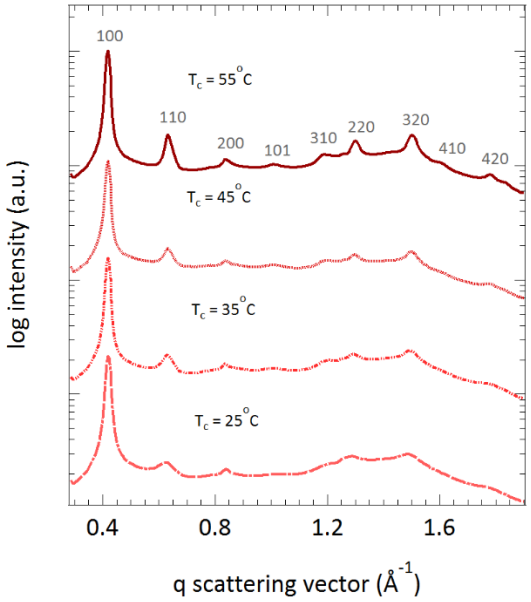

Figure 2.7 T_c dependent WAXS traces of P3EHT-*b*-PMA

Reduced 1-D WAXS traces of P3EHT-*b*-PMA-11.1/6.0k after isothermal crystallization from the melt at various degrees of undercooling. Increasing crystallization temperature (decreased undercoolings) result in improved crystal size/perfection, especially in the 110 reflection (correlated with π-π stacking) comparable to P3EHT homopolymer.

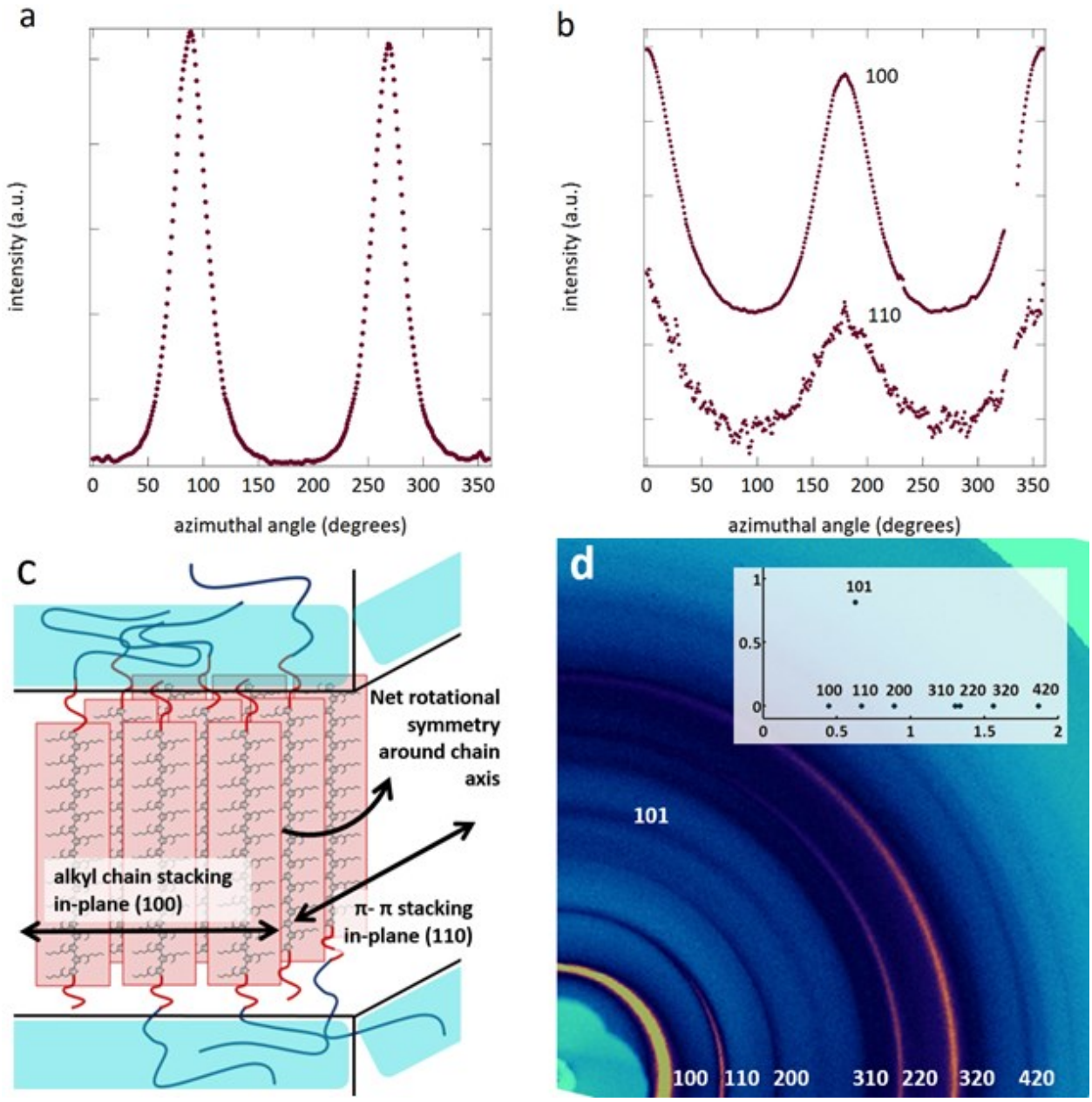

Figure 2.8 Orientation of P3EHT crystallites in confinement

Azimuthal angular dependence of (a) primary SAXS and (b) primary WAXS peaks of aligned P3EHT-*b*-PMA with maximum intensities offset by 90° (100 and 110 not to scale) implying that P3EHT adopts (c) an orientation of P3EHT crystallites with the chains perpendicular to domain interfaces. This orientation is further supported by (d) 2-D WAXS of aligned P3EHT-*b*-PMA diblock crystallized at 55°C which displays many higher-order peaks and agrees with the (inset) predicted peak positions for rotational symmetry around the chain axis.

2.5 Role of Microdomains in Inducing Crystallite Orientation

Both the thermal dependence of crystallite growth and a melt-recrystallization process is retained for P3EHT in confinement, suggesting that the π-π stacking direction is free to grow unhindered within P3EHT lamellae as illustrated in Figure 2.8c. However, to directly understand the role of diblock microdomains in inducing P3EHT crystallite growth habits, the relative orientation of microphase separated domains and P3EHT crystal structure may be directly probed via SAXS/WAXS of P3EHT-*b*-PMA aligned via a channel-flow die.[29] Figure 2.8a presents SAXS intensity of the primary scattering peaks taken with the X-ray beam along the highly oriented constraint direction[29] (X-ray beam parallel to lamellar interfaces) as a function of azimuthal intensity. The two sharp scattering peaks at 90° and 270° confirm that P3EHT-*b*-PMA domains are highly aligned. All 2-D scattering patterns and a discussion of orientational order parameter calculations may be found in the Appendix. Figure 2.8b, by contrast, examines the relative orientation of crystalline 100 (alkyl chain stacking) and 110 (π-π stack) peaks, also in the constraint direction, for a sample crystallized at 25°C. The crystalline peaks are precisely perpendicular to maximums in SAXS intensity at 0°, 180°, and 360°, placing both the alkyl chain and π-π stacking directions parallel to the lamellar interface; this orientation is maintained through melting (Figure 2.13). Thus, as suggested by the WAXS/DSC analysis, P3EHT X-ray scattering analysis of aligned samples directly confirms that crystallization from the confined melt permits unconstrained in-plane crystal growth in the π-π direction. The resulting structure places individual P3EHT chains extending perpendicular from the lamellar interface, as depicted in Figure 8c. This orientation is further supported by crystallizing the aligned diblock at a higher T_c of 55°C, resulting in more pronounced higher order crystalline peaks (Figure 2.8d). These match well with the scattering pattern expected for net rotational symmetry around the polymer chain axis (Figure 2.8d, inset).

2.6 Changes in P3EHT Chain Conformation during P3EHT Confined Crystallization

Since the P3EHT crystalline chain axis sits perpendicular to lamellar microdomains interfaces (refer to Figure 2.8c), the degree of P3EHT chain folding can be inferred from the domain spacing post-crystallization. Specifically, the shift in the primary SAXS peak of P3EHT-*b*-PMA during melting reveals an overall domain spacing contraction by ~20% (Figure 2.15a). Remarkably, it displays this behavior despite the expansion of P3EHT during melting. Based on simple density arguments, one would naively expect domains to expand during melting due to the increase in P3EHT's specific volume. A closer analysis reveals that if P3EHT expands upon crystallization, PMA domains must likewise expand in order to maintain a constant volume (Figure 2.15b,c). After calculating the d_{P3EHT} values after crystallization, we find the width of crystalline P3EHT microdomains closely matches the calculated contour lengths of P3EHT chains (Table 2.3). These results are consistent with P3EHT chains adopting a fully extended conformation in order to crystallize within lamellar confinement. Here, this simply emphasizes that amorphous block stretching penalties are insufficient to overcome the energy penalty for bending the semiflexible P3EHT. Meanwhile, P3EHT confined within P3EHT-*b*-PS demonstrates minimal expansion/contraction (Table 2.3), re-emphasizing the effect of glassy confinement on chain conformation and resulting lack of crystallinity in this system.

Table 2.3 Confined P3EHT contour lengths and domain sizes

P3EHT-*b*-PMA	L_c P3EHT[a] (nm)	*d* P3EHT 145°C (nm)	*d* P3EHT 35°C (nm)[b]
11.1/6.0k	22.3	17.9	23.4
11.1/8.1k	22.3	16.8	21.5
8.3/9.8k	16.6	14.3	17.4
8.3/8.8k	16.6	14.2	18.3
7.6/9.5k	15.3	13.1	16.5
P3EHT-*b*-PS			
8.3/6.0k	16.6	13.0	13.2
8.3/4.6k	16.6	13.0	13.3

[a]Contour lengths calculated using a monomer length of 0.39 nm standard to P3ATs.[19]
[b]Density of crystallized P3EHT via gas pycnometry of semicrystalline P3EHT homopolymer, $\rho_{semicrystalline}$= 1.10 g/cm^3.

2.7 Conclusions

Insights into both the organization of P3EHT crystallites and the detailed crystallization and melting behavior are gleaned from examination of P3EHT crystallization within lamellar confinement in both soft-confined P3EHT-*b*-PMA and hard-confined P3EHT-*b*-PS diblock systems. Within P3EHT-*b*-PMA, the tunability of size/perfection in the π-π stack, and melt-recrystallization behavior (with slowed kinetics) that has been previously reported in P3EHT homopolymer is retained,[10] emphasizing that the length scales of crystallite growth in homopolymer P3EHT are essentially maintained within lamellar confinement. The impact of lamellar microdomains on P3EHT growth habits was examined by aligning P3EHT-*b*-PMA diblocks using a channel flow die, and subsequently characterizing via both SAXS and WAXS, showing that the 100 (alkyl chain stacking direction) and 110 (π-π stack) preferentially grow within the plane of P3EHT microdomains. Thus, the remarkably similar thermal tunability of crystallite size/perfection and melt-recrystallization behavior between homopolymer and P3EHT-*b*-PMA diblock is attributed to the confined P3EHT's ability to maintain the direction of preferential crystal growth within the plane of lamellar microdomains. Finally, by tracking the ~20% decrease in total domain spacing during melting and calculating d_{P3EHT} both in the melt and after crystallization, we conclude that P3EHT must be fully extended after crystallization in the structures examined. Additionally, we attribute the poor crystallinity in P3EHT-*b*-PS to a combination of the inability of P3EHT chains to adopt this fully extended conformation in the glassy matrix and the tethering of the P3EHT to the glassy interface interfering with chain organization. Based on theoretical work by Whitmore and Noolandi[42] and experimental results indicating a critical molecular weight to achieve chain folding in poly(3-alkylthiophene)s,[43] we expect that chain folding in confinement may be observed at larger P3EHT molecular weights than those examined here. Finally, we show that hard versus soft confinement can have significant effects on not only the retention of the melt structure following crystallization (as observed in flexible systems), but also the resulting associations (conformation and local packing interactions) between conjugated chains. These findings show that through proper design of P3AT-containing block copolymer architectures, significant control over the spatial organization of both the microdomains and the crystallites can be achieved. Such control may facilitate additional studies into how crystallite size/perfection as well as orientation affects the resulting optoelectronic properties.

2.8 Appendix

2.8.1 2-D SAXS/WAXS of Aligned Samples

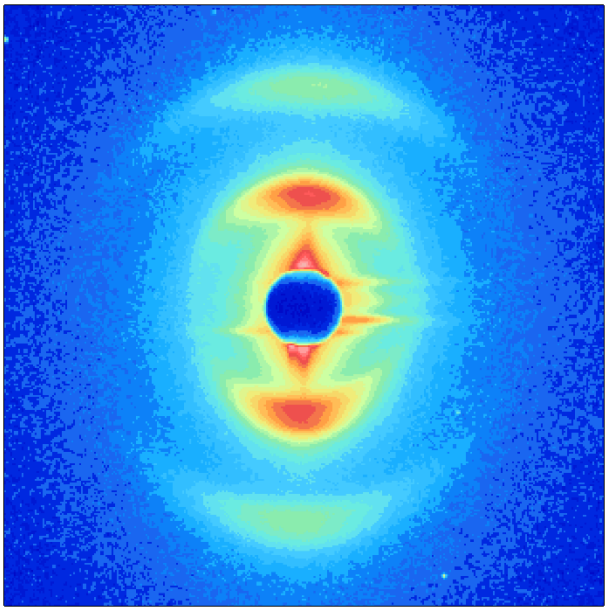

Figure 2.9 SAXS of aligned P3EHT-*b*-PMA 11.1k/6.0k
First and second order reflections of lamellar structure visible. Localized reflections as a result of domain alignment are clear.

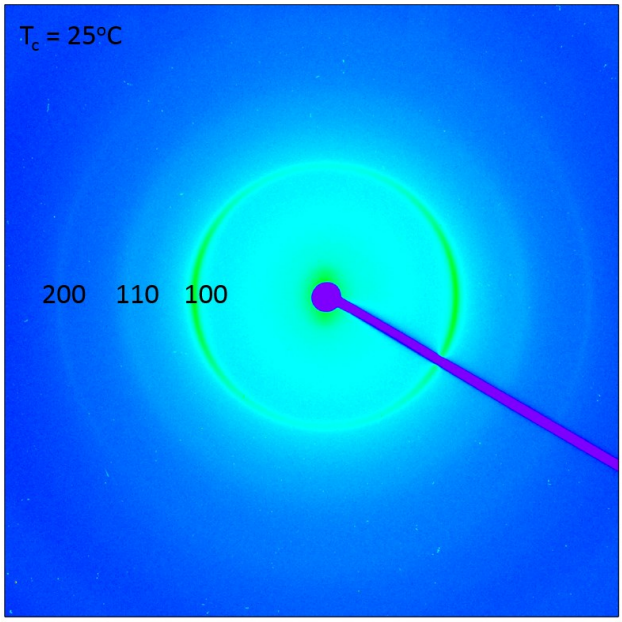

Figure 2.10 2D WAXS of aligned P3EHT-*b*-PMA 11.1k/6.0k

Crystalline P3EHT 100, 110, and 200 reflections visible. Reflections are clearly perpendicular to reflection peaks in the SAXS.

2.8.2 Orientational Order Parameter

Angular traces in Figure 2.8 (a) and (b) (T_c = 25°C) were fit to the Hermans orientation function to quantify alignment. The orientational order parameter $\langle P_2 \rangle$ is defined as:

$$\langle P_2 \rangle = \frac{3\langle \cos^2 \varphi \rangle - 1}{2}$$

where

$$\langle \cos^2 \varphi \rangle = \frac{\int_0^{2\pi} I(\varphi) \cos^2 \varphi \, |\sin \varphi| d\varphi}{\int_0^{2\pi} I(\varphi) |\sin \varphi| \, d\varphi}$$

Here, φ is the azimuthal angle of the primary SAXS peak q^* (or highest order WAXS peaks - the 100 and 010) relative to the direction of alignment. Oriented data was taken along the compression direction of oriented lamellar samples, so φ is defined as 0° where it is perpendicular to the direction of flow in the channel flow die. Thus, perfectly oriented lamellae in SAXS would yield $\langle \cos^2 \varphi \rangle$ of 1, and therefore $\langle P_2 \rangle$ of 1. Isotropically oriented lamellae yield $\langle \cos^2 \varphi \rangle$ of 1/3, and therefore $\langle P_2 \rangle$ of 0. Perfectly perpendicular lamellae, by contrast, yield $\langle \cos^2 \varphi \rangle$ of 0, and $\langle P_2 \rangle$ of -0.5. We can extend this analysis to examine the orientation of WAXS (P3EHT crystal structure) peaks relative to the SAXS via the orientational order parameter. For WAXS calculations, WAXS peak intensities were linearly interpolated across the beamstop.

Alignment via the channel flow die yielded $\langle P_2 \rangle$ of 0.68 for domain alignment. Periodicity in the crystal structure as detected by WAXS or aligned samples was clearly perpendicular to the lamellar alignment: $\langle P_2 \rangle$ for the 100 (alkyl chain stacking) reflection was -0.24, while $\langle P_2 \rangle$ for the 110 (π-π) stacking reflection was -0.14.

2.8.3 WAXS temperature evolution in confinement

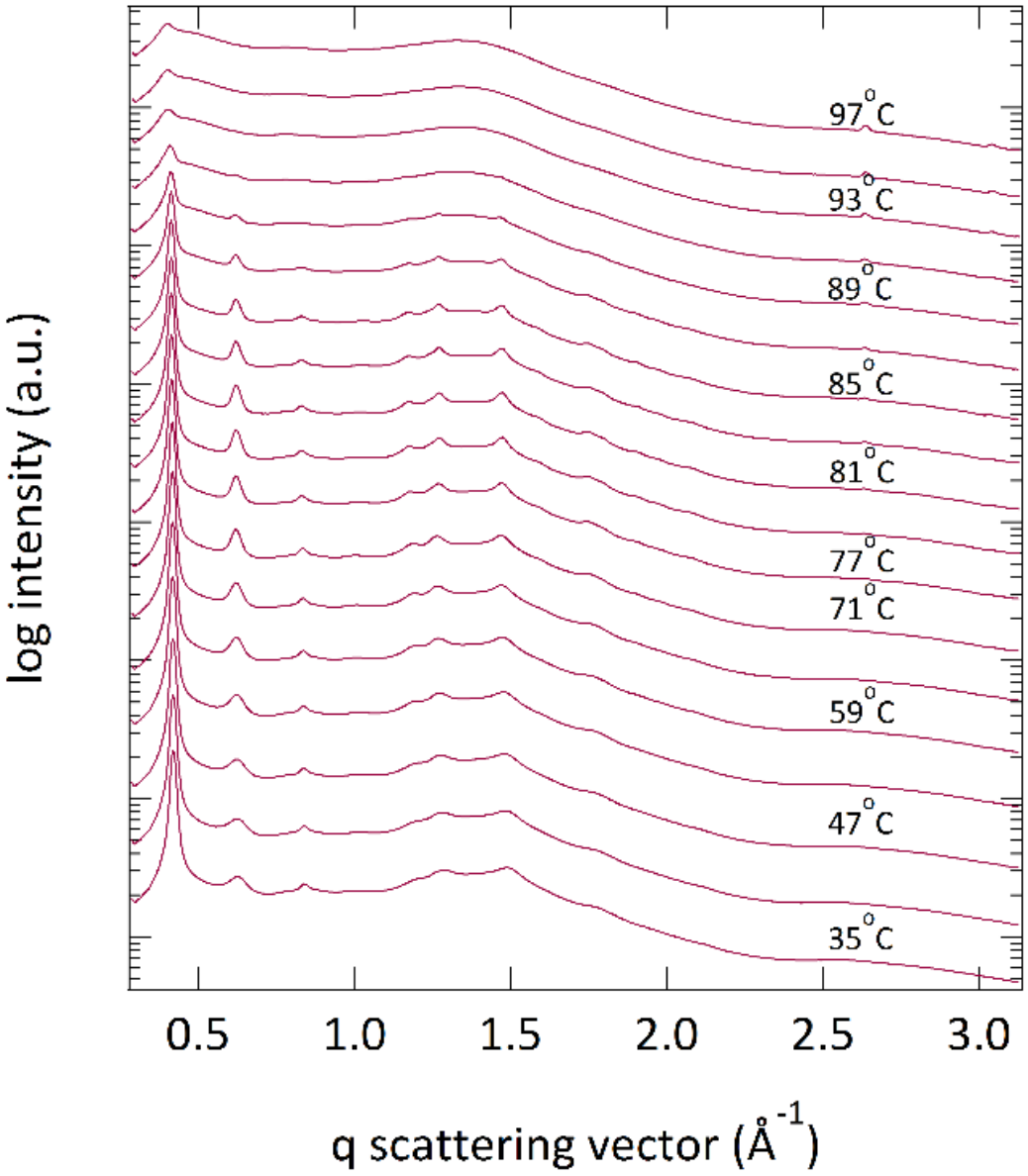

Figure 2.11 Temperature evolution of WAXS spectra of P3EHT-*b*-PMA 11.1k/6.0k crystallized at 25°C

Growth of 110 and higher order peaks with increasing temperature provides evidence that confined crystallites participate in a melt-recrystallization mechanism comparable to P3EHT homopolymer. However, higher order peaks clearly do not reach the intensity seen in Figure 2.12, indicating that isothermal crystallization at low degrees of undercooling is essential to attaining highly perfect crystallites in confinement.

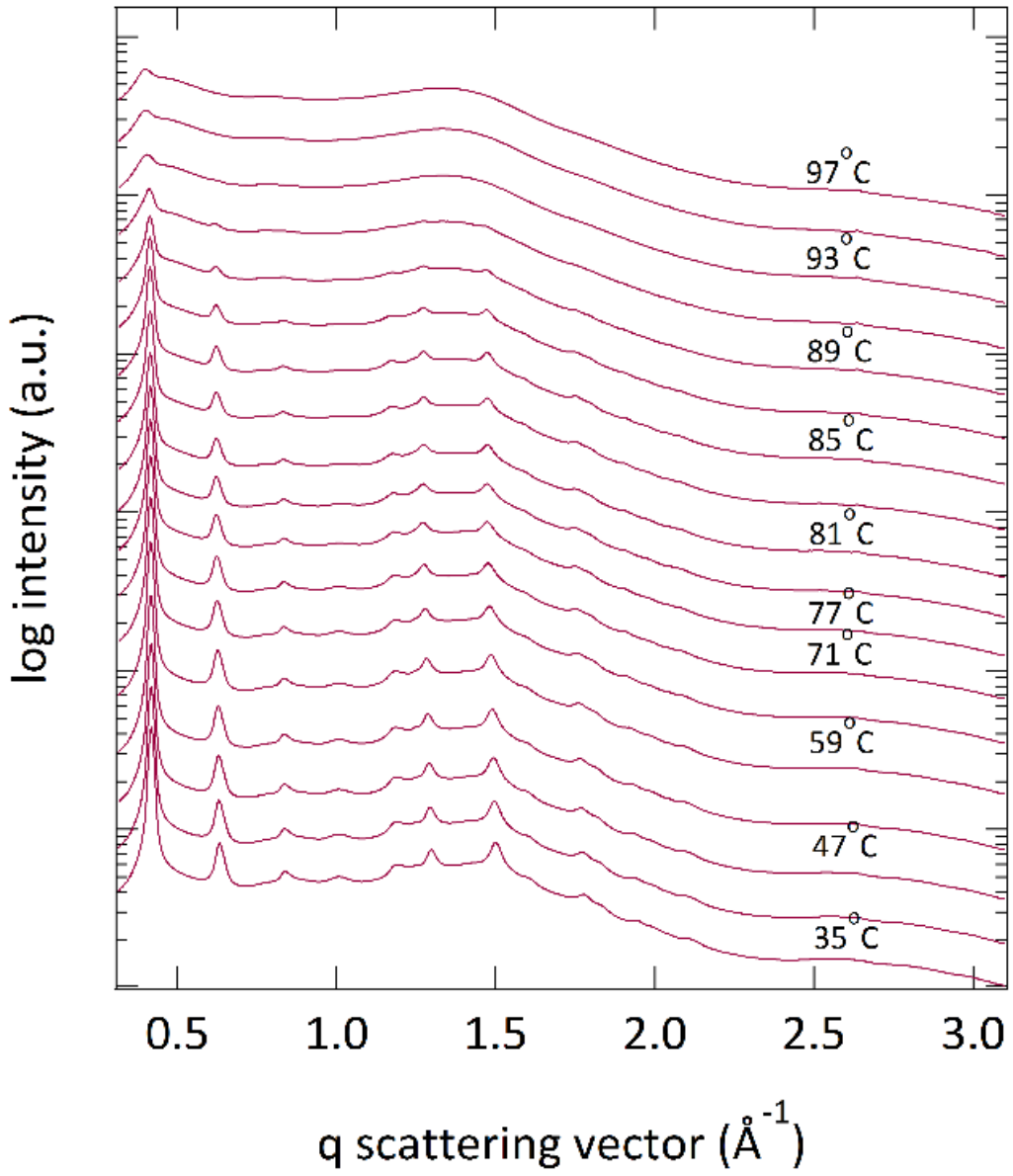

Figure 2.12 Temperature evolution of WAXS spectra of P3EHT-*b*-PMA 11.1k/6.0k crystallized at 55°C

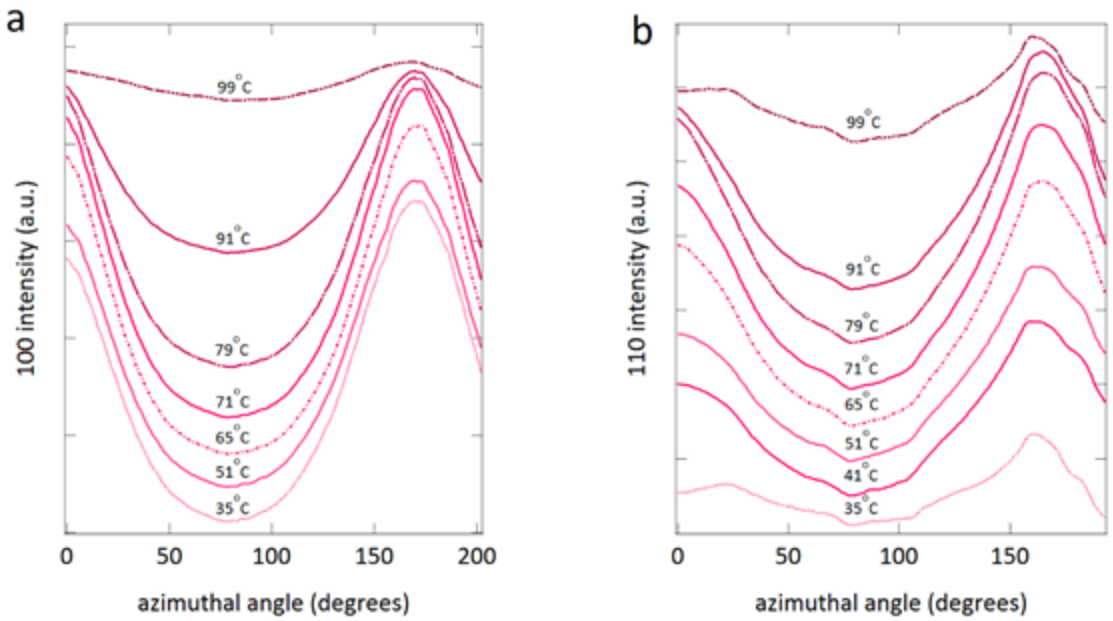

Figure 2.13 Temperature evolution of P3EHT crystal orientation with melting

Temperature evolution of orientation of (a) 100 (alkyl chain stacking peak) and (b) 110 of P3EHT-*b*-PMA 11.1/6.0k crystallized at 25°C during melting. Orientation changes negligibly until final melting, although the 110 displays a notable increase in signal to noise. Only 200 degrees of imaging on a 2D detector were available while collecting these WAXS spectra.

2.8.4 Diblock GPC profiles

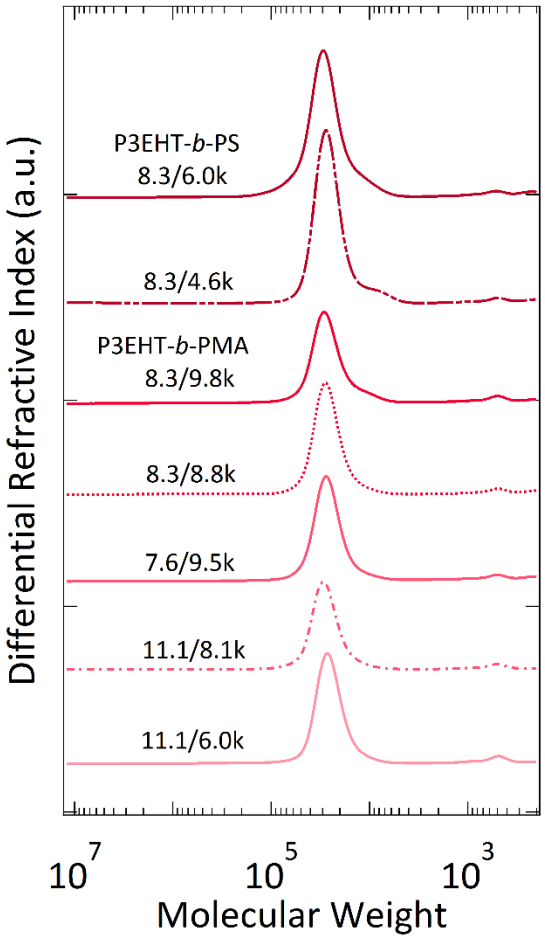

Figure 2.14 GPC profiles of diblock copolymers

GPC profiles in THF by refractive index detector of diblock copolymers used in this study. Plotted against polystyrene-equivalent molecular weight.

2.8.5 Density calculations

Temperature-dependent values for the density of PMA and PS as a function of temperature were calculated from Bunacci et al.[35] and Richardson et al.[36] respectively from fits to the form:

$$v = a + b \times 10^{-4} T + c \times 10^{-7} T^2$$

Where the specific volume v is in $cm^3\ g^{-1}$ and T is in ^oC. Polystyrene parameters were calculated as a function of PS molecular weight and for both below and above the PS glass transition; a linear interpolation was used to determine the parameters for each given molecular weight. PMA containing block copolymers were examined only above the PMA glass transition.

P3EHT densities were calculated for a 12k homopolymer both directly after quenching to room temperature (note that P3EHT has an induction time of ~40 minutes) and after 6 hours of crystallization at room temperature (after which no more crystallization is observed in dry homopolymer) via gas (helium) pycnometry. Amorphous P3EHT density was measured in a pre-analyzed, homemade aluminum pan. Measurements were made with ~0.2 mL of material and masses were measured on a high-precision balance, allowing accuracy of +/- 0.01 mg/ cm^3. The density of amorphous P3EHT was found to be 0.97 g/mL, and the density of semicrystalline P3EHT was found to be 1.10 g/ cm^3. Temperature-dependent densities were not collected, and crystalline densities within confined P3EHT domains were assumed to be identical to those of semicrystalline homopolymer. Notably, using the 1.16 g/cm^3 value for fully crystalline P3EHT,[44] a degree of crystallinity of 68% may be calculated for this material. This is in good agreement with the degree of crystallinity of 62% determined via DSC analysis by Beckingham et al. for P3EHT of a comparable molecular weight.[10]

2.8.6 P3EHT Domain Structure During Melting

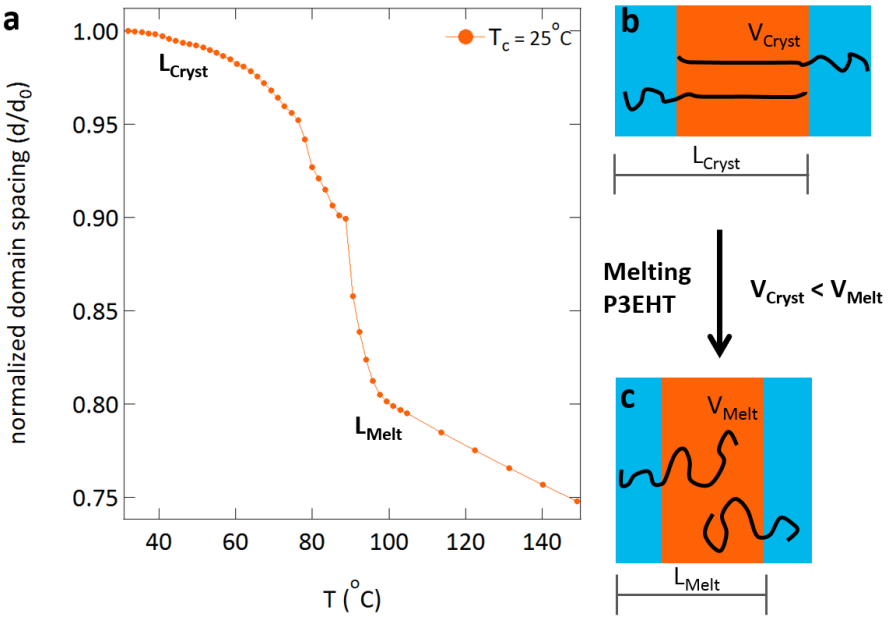

Figure 2.15 Domain spacing of P3EHT-*b*-PMA on melting

(a) Domain spacing of P3EHT-*b*-PMA 11.1/6.0k decreases sharply by ~20% at the P3EHT melting temperature even though specific P3EHT volume in the melt, v_{Melt} is greater than specific volume of crystalline P3EHT v_{Cryst}. (b) P3EHT (orange) chains are fully extended in crystallized P3EHT (c) P3EHT and PMA domains shrink due to relaxation of P3EHT chains with melting.

2.9 Acknowledgements

We gratefully acknowledge support from the NSF-DMR Polymers Program through grant no. 1206296. This work made significant use of user facilities at the Advanced Light Source and Stanford Synchrotron Radiation Light Source, supported by the Director, Office of Science, Office of Basic Energy Sciences, of the U.S. Department of Energy under Contracts No DE-AC02-05CH11231 and DE-AC02-76SF00515, respectively. We also gratefully acknowledge use of the UCSB MRL Shared Experimental Facilities supported by the MRSEC Program of the NSF under Award No. DMR 1121053; a member of the NSF-funded Materials Research Facilities Network. In addition, the authors appreciate the help of Stephan Kramer for providing support for TEM imaging

2.10 References

1. Salleo, A., Charge transport in polymeric transistors. *Materials Today* **2007,** *10* (3), 38-45.

2. Thompson, B. C.; Fréchet, J. M. J., Polymer–Fullerene Composite Solar Cells. *Angewandte Chemie International Edition* **2008,** *47* (1), 58-77.

3. Duong, D. T.; Toney, M. F.; Salleo, A., Role of confinement and aggregation in charge transport in semicrystalline polythiophene thin films. *Physical Review B* **2012,** *86* (20), 205205.

4. Jimison, L. H.; Himmelberger, S.; Duong, D. T.; Rivnay, J.; Toney, M. F.; Salleo, A., Vertical confinement and interface effects on the microstructure and charge transport of P3HT thin films. *Journal of Polymer Science Part B: Polymer Physics* **2013,** *51* (7), 611-620.

5. Sauvé, G.; McCullough, R. D., High Field-Effect Mobilities for Diblock Copolymers of Poly(3-hexylthiophene) and Poly(methyl acrylate). *Advanced Materials* **2007,** *19* (14), 1822-1825.

6. Iovu, M. C.; Jeffries-El, M.; Zhang, R.; Kowalewski, T.; McCullough, R. D., Conducting Block Copolymer Nanowires Containing Regioregular Poly(3-Hexylthiophene) and Polystyrene. *Journal of Macromolecular Science, Part A* **2006,** *43* (12), 1991-2000.

7. Iovu, M. C.; Zhang, R.; Cooper, J. R.; Smilgies, D. M.; Javier, A. E.; Sheina, E. E.; Kowalewski, T.; McCullough, R. D., Conducting Block Copolymers of Regioregular Poly(3-hexylthiophene) and Poly(methacrylates): Electronic Materials with Variable Conductivities and Degrees of Interfibrillar Order. *Macromolecular Rapid Communications* **2007,** *28* (17), 1816-1824.

8. Lim, H.; Chao, C.-Y.; Su, W.-F., Modulating Crystallinity of Poly(3-hexylthiophene) via Microphase Separation of Poly(3-hexylthiophene)–Polyisoprene Block Copolymers. *Macromolecules* **2015,** *48* (10), 3269-3281.

9. Ho, V.; Boudouris, B. W.; Segalman, R. A., Tuning Polythiophene Crystallization through Systematic Side Chain Functionalization. *Macromolecules* **2010,** *43* (19), 7895-7899.

10. Beckingham, B. S.; Ho, V.; Segalman, R. A., Melting Behavior of Poly(3-(2′-ethyl)hexylthiophene). *Macromolecules* **2014,** *47* (23), 8305-8310.

11. Beckingham, B. S.; Ho, V.; Segalman, R. A., Formation of a Rigid Amorphous Fraction in Poly(3-(2′-ethyl)hexylthiophene). *ACS Macro Letters* **2014,** *3* (7), 684-688.

12. Boudouris, B. W.; Ho, V.; Jimison, L. H.; Toney, M. F.; Salleo, A.; Segalman, R. A., Real-Time Observation of Poly(3-alkylthiophene) Crystallization and Correlation with Transient Optoelectronic Properties. *Macromolecules* **2011,** *44* (17), 6653-6658.

13. Duong, D. T.; Ho, V.; Shang, Z.; Mollinger, S.; Mannsfeld, S. C. B.; Dacuña, J.; Toney, M. F.; Segalman, R.; Salleo, A., Mechanism of Crystallization and Implications for Charge Transport in Poly(3-ethylhexylthiophene) Thin Films. *Advanced Functional Materials* **2014,** *24* (28), 4515-4521.

14. Ho, V.; Boudouris, B. W.; McCulloch, B. L.; Shuttle, C. G.; Burkhardt, M.; Chabinyc, M. L.; Segalman, R. A., Poly(3-alkylthiophene) Diblock Copolymers with Ordered Microstructures and Continuous Semiconducting Pathways. *Journal of the American Chemical Society* **2011,** *133* (24), 9270-9273.

15. Patel, S. N.; Javier, A. E.; Beers, K. M.; Pople, J. A.; Ho, V.; Segalman, R. A.; Balsara, N. P., Morphology and Thermodynamic Properties of a Copolymer with an Electronically Conducting Block: Poly(3-ethylhexylthiophene)-block-poly(ethylene oxide). *Nano Letters* **2012,** *12* (9), 4901-4906.

16. Moon, H. C.; Bae, D.; Kim, J. K., Self-Assembly of Poly(3-dodecylthiophene)-block-poly(methyl methacrylate) Copolymers Driven by Competition between Microphase Separation and Crystallization. *Macromolecules* **2012,** *45* (12), 5201-5207.

17. Zhu, L.; Cheng, S. Z. D.; Calhoun, B. H.; Ge, Q.; Quirk, R. P.; Thomas, E. L.; Hsiao, B. S.; Yeh, F.; Lotz, B., Crystallization Temperature-Dependent Crystal Orientations within Nanoscale Confined Lamellae of a Self-Assembled Crystalline−Amorphous Diblock Copolymer. *Journal of the American Chemical Society* **2000,** *122* (25), 5957-5967.

18. Quiram, D. J.; Register, R. A.; Marchand, G. R.; Adamson, D. H., Chain Orientation in Block Copolymers Exhibiting Cylindrically Confined Crystallization. *Macromolecules* **1998,** *31* (15), 4891-4898.

19. McCulloch, B.; Ho, V.; Hoarfrost, M.; Stanley, C.; Do, C.; Heller, W. T.; Segalman, R. A., Polymer Chain Shape of Poly(3-alkylthiophenes) in Solution Using Small-Angle Neutron Scattering. *Macromolecules* **2013,** *46* (5), 1899-1907.

20. Zhang, W.; Gomez, E. D.; Milner, S. T., Predicting Chain Dimensions of Semiflexible Polymers from Dihedral Potentials. *Macromolecules* **2014,** *47* (18), 6453-6461.

21. Gettinger, C. L.; Heeger, A. J.; Drake, J. M.; Pine, D. J., The Effect of Intrinsic Rigidity on the Optical Properties of PPV Derivatives. *Molecular Crystals and Liquid Crystals Science and Technology. Section A. Molecular Crystals and Liquid Crystals* **1994,** *256* (1), 507-512.

22. Loo, Y.-L.; Register, R. A.; Ryan, A. J., Modes of Crystallization in Block Copolymer Microdomains: Breakout, Templated, and Confined. *Macromolecules* **2002,** *35* (6), 2365-2374.

23. Loo, Y.-L.; Register, R. A.; Ryan, A. J.; Dee, G. T., Polymer Crystallization Confined in One, Two, or Three Dimensions. *Macromolecules* **2001,** *34* (26), 8968-8977.

24. Loo, Y.-L.; Register, R. A.; Adamson, D. H., Polyethylene Crystal Orientation Induced by Block Copolymer Cylinders. *Macromolecules* **2000,** *33* (22), 8361-8366.

25. Douzinas, K. C.; Cohen, R. E.; Halasa, A. F., Evaluation of domain spacing scaling laws for semicrystalline diblock copolymers. *Macromolecules* **1991,** *24* (15), 4457-4459.

26. Hamley, I. W.; Patrick, J.; Fairclough, A.; Ryan, A. J.; Bates, F. S.; Towns-Andrews, E., Crystallization of nanoscale-confined diblock copolymer chains. *Polymer* **1996,** *37* (19), 4425-4429.

27. Hamley, I. W.; Fairclough, J. P. A.; Terrill, N. J.; Ryan, A. J.; Lipic, P. M.; Bates, F. S.; Towns-Andrews, E., Crystallization in Oriented Semicrystalline Diblock Copolymers. *Macromolecules* **1996,** *29* (27), 8835-8843.

28. Beckingham, B. S.; Register, R. A., Architecture-Induced Microphase Separation in Nonfrustrated A–B–C Triblock Copolymers. *Macromolecules* **2013,** *46* (9), 3486-3496.

29. Lee, H. H.; Register, R. A.; Hajduk, D. A.; Gruner, S. M., Orientation of triblock copolymers in planar extension. *Polymer Engineering & Science* **1996,** *36* (10), 1414-1424.

30. Loewe, R. S.; Ewbank, P. C.; Liu, J.; Zhai, L.; McCullough, R. D., Regioregular, Head-to-Tail Coupled Poly(3-alkylthiophenes) Made Easy by the GRIM Method: Investigation of the Reaction and the Origin of Regioselectivity. *Macromolecules* **2001,** *34* (13), 4324-4333.

31. Iovu, M. C.; Sheina, E. E.; Gil, R. R.; McCullough, R. D., Experimental Evidence for the Quasi-"Living" Nature of the Grignard Metathesis Method for the Synthesis of Regioregular Poly(3-alkylthiophenes). *Macromolecules* **2005,** *38* (21), 8649-8656.

32. Jeffries-El, M.; Sauvé, G.; McCullough, R. D., Facile Synthesis of End-Functionalized Regioregular Poly(3-alkylthiophene)s via Modified Grignard Metathesis Reaction. *Macromolecules* **2005,** *38* (25), 10346-10352.

33. Matyjaszewski, K., Atom Transfer Radical Polymerization (ATRP): Current Status and Future Perspectives. *Macromolecules* **2012,** *45* (10), 4015-4039.

34. Duxbury, C. J.; Cummins, D.; Heise, A., Glaser coupling of polymers: Side-reaction in Huisgens "click" coupling reaction and opportunity for polymers with focal diacetylene units in combination with ATRP. *Journal of Polymer Science Part A: Polymer Chemistry* **2009,** *47* (15), 3795-3802.

35. Brunacci, A.; Pedemonte, E.; Turturro, A., Determination of the Equation-of-State Parameters of Poly(Methyl Acrylate). *Polymer* **1992,** *33* (20), 4428-4431.

36. Richardson, M. J.; Savill, N. G., Volumetric properties of polystyrene: influence of temperature, molecular weight and thermal treatment. *Polymer* **1977,** *18* (1), 3-9.

37. Huang, T. C.; Toraya, H.; Blanton, T. N.; Wu, Y., X-ray powder diffraction analysis of silver behenate, a possible low-angle diffraction standard. *Journal of Applied Crystallography* **1993,** *26* (2), 180-184.

38. Ilavsky, J., Nika: software for two-dimensional data reduction. *Journal of Applied Crystallography* **2012,** *45* (2), 324-328.

39. Cochran, E. W.; Garcia-Cervera, C. J.; Fredrickson, G. H., Stability of the Gyroid Phase in Diblock Copolymers at Strong Segregation. *Macromolecules* **2006,** *39* (7), 2449-2451.

40. Liu, J.; Arif, M.; Zou, J.; Khondaker, S. I.; Zhai, L., Controlling Poly(3-hexylthiophene) Crystal Dimension: Nanowhiskers and Nanoribbons. *Macromolecules* **2009,** *42* (24), 9390-9393.

41. Lee, L.-B. W.; Register, R. A., Equilibrium Control of Crystal Thickness and Melting Point through Block Copolymerization. *Macromolecules* **2004,** *37* (19), 7278-7284.

42. Whitmore, M. D.; Noolandi, J., Theory of crystallizable block copolymers. *Makromolekulare Chemie. Macromolecular Symposia* **1988,** *16* (1), 235-249.

43. Snyder, C. R.; Nieuwendaal, R. C.; DeLongchamp, D. M.; Luscombe, C. K.; Sista, P.; Boyd, S. D., Quantifying Crystallinity in High Molar Mass Poly(3-hexylthiophene). *Macromolecules* **2014,** *47* (12), 3942-3950.

44. Himmelberger, S.; Duong, D. T.; Northrup, J. E.; Rivnay, J.; Koch, F. P. V.; Beckingham, B. S.; Stingelin, N.; Segalman, R. A.; Mannsfeld, S.; Salleo, A., Role of Side-chain Branching on Thin-film Structure and Electronic Properties of Polythiophenes. *Advanced Functional Materials* **2015**.

Chapter 3. Confined Crystallization within Cylindrical P3EHT Block Copolymer Microdomains

Confinement of crystallites within block copolymer microdomains is a promising approach to study conjugated polymer crystallization due to interfacial chain tethering and defined geometries. The nanoscale organization of crystallites is often critical to determining the charge transport properties of conjugated polymers. Here, a poly(3-(2′-ethyl)hexylthiophene)-*block*-poly(methyl acrylate) (P3EHT-*b*-PMA) system is leveraged to study the impact of confinement within cylindrical microdomains. The crystalline P3EHT permits accessible melting temperatures and robust formation of traditional microphase separated morphologies, while the rubbery PMA allows the local deformations required to permit P3EHT crystallization. Crystallites form with chains perpendicular to the diblock interface, causing domain expansion; TEM reveals that this is accommodated in the cylindrical geometry via local anisotropic deformation. Surprisingly, complementary SAXS/WAXS of aligned diblocks shows preferential orientation of the alkyl chain stacks down domains. Furthermore, cylindrically confined P3EHT demonstrates a smaller window of thermal control over crystalline perfection via isothermal crystallization conditions than homopolymer P3EHT or block copolymer P3EHT in lamellar confinement. This work demonstrates that post-crystallization annealing is an alternative route to generating uniformly high quality crystallites in cylindrically confined P3EHT. These results are important for considering routes to optimizing and controlling crystallinity in nanoscale confined geometries.

3.1 Introduction

Conjugated polymers have been applied to light emitting diodes, solar cells, and transistors which rely crucially on charge mobility.[1-3] In these materials, charge mobility is highly influenced by structural details of the resulting crystallinity – particularly crystalline orientation – as influenced by factors including confinement,[4, 5] processing conditions,[6-10] mechanism of crystallization,[11-15] and details of molecular design and architecture.[12, 16, 17] The study of confinement within controlled geometries and tethering of chain ends presents a unique opportunity to template and control conjugated polymer crystallization. In particular, microphase separated diblock copolymers present a model system in which confinement geometry and curvature may be controlled to understand their impacts upon the resulting polymer crystallization. Ultimately, this allows us to understand more deeply the mechanism of crystallite growth in conjugated polymers, the forces impacting preferred crystallite growth directions, and the limits of how curved geometries may accommodate extended-chain crystallites. These details have important implications for how conjugated polymer crystallinity can be controlled, as well as the ability of these confined crystallites to transport charge.

Conjugated diblock copolymer systems tend to have high melting points, causing crystallization to dominate self-assembly.[18-24] Poly(3-(2′-ethyl)hexylthiophene) features accessible melting temperatures, while maintaining key features of the many more extensively studied conjugated polymers.[25-28] In particular, P3EHT in block copolymers leads to robust formation of microphase separated morphologies, and maintains them following crystallization.[29] In lamellar diblock copolymer confinement, the P3EHT crystallite orientation is templated

relative to the diblock interface. Furthermore, conjugated polymer chains demonstrate a driving force to extend upon crystallization and drive domain expansion during crystallization.[30] Surprisingly in these lamellar systems, confinement does not appear to significantly impact the stability of the resulting crystallite populations; P3EHT melting points remain comparable to the constitutive homopolymers. Furthermore, charge mobilities of P3EHT in diblocks measured via time of flight remain comparable to those of the constitutive homopolymers.[29]

Cylindrical geometries are of interest as a template for organic photovoltaics, or as a model system for controlled charge transport in one dimension. However, these geometries present new challenges to the confined crystallization of conjugated polymers. While the lamellar system adopts uniaxial symmetry in-plane (π- π and alkyl chain stacking are both in-plane),[30] the question remains of what crystallite growth direction is preferred along the long axis of the cylinders. Notably, in the homopolymer, long crystalline 'fibrils' form with the π - π stack along the long-axis. Interestingly, crystallization-driven self-assembly of P3HT diblocks, while lacking the long-range order of diblocks microphase separated in the melt, features locally fibrillar morphologies similar to the homopolymer.[15, 18] By contrast, model studies of P3HT crystallized within anodized alumina nanopores displayed diameter-dependent orientation: at large diameters (above 120 nm), the π - π stacking was found to run parallel to the cylinder long axis, while at small diameters (50 nm-15 nm) the orientation with π - π direction perpendicular to the cylinder long axis began to predominate; the authors hypothesize that at small diameters, local nucleation from the edge of the pore walls dominates the crystallization mechanism and results in the change in orientation.[31] However in this case, nucleation from the diblock interface is unexpected; since conjugated polymers are typically characterized by strong π - π stacking interactions that drive crystallization, it was expected that the π - π interactions would dominate along the length of the cylinder. Essentially, this orientation would result in a 'fibril' within a microphase templated cylinder (Figure 3.2). Importantly, the resulting orientation is critical for determining the potential material applications given that charge transport with crystallites is fastest along the chain backbone, and slowest in the π - π stacking direction. Furthermore, while the impact of confined crystallization within cylindrical geometries on templated crystallite orientation and crystallization kinetics have been studied in traditional flexible polymers,[32-35] new competing preferences arise in conjugated systems. In the cylindrical microdomains it is clearly impossible for all conjugated chains to both participate in extended-chain crystallites and to orient perpendicular to domains, raising the question of how crystallization within the microdomains will attempt to satisfy these conflicting demands (Figure 3.1).

The mode of crystallization and the stability of the resulting crystallites may also be impacted by confinement.[35-37] Previous works studying the nucleation mechanism of flexible polymers in confinement have noted either a shift from a heterogenous to a homogenous nucleation mechanism or reduced degrees of crystallinity attributed to glassy walls arresting the mobility of tethered crystalline chains.[37-41] Such shifts in nucleation mechanism could require critical changes in material processing conditions to achieve high quality crystallites within these nanostructured conjugated polymers. Importantly, this dramatic shift in mechanism is not necessarily expected within conjugated polymers. Standard crystalline homopolymers are composed of micron-scale spherulites; these are known to follow a heterogenous nucleation mechanism characterized by one nucleation site (typically attributed to dust or other defects) per

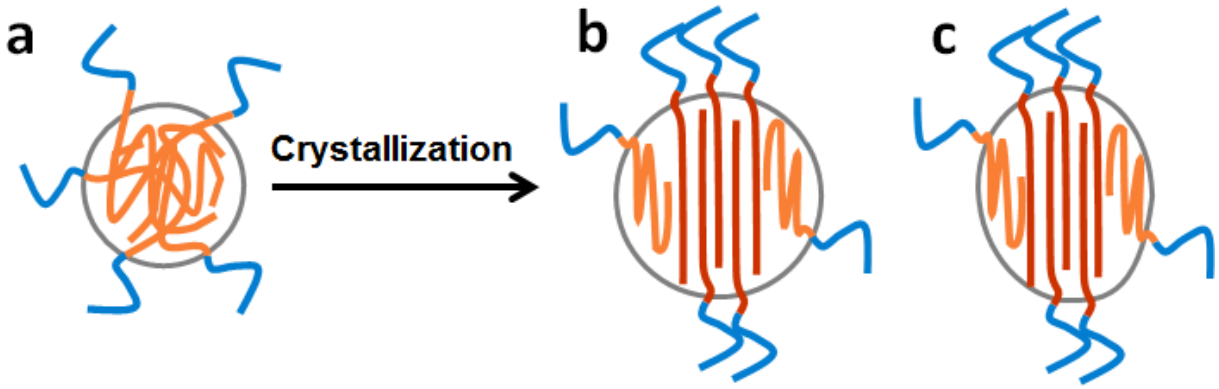

Figure 3.1 Potential impact of extended-chain crystallization in a cylindrical domain
(a) P3EHT-*b*-PMA cylinders in the melt undergo crystallization with concurrent increase in the apparent size of cylinders. Extended-chain P3EHT crystallites may be accommodated by (b) the entire domain expanding, with some amorphous material excluded at the edges, or (c) by resulting anisotropic deformation of domains

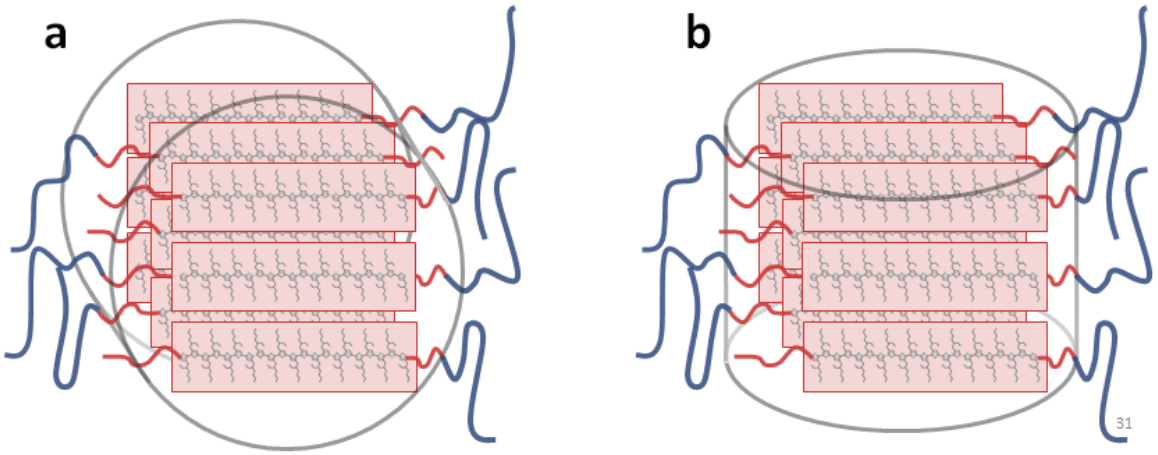

Figure 3.2 Possible P3EHT orientations within cylindrical microdomains

P3EHT is known to form fibrils with P3EHT π-stacking down the long axis; the orientation of crystals in (a) would allow P3EHT to crystallize with long-range π-stacking similar to a fibril down the center of the cylinder. The orientation in (b) is also possible, with alkyl chain stacking down the long-axis of the cylinder.

spherulite.[42] Thus, a decrease in cylinder volume below the length scales of the typical nucleation site distribution induces a fundamental change in nucleation mechanism.[36] By contrast, conjugated polymers readily aggregate driven by π-π interactions. When these aggregates are sufficiently well-ordered and large in size they are considered crystalline, and form fibrillar crystals with dimensions of approximately 15 nm in diameter and order of 200 nm in length; assuming a single nuclei per fibril, this result implies a typical nucleation density on the order of the volume of a cylindrical microdomain.[10, 43] Thus, it is expected that the cylindrical microdomains will have a comparable nucleation density to P3EHT homopolymer; a change in nucleation mechanism is not necessarily anticipated. However, the tethering of P3EHT chains to the edges of crystallites is expected to, similar to in the lamellar system, dramatically slow the crystallization dynamics.

This work examines P3EHT crystallization confined within cylindrical microdomains, and seeks to understand how the shift from lamellar to cylindrical confinement impacts the resulting crystallinity. In particular, the impact of cylindrical geometry on crystallite orientation is investigated, revealing that – surprisingly – crystallites orient with the alkyl chains stacking direction along the long axis and π-stacking across the short axis. Further, lateral expansion of domains upon crystallization (despite densification of the P3EHT) emphasizes that conjugated chains preferentially extend upon crystallization; imaging studies via TEM find that curved domains accommodate crystallites composed of extended chains via local anisotropic deformation. Finally, since the impact of confinement on the crystallization dynamics and stability are critically important for developing processing methods leading to property optimization, the melting behavior is investigated as a function of time, temperature, and degree of confinement. Crystallization kinetics are limited – in particular at high temperature – at small volume fractions relative to in lamellar confinement, implying a potential change of nucleation mechanism. Importantly, while in lamellar confinement the manipulation of crystallization temperature permits manipulation of the degree of crystalline perfection, the range of accessible crystallization temperatures is smaller in cylindrical confinement. This work shows that despite this limited range, the P3EHT melt-recrystallization mechanism can be manipulated to produce crystallites with high and uniform melting points via annealing.

3.2 Experimental

3.2.1 Synthesis

Reagents and solvents used as received from Sigma Aldrich unless otherwise noted. P3EHT monomer, end-functionalized polymer, and diblocks were synthesized as previously described.[28, 30]

3.2.2 Molecular Characterization

Molecular weights and dispersity according to PS standards were determined via gel permeation chromatography (GPC) on a Waters instruments using a refractive index detector and Agilent PLgel 5μm MiniMIX-D columns (GPC traces in Figure 3.8). THF at 35°C was used as the mobile phase with a flow rate of 0.3 mL/min. ^{1}H NMR spectra were collected on a Bruker

Table 3.1 Molecular and morphological characteristics of P3EHT-*b*-PMA cylinder forming diblocks

P3EHT-*b*-PMA composition	*Đ*	$\varphi_{melt,\ P3EHT}$	Contour length, P3EHT (nm)	Cylinder diameter, melt[a]	Cylinder diameter, crystalline[a]
8.3k/14.9k	1.23	0.38	16.6	12.8	14.9
8.3k/24.6k	1.24	0.21	16.6	11.3	11.8
11.1k/20.6k	1.19	0.33	22.3	14.6	19.8

[a]Cylinder diameters calculated from hexagonally packed cylinder geometry and melt and crystalline volume fractions. Crystalline diameter assumes a crystalline P3EHT density of 1.10 g/cm^3.

AV-500 MHz spectrometer and on a Varian VNMRS 600 MHz spectrometer using deuterated chloroform (Cambridge) as the solvent with ~1 weight % polymer. Reported molecular weights are by end group analysis. Densities were collected via gas pycnometry (P3EHT)[30] or are calculated from literature (PMA[44] and PS[45]).

3.2.3 SAXS/WAXS

Both aligned and isotropic samples for X-ray scattering were prepared. Isotropic samples were melt-pressed into 1 mm thick aluminum washers at 150°C while aligned strips were created with a channel flow die.[46] Material is initially loaded into the center of the die (and long, flat channel with walls on either side). Upon compressing a top part onto the channel, the sample flows out away from the load position (in the 'load direction') but is constrained by the walls ('constraint direction') in addition to the top/bottom of the channel ('load direction').[46] Samples were isothermally crystallized for one week within temperature-controlled ovens prior to data collection. For annealing studies, samples were annealed overnight following crystallization. SAXS and WAXS patterns were collected at beamline 7.3.3. of LBNL's Advanced Light Source (ALS) and beamlines 1-5 and 11-3 of the Stanford Synchrotron Radiation Laboratory (SSRL). Scattering patterns were calibrated against silver behenate (AgBe).[47] Scattering intensity is plotted versus the momentum transfer vector $q = (4\pi/\lambda) \sin \theta$. Scattering data was reduced using the Nika package for Igor.[48]

3.2.4 TEM

Samples for TEM were prepared by melt pressing polymer at 150°C between two sheets of Kapton or Teflon followed by isothermal crystallization in temperature controlled ovens for one week. 100 nm thick thin sections for TEM were sliced from these samples using a Leica UC7 Ultramicrotome with FC7 cryo attachment. P3EHT-*b*-PMA samples were cryomicrotomed at -25°C and collected directly from the dry diamond knife. Thin sections were placed on CF300 amorphous carbon coated Cu grids from Electron Microscopy Sciences. Sections were stained by 20 minute exposure to RuO_4 (2% aqueous RuO_4 solution, Electron Microscopy Sciences) vapor. Imaging was performed on an FEI Tecnai G2 Sphera microscope operating at 200 kV.

3.2.5 DSC

Differential scanning calorimetry (DSC) measurements were performed using a TA Q2000 calorimeter. Samples (2-10 mg each) were hermetically sealed inside TZero aluminum pans. Samples in pans were heated to 150°C offline and held for ten minutes to clear thermal history, then isothermally crystallized for one week in temperature controlled ovens. For annealing studies, samples were first crystallized for one week at room temperature, and then annealed overnight at the desired temperature in temperature controlled ovens. Samples were heated from -20°C to 150°C at 10°C/min to observe both the PMA glass transition at ~10°C and P3EHT melting transitions ~60-90°C.

3.3 Results and Discussion

Three cylinder-forming diblock copolymers containing a semiflexible P3EHT conjugated block and flexible PMA rubbery block were utilized to study conjugated polymer crystallization within curved geometries (Figure 3.3). Notably, PMA is highly distinct from PMMA; removing the backbone methyl group to form PMA decreases the glass transition from ~120°C to ~10°C. Here, the rubbery PMA block was chosen because prior studies in lamellar-forming diblocks demonstrated that a rubbery second block is critical for permitting the chain reorganization necessary for crystallization (namely, local chain extension in addition to P3EHT densification upon crystallization).[30] Interestingly, the cylinder-forming composition window studied here (minority semiflexible P3EHT; P3EHT confined within cylinders) appears to be favored over the opposite composition window (majority semiflexible P3EHT). Importantly, all cylinder-forming diblocks demonstrated crystallization with the same unit cell as homopolymer and lamellar-confined P3EHT. Here, the cylindrical geometry imposes unique constraints upon the crystallization. In particular, the volume of each continuously-connected region in cylindrical geometries is clearly smaller than in lamellar confinement, and is expected to result in less stable (lower-melting) crystallites and slower nucleation processes. Additional constraints appear initially contradictory; from simple packing considerations, the polymer clearly cannot both allow all chains to extend upon crystallization and maintain a circular geometry.

3.3.1 P3EHT-*b*-PMA Forms Cylindrical Morphologies Confining P3EHT

In designing block copolymers containing functional materials for targeted morphology-dependent applications, it is critical to consider how the relative chain shape and stiffness of the blocks impact the resulting phase behavior. Here, the P3EHT-*b*-PMA system displays asymmetric phase behavior, strongly favoring lamellar morphologies at high volume fractions of P3EHT (φ_{P3EHT}=0.46 to φ_{P3EHT} = 0.67).[30] Meanwhile, over a composition window from φ_{P3EHT}=0.12 to φ_{P3EHT} = 0.39, the system confines P3EHT within cylindrical morphologies. P3EHT and other poly(3-alkylthiophenes) are considerably stiffer than traditional flexible polymers with persistence lengths on the order of 3 nanometers.[49, 50] By contrast, poly(methyl acrylate), used here, has a persistence length of only 0.74 nm.[51] At moderate molecular weights of ~10k P3ATs display contour lengths on the order of 20 nm, emphasizing that the chain conformation in the melt is still well-described by a random walk. These differences in chain stiffness can be parameterized in terms of a conformational asymmetry parameter, ε,

$$\varepsilon = (\beta_A/\beta_B)^2$$

that describes the differences in both conformational and volume-filling characteristics.[52, 53] Here, $\beta^2 = R_g^2/V$, where R_g is the radius of gyration, and V is the volume of the block. Importantly, even two polymers with chain conformations well-described by random walk statistics but with different persistence lengths will have considerably different volume-filling characteristics. Thus, significant degrees of conformational asymmetry can arise purely from a difference in local chain stiffness. Seen here, the difference in persistence length leads to conformational asymmetry that induces the observed composition window where curved interfaces are favored at high fractions of the more flexible block.[54-56] Importantly, the impacts of conformational asymmetry on self-assembly should not be confused with the impacts of liquid

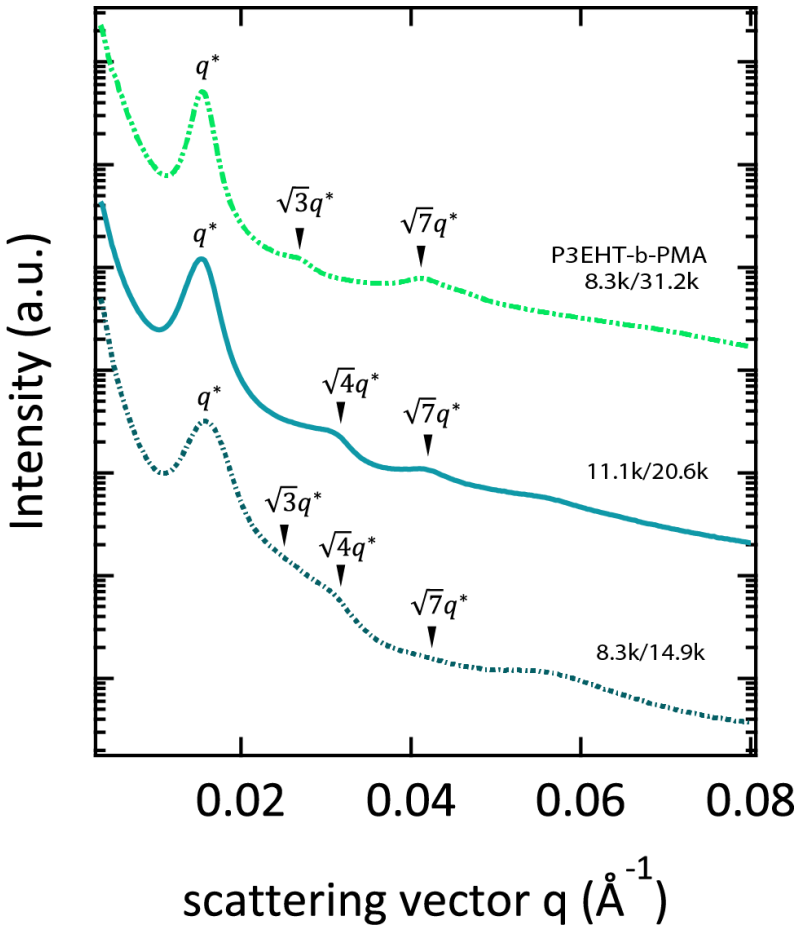

Figure 3.3 SAXS of cylinder forming P3EHT-*b*-PMA diblocks
Small angle X-ray scattering of cylinder-forming P3EHT-*b*-PMA diblocks

crystalline and crystalline interactions. While liquid crystalline interactions can induce smectic and nematic block copolymer phases in some systems,[57, 58] and the competition between enthalpy-driven microphase separation and crystallization can lead to crystallization-dominated morphologies,[59] the simple difference in stiffness between chains in a molten diblock – described via conformational asymmetry – can lead to significant shifts in the composition window over which each morphology is favored.

Importantly, this behavior highlights key design rules for the self-assembly of conjugated-amorphous block copolymers. In particular, it highlights that chain stiffness does not merely impact liquid crystalline and crystalline behavior. For targeting specific morphologies in the melt it is also critical to consider the impact of local chain conformation on the block copolymer phase diagram. Here, we specifically examine three cylinder-forming compositions within this window to understand the impact of P3EHT volume fraction and crystallization conditions on the resulting P3EHT crystallinity, finding that cylinders promote a crystallite orientation with alkyl chain stacking along the long axis and, and at small volume fractions results in inaccessibly slow kinetics at temperatures previously used to manipulate the degree of crystalline perfection. Characteristic SAXS patterns (Figure 3.3) identify the diblocks which form curved interfaces; cylindrical morphologies are further confirmed via transmission electron microscopy (Figure 3.4).

3.3.2 P3EHT Crystallization Induces Local Domain Deformation

The cylindrical microdomains and initial morphology are formed here in the melt, but ultimately the rubbery matrix permits deformation during the course of crystallization. Similar to lamellar morphologies, the diameter of P3EHT cylinders clearly increases upon crystallization despite densification of P3EHT (Table 3.1), emphasizing that the drive for chain extension is a key driving force during cylindrically confined crystallization. However, the average diameter of each cylinder does not approach the full contour length of the component P3EHT, emphasizing that either chains are not fully extended, or domains do not experience uniform deformation due to local frustrations. Clearly, to accommodate extended conformations, the fraction of polymer chains capable of participating in the crystallite without completely disrupting the microdomain morphology is limited relative to the lamellar case. In order to directly probe the degree of anisotropic deformation and understand how domains accommodate the chain extension, crystallites and microdomains were visualized via TEM. By selectively staining thin sections of crystallized cylinder-forming diblocks with RuO_4, TEM imaging clearly defines the difference between non-crystalline regions (where staining agent diffuses quickly) and crystalline regions (where staining agent diffuses more slowly).[60] The contrast between unstained and selectively stained P3EHT-*b*-PMA is clear in Figure 3.9. Distinguishing the actual shape of the interior crystallites is challenging, but upon crystallization the resulting crystallites and microdomains are clearly not perfectly round, especially in the case (Figure 3.9b) of relatively high volume fractions of P3EHT. P3EHT-*b*-PS cylinders, by contrast, display no such deformation; staining and direct imaging yields no imagine of crystallites and emphasizes DSC and WAXS results which emphasize the lack of crystallinity in these systems (Figure 3.11). These deformed microdomain shapes in P3EHT-*b*-PMA crystallized cylinder-formers imply that these extended-

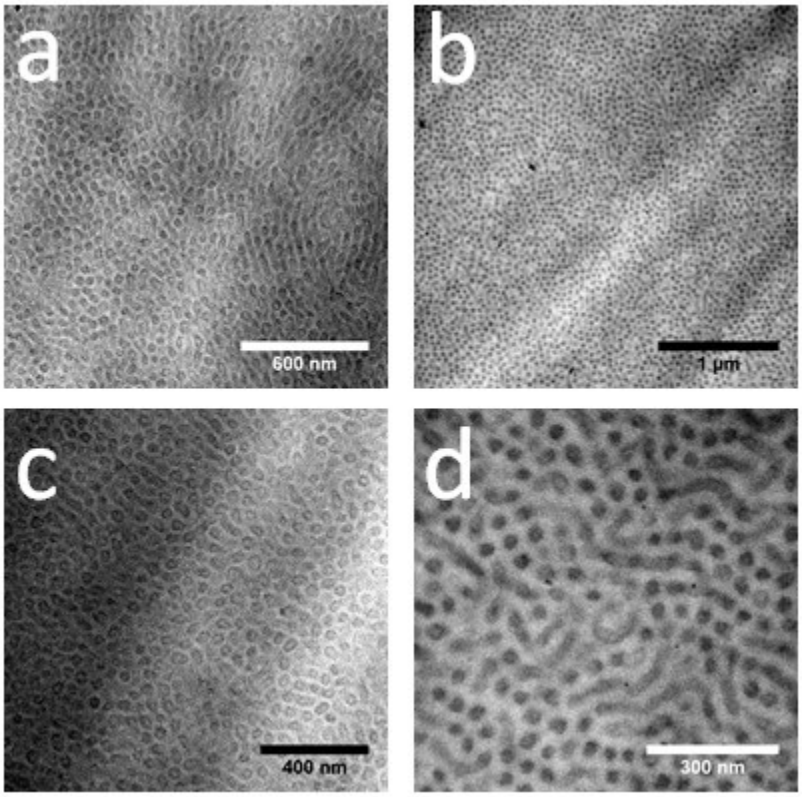

Figure 3.4 Bright field TEM of cylinder forming P3EHT-*b*-PMA

Bright field TEM of cylindrical P3EHT domains at $\varphi_{P3EHT} = 0.4$ (a, c) and $\varphi_{P3EHT} = 0.2$ (b, d). Crystallites are visualized via selective RuO_4 staining; crystallization clearly induces local deformation of the P3EHT and surrounding domains.

chain crystallites are achieved through limited local deformation of the microdomains. Interestingly, while some chains can easily participate in these crystallites while maintaining a perpendicular orientation relative to the microdomain interface, other chains must either remain excluded or accommodate a significant conformational bend near the microdomain interface in order to participate in the crystallite.

3.3.3 Preferential Orientation of P3EHT within Cylindrical Microdomains

The preferred orientation of the resulting crystallites within microdomains is expected to have significant implications for potential applications. The incorporation of alkyl side chains in P3ATs is typically considered a necessary tradeoff between performance and processability; while alkyl side chains permit solvent and thermal processing of the intractable polythiophene backbone, they are known to cause P3AT crystallites to be more resistive along the alkyl chain stacking direction.[61] While SAXS studies establish that cylinders expand upon crystallization, and TEM shows that this expansion is anisotropic, these studies do not uniquely identify the preferred crystallite orientation within the microdomains. To identify this orientation, complementary SAXS/WAXS of shear-aligned materials is leveraged. The polymer is first shear-aligned via a channel flow die.[46] Shear-aligned cylinders adopt a uniaxial symmetry as confirmed by SAXS both perpendicular to (Figure 3.5a) and along (Figure 3.5b) the flow direction. Complementary WAXS in these geometries emphasizes the preferential orientation of the 100 (alkyl chain stacking) crystal stacking direction along the long axis of the confined cylinders, and the lack of preferred orientation within the face of the cylinder itself. This preferred orientation is initially surprising given that the π-stacking crystal growth is commonly considered to be the strongest direction of crystallite growth in poly(3-alkylthiophenes) and the driving force for fibril formation. Furthermore, this implies that π-stacking occurs primarily across the short-axis of the cylindrical morphologies. Notably for all diblock morphologies, the area per chain at the interfaces significantly decreases upon crystallization due to both (1) the preference for individual chains to extend upon crystallization, and (2) the densification of P3EHT upon crystallization. Both the π-stacking and the alkyl chain stacking directions of the crystallite extend perpendicular to the intersection of the P3EHT chain with the microdomain interface. The P3EHT crystal structure contains a fundamental asymmetry in chain-chain distance in the two different packing directions. Assuming chains extend across the entire domain, the average interfacial chain-chain distance around the circumference of the cylinders is merely 0.97 nm (corresponding to roughly twice the π-stacking distance), while the average interfacial chain-chain distance along the long axis of the cylinders is 2.96 nm (corresponding to approximately double the alkyl chain stacking direction). Given the chain extension and expansion in the plane of the cylinder, the system may minimize further expansion in this dimension by localizing π-stacking along this dimension. By contrast, symmetry prevents crystallites confined within lamellae from having such preferences.

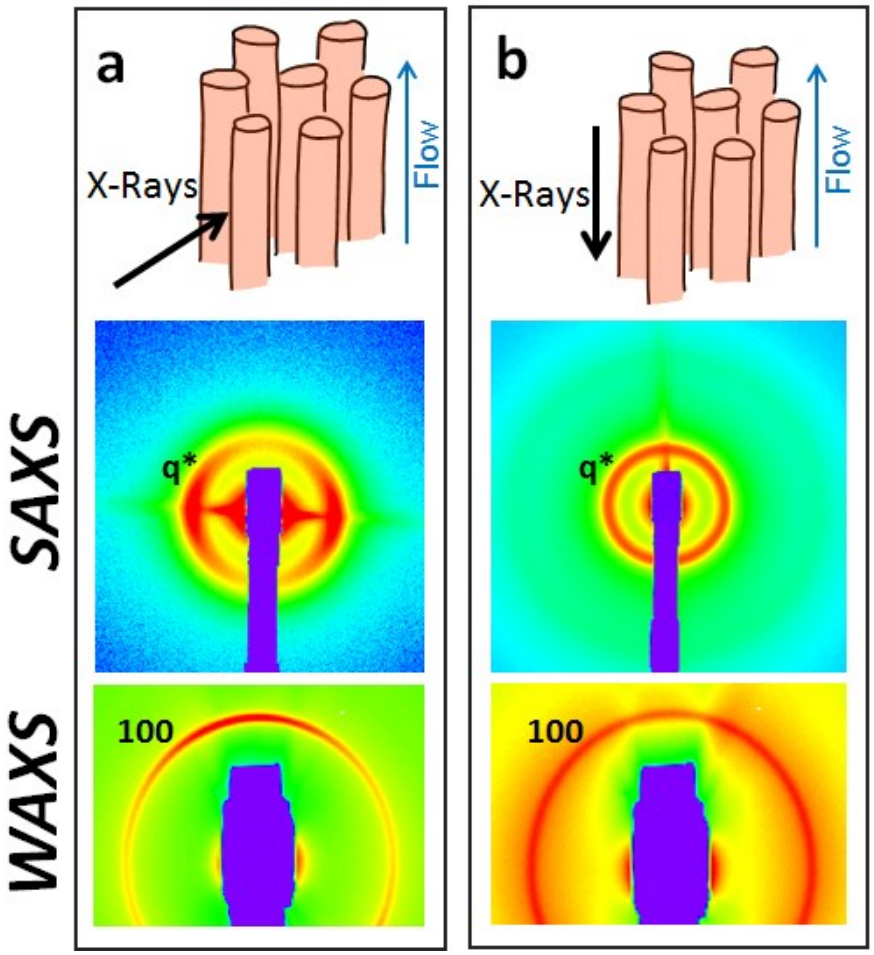

Figure 3.5 2-D SAXS/WAXS of aligned cylinders

2-D SAXS/WAXS of aligned cylinder-forming P3EHT-*b*-PMA 8.3/31.2k. Only 200 degrees of WAXS were available. Cylinders align along the flow direction of the channel flow die.[46] Note the apparent loss of intensity in WAXS (b) is due to the shadow above the beamstop.

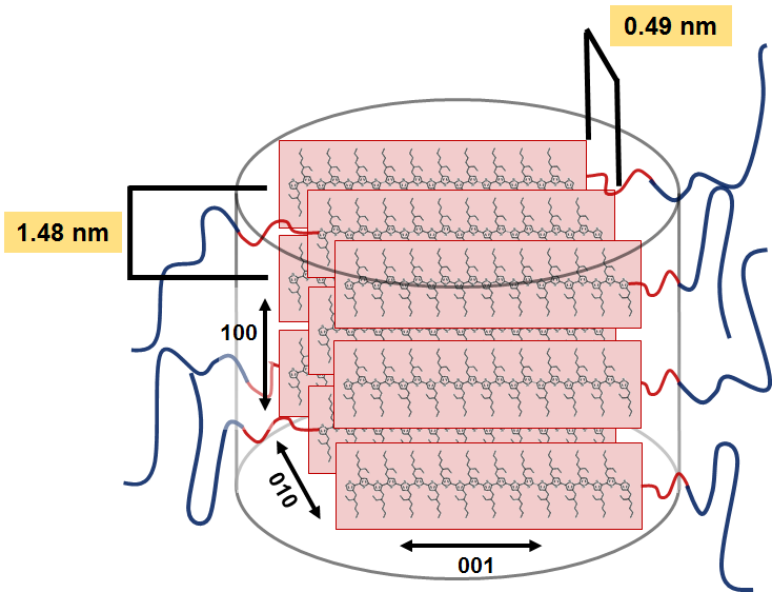

Figure 3.6 Dimensions and preferred orientation of P3EHT chains within confined cylinders.

Preferred orientation of P3EHT chains within confined cylinders. Chains are perpendicular to the diblock interface. Given fully extended chains, the system contracts to an area of 1.43 nm^2 per chain spanning the interface. Within crystals, chains are 1.48 nm apart vertically, and 0.48 nm apart horizontally. Note that the crystal structure has been is drawn for simplicity; P3EHT adopts a triclinic unit cell with a true alkyl-stacking distance of 1.41 nm and π-stacking distance of 0.51 nm.[12]

3.3.4 Impact of Cylindrical Confinement on Crystallization dynamics and Crystallite Population

While crystallite orientation and how crystallites are accommodated are critical to the resulting material properties, confinement within microdomains also has the possibility of impacting the resulting crystallization dynamics and stability. By leveraging controlled crystallization conditions and analyzing the resultant crystallite populations by differential scanning calorimetry, we find that confinement controls the resulting crystallite population and nucleation processes. Under standard conditions – crystallization at 25°C – the crystallite populations observed in cylindrically-confined P3EHT are immediately distinct from those observed in either lamellar-confined or homopolymer P3EHT. In particular, cylindrically-confined P3EHT displays a distinct 'two-peak' melting behavior (Figure 3.7a,b) in contrast to lamellar-confined (Figure 3.7c) and homopolymer P3EHT which consistently displays 'three-peak' melting.[25, 26, 30] In lamellar-confined and homopolymer P3EHT, these three peaks have been assigned to a combination of (low-melting) either a rigid amorphous fraction or secondary crystallization and (high-melting) a melt-recrystallization process. In cylindrically-confined P3EHT, the lower-melting of these peaks appears to vanish with increasing isothermal crystallization temperature (Figure 3.11), or with controlled annealing conditions (Figure 3.7d) implying that it corresponds to a less-perfect population of crystallites.

For processing considerations it is important to consider the impact of confinement on the time scales of crystallization. Notably, all P3EHT-*b*-PMA diblocks require on the order of a week to fully crystallize – considerably longer than the constituent homopolymer P3EHT, which only requires ~six hours for reaching a maximum degree of crystallinity of the bulk material.[26, 30] Directly probing the crystallization kinetics in confinement is challenging due to the long time scales involved; however significant insight can be gleaned by examining several basic comparisons. In particular, P3EHT-*b*-PMA cylindrically confined diblocks require considerably more time to crystallize than the corresponding lamellar diblock with identical P3EHT block. Furthermore, even for confined cylinders with identical P3EHT blocks, increasing the relative PMA volume fraction appears to further decrease the crystallization kinetics. The question is whether this is merely a function of slowed dynamics with increasing molecular weight, or is truly attributable to shifts in the morphology of confinement. Interestingly, the crystallization dynamics in cylindrical confinement at small P3EHT volume fractions become inaccessibly slow with increasing isothermal crystallization temperature above 35°C (Figure 3.11). By contrast, P3EHT homopolymer and P3EHT in lamellar confinement both crystallize with accessible kinetics across a range of temperatures from 15°C to 55°C.[26, 30] If the decreased kinetics were due to slowed dynamics alone, the higher crystallization temperatures would be expected to promote, not suppress, crystallization in all cases. Therefore, while we expect the crystallization kinetics can be partially attributed to slowed dynamics, we also attribute it to a decrease in the stability of the crystallite nuclei which grow into the resulting crystallites. While individual chain diffusion dynamics may play a role in the slowed kinetics in cylindrical confinement, a significant effects also seems to be the shift in nucleation mechanism.

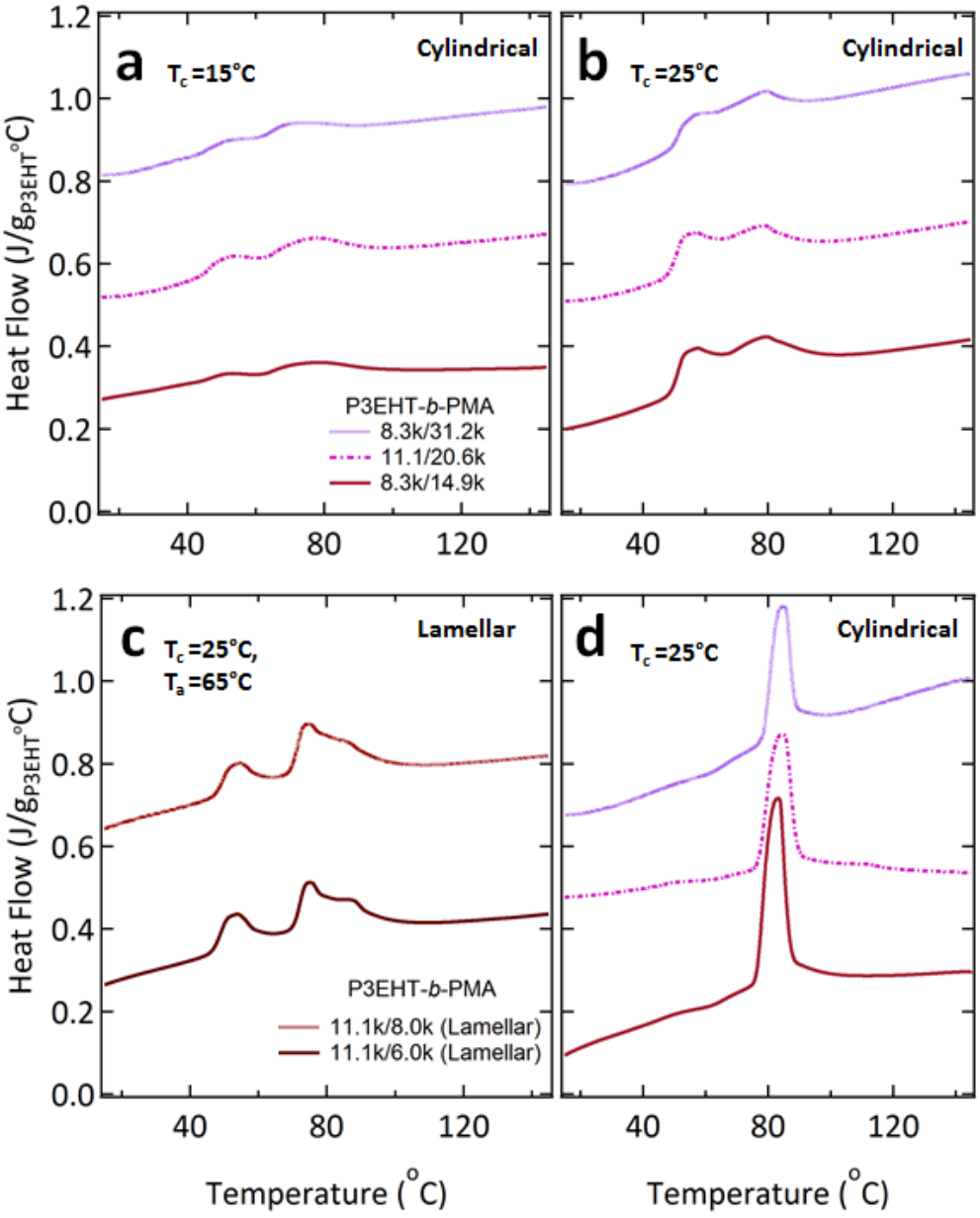

Figure 3.7 Differential scanning calorimetry of cylinder versus lamellar forming P3EHT-*b*-PMA

Differential scanning calorimetry of P3EHT crystallized in cylindrical confinement (A) crystallized at 15°C (B) crystallized at 25°C (C) crystallized at 25°C followed by annealing overnight at 65°C.

Previously in the P3EHT homopolymer and in lamellar confinement, it has been shown that increasing the isothermal crystallization temperature improves the resulting degree of crystalline perfection. While this tunability is an important processing consideration for the resulting charge transport properties, in the cylindrically confined system it is not as powerful: the window of accessible crystallization kinetics becomes quite small (T_c<35°C, as opposed to <55°C), limiting the degree to which this processing strategy can manipulate the resulting crystallites. Importantly, here it is possible to take advantage of the ease with which these materials exhibit 'melt-recrystallization' behavior. The material is first allowed to fully form low-quality crystallites at 25°C, where nucleation processes are favored. Then, confined cylinders are heated to 65°C – a temperature at which crystallites are stable yet could not intrinsically crystallize due to instability of the nuclei. The resulting crystallites form a single uniform population as observed by DSC (Figure 3.7d). Thus, taking advantage of mechanisms for seeding nuclei and then improving crystallinity via annealing steps are promising routes to attaining high-quality crystallites when traditional crystallization routes are unsuccessful.

3.4 Conclusions

Here, the impact of confinement within curved microdomains on the crystallization of conjugated polymers is investigated. Crystallization of conjugated polymers within confinement is impacted by a range of factors, including the interfacial tethering due to the diblock nature of the materials, the mechanical nature of the second block it is attached to, nucleation properties associated with the coherence and volume of confined polymer, and the preference for extended-chain crystallization. This work demonstrates the synthesis of P3EHT-*b*-PMA diblocks which confine P3EHT within cylindrical microdomains, and perform a detailed investigation into how confinement within cylindrical microdomains impacts conjugated polymer crystallization. Importantly, it is observed that confinement templates crystallite orientation such that the 100 (alkyl chain stacking direction) extends down the long axis of the cylinder, while the extended chain and 110 (π-stacking) direction lie within the plane of the cylinder. These observed orientations pose a challenge, as a strategy for templating crystallinity with a faster transport direction – ie: π-stacking – along the long axis of the cylinder must be developed to use these materials as model systems for studying 1-D transport. Furthermore, the combination of TEM and SAXS emphasize the local deformation that is required to accommodate extended-chain crystallites: not only do the cylinders expand in diameter (as measured by SAXS), but they experience local anisotropic deformations (visible via TEM). Importantly, these confined crystallites also display an apparent change in nucleation mechanism, reducing the ability to tune crystalline perfection merely via isothermal crystallization conditions. Instead, excellent crystallinity is achieved via an initial, accessible crystallization followed by subsequently taking advantage of melt-recrystallization mechanisms. This work examines the unique impacts that crystallization tethered within cylindrical microdomains has on conjugated polymers, and highlights both the challenges and promises for achieving additional control over functional polymer nanostructured materials for devices or fundamental charge transport studies.

3.5 Appendix

3.5.1 Gel Permeation Chromatography

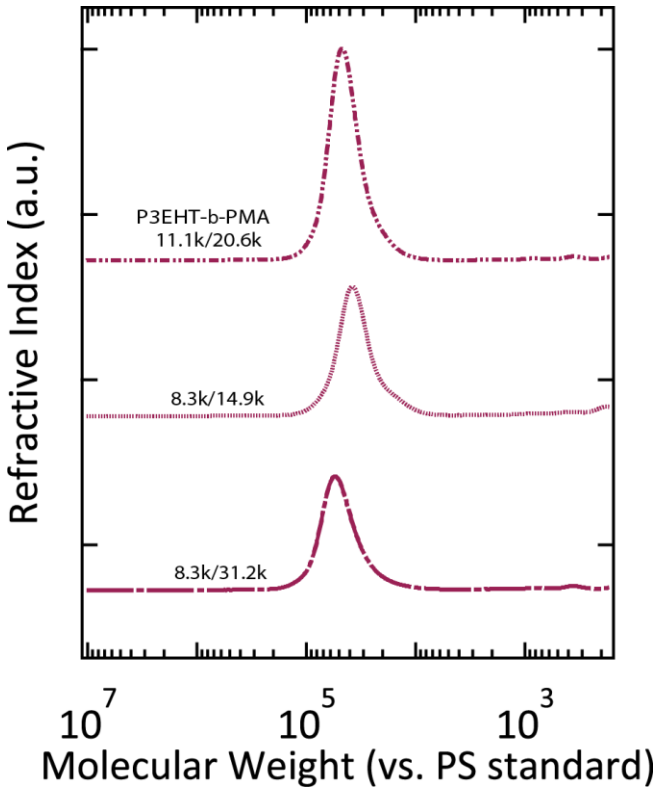

Figure 3.8 GPC of cylinder-forming P3EHT-*b*-PMA diblock copolymers

GPC of studied P3EHT-*b*-PMA cylinder-forming diblocks. Molecular weight calibrated via polystyrene standards.

3.5.2 Impact of staining on TEM of P3EHT-*b*-PMA cylinders

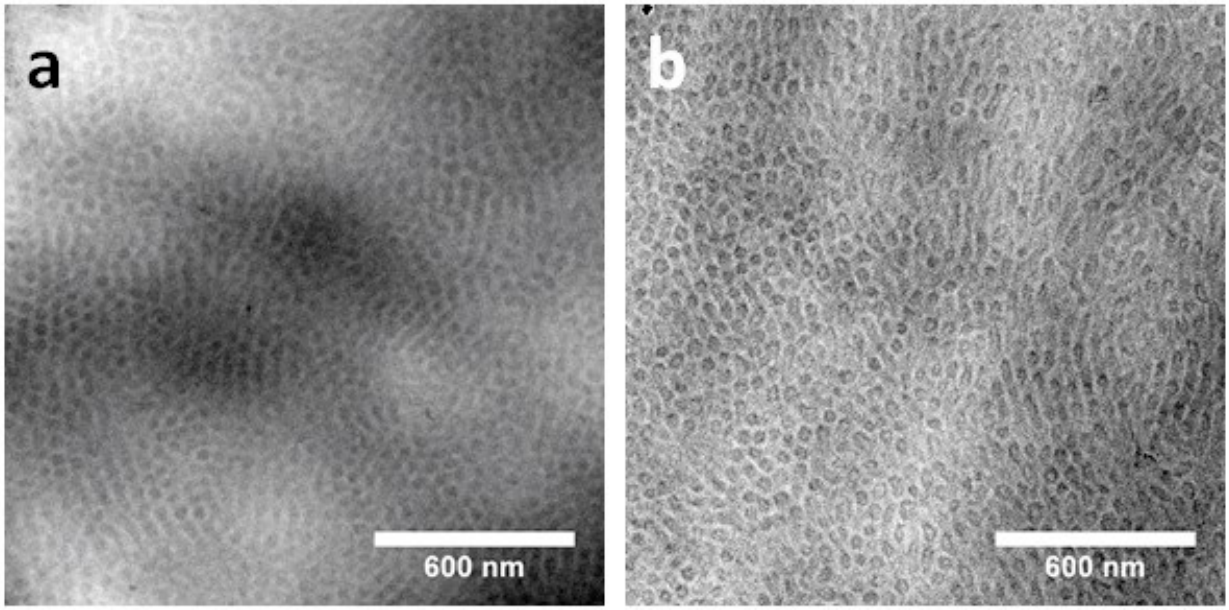

Figure 3.9 TEM of stained versus unstained crystalline P3EHT-*b*-PMA

While unstained P3EHT-*b*-PMA (here, P3EHT-*b*-PMA 11.1/20.6k provides sufficient contrast for TEM bright-field imaging of microdomains (left), staining with RuO_4 enhances contrast, particularly between amorphous and crystalline components within cylindrical microdomains (right).

3.5.3 Morphology of P3EHT-b-PS cylinders

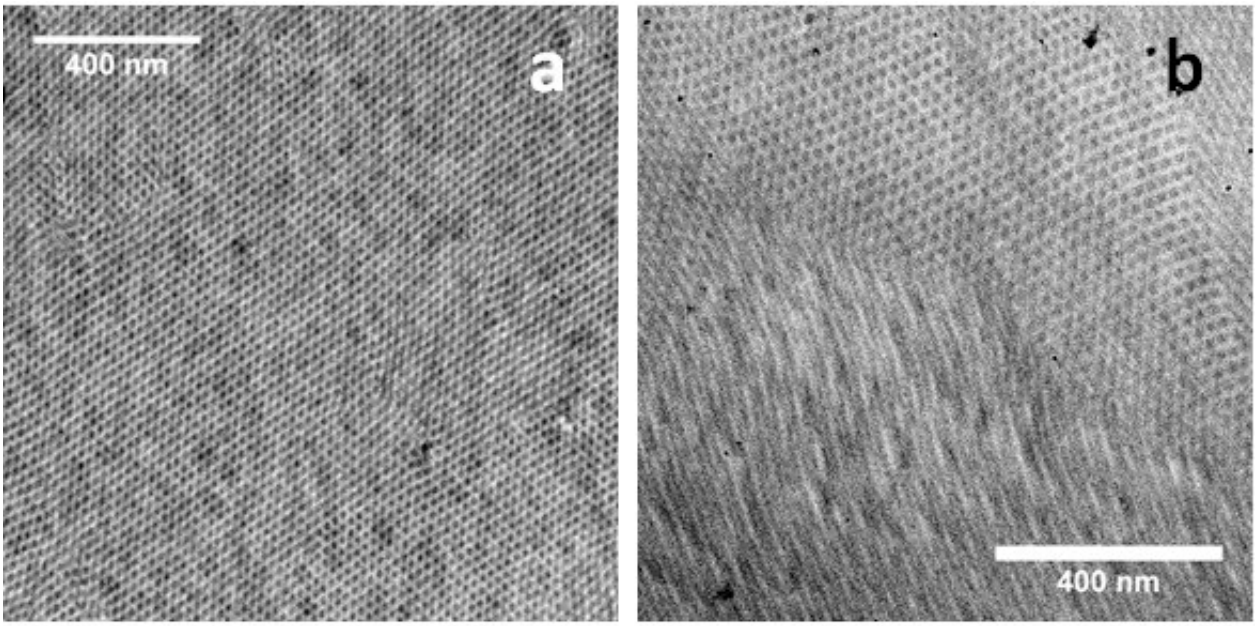

Figure 3.10 TEM of P3EHT-*b*-PS cylinder forming morphologies
TEM of RuO_4 stained cylinder-forming P3EHT-*b*-PS cylinder forming diblocks (a) 8.3k/14.1k (b) 8.3k/12.5k

3.5.4 Supplementary Differential Scanning Calorimetry

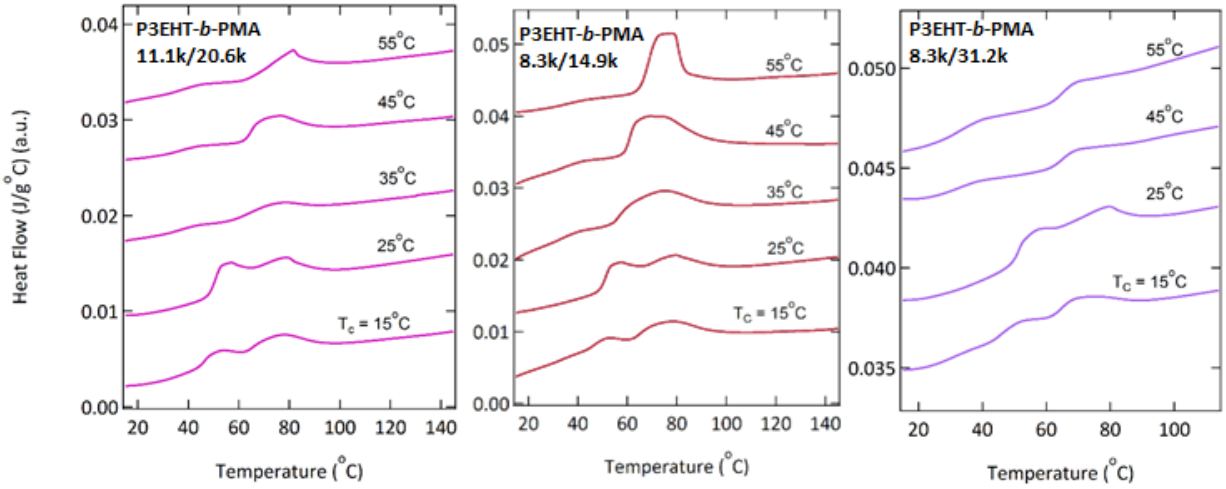

Figure 3.11 DSC of temperature-dependent crystallization in cylindrical confinement

Crystallization temperature-dependent crystallization from T_c = 15°C to T_c = 55°C for cylindrically confined P3EHT. Note that samples were exposed to room temperature on a DSC autosampler for ~1 day prior to running after being removed from temperature controlled ovens leading to the weak crystallinity in P3EHT-*b*-PMA 8.3k/31.2k 45°C and 55°C traces.

3.6 Acknowledgements

We gratefully acknowledge support from the NSF-DMR Polymers Program through grant no. 1206296. This work used user facilities at the Advanced Light Source and at the Stanford Synchrotron Radiation Light Source, supported by the Director, Office of Science, Office of Basic Energy Sciences, of the U.S. Department of Energy under Contracts No DE-AC02-05CH11231 and DE-AC02-76SF00515. We also gratefully acknowledge use of the UCSB MRL Shared Experimental Facilities supported by the MRSEC Program of the NSF under Award No. DMR 1121053; a member of the NSF-funded Materials Research Facilities Network. We also thank Stephan Kramer for support with TEM imaging.

3.7 References

1. Salleo, A., Charge transport in polymeric transistors. *Mater Today* **2007,** *10* (3), 38-45.

2. Sirringhaus, H.; Tessler, N.; Friend, R. H., Integrated optoelectronic devices based on conjugated polymers. *Science* **1998,** *280* (5370), 1741-1744.

3. Thompson, B. C.; Frechet, J. M. J., Organic photovoltaics - Polymer-fullerene composite solar cells. *Angew Chem Int Edit* **2008,** *47* (1), 58-77.

4. Himmelberger, S.; Dacuna, J.; Rivnay, J.; Jimison, L. H.; McCarthy-Ward, T.; Heeney, M.; McCulloch, I.; Toney, M. F.; Salleo, A., Effects of Confinement on Microstructure and Charge Transport in High Performance Semicrystalline Polymer Semiconductors. *Adv Funct Mater* **2013,** *23* (16), 2091-2098.

5. Jimison, L. H.; Himmelberger, S.; Duong, D. T.; Rivnay, J.; Toney, M. F.; Salleo, A., Vertical Confinement and Interface Effects on the Microstructure and Charge Transport of P3HT Thin Films. *J Polym Sci Pol Phys* **2013,** *51* (7), 611-620.

6. Hellmann, C.; Treat, N. D.; Scaccabarozzi, A. D.; Hollis, J. R.; Fleischli, F. D.; Bannock, J. H.; de Mello, J.; Michels, J. J.; Kim, J. S.; Stingelin, N., Solution Processing of Polymer Semiconductor: Insulator Blends-Tailored Optical Properties Through Liquid-Liquid Phase Separation Control. *J Polym Sci Pol Phys* **2015,** *53* (4), 304-310.

7. Tseng, H. R.; Phan, H.; Luo, C.; Wang, M.; Perez, L. A.; Patel, S. N.; Ying, L.; Kramer, E. J.; Nguyen, T. Q.; Bazan, G. C.; Heeger, A. J., High-Mobility Field-Effect Transistors Fabricated with Macroscopic Aligned Semiconducting Polymers. *Adv Mater* **2014,** *26* (19), 2993-2998.

8. Patel, S. N.; Su, G. M.; Luo, C.; Wang, M.; Perez, L. A.; Fischer, D. A.; Prendergast, D.; Bazan, G. C.; Heeger, A. J.; Chabinyc, M. L.; Kramer, E. J., NEXAFS Spectroscopy Reveals the Molecular Orientation in Blade-Coated Pyridal[2,1,3]thiadiazole-Containing Conjugated Polymer Thin Films. *Macromolecules* **2015,** *48* (18), 6606-6616.

9. Hu, H. L.; Zhao, K.; Fernandes, N.; Boufflet, P.; Bannock, J. H.; Yu, L. Y.; de Mello, J. C.; Stingelin, N.; Heeney, M.; Giannelise, E. P.; Amassian, A., Entanglements in marginal solutions: a means of tuning pre-aggregation of conjugated polymers with positive implications for charge transport. *J Mater Chem C* **2015,** *3* (28), 7394-7404.

10. Kline, R. J.; McGehee, M. D.; Kadnikova, E. N.; Liu, J. S.; Frechet, J. M. J.; Toney, M. F., Dependence of regioregular poly(3-hexylthiophene) film morphology and field-effect mobility on molecular weight. *Macromolecules* **2005,** *38* (8), 3312-3319.

11. Duong, D. T.; Ho, V.; Shang, Z. R.; Mollinger, S.; Mannsfeld, S. C. B.; Dacuna, J.; Toney, M. F.; Segalman, R.; Salleo, A., Mechanism of Crystallization and Implications for Charge Transport in Poly(3-ethylhexylthiophene) Thin Films. *Adv Funct Mater* **2014,** *24* (28), 4515-4521.

12. Himmelberger, S.; Duong, D. T.; Northrup, J. E.; Rivnay, J.; Koch, F. P. V.; Beckingham, B. S.; Stingelin, N.; Segalman, R. A.; Mannsfeld, S. C. B.; Salleo, A., Role of Side-Chain Branching on Thin-Film Structure and Electronic Properties of Polythiophenes. *Adv Funct Mater* **2015,** *25* (17), 2616-2624.

13. Muller, C.; Zhigadlo, N. D.; Kumar, A.; Baklar, M. A.; Karpinski, J.; Smith, P.; Kreouzis, T.; Stingelin, N., Enhanced Charge-Carrier Mobility in High-Pressure-Crystallized Poly(3-hexylthiophene). *Macromolecules* **2011,** *44* (6), 1221-1225.

14. Treat, N. D.; Malik, J. A. N.; Reid, O.; Yu, L. Y.; Shuttle, C. G.; Rumbles, G.; Hawker, C. J.; Chabinyc, M. L.; Smith, P.; Stingelin, N., Microstructure formation in molecular and polymer semiconductors assisted by nucleation agents. *Nat Mater* **2013,** *12* (7), 628-633.

15. Zhang, R.; Li, B.; Iovu, M. C.; Jeffries-EL, M.; Sauve, G.; Cooper, J.; Jia, S. J.; Tristram-Nagle, S.; Smilgies, D. M.; Lambeth, D. N.; McCullough, R. D.; Kowalewski, T., Nanostructure dependence of field-effect mobility in regioregular poly(3-hexylthiophene) thin film field effect transistors. *J Am Chem Soc* **2006,** *128* (11), 3480-3481.

16. Baklar, M.; Barard, S.; Sparrowe, D.; Wilson, R. M.; McCulloch, I.; Heeney, M.; Kreouzis, T.; Stingelin, N., Bulk charge transport in liquid-crystalline polymer semiconductors based on poly(2,5-bis(3-alkylthiophen-2-yl)thieno[3,2-b]thiophene). *Polym Chem-Uk* **2010,** *1* (9), 1448-1452.

17. DeLongchamp, D. M.; Kline, R. J.; Jung, Y.; Lin, E. K.; Fischer, D. A.; Gundlach, D. J.; Cotts, S. K.; Moad, A. J.; Richter, L. J.; Toney, M. F.; Heeney, M.; McCulloch, I., Molecular basis of mesophase ordering in a thiophene-based copolymer. *Macromolecules* **2008,** *41* (15), 5709-5715.

18. Sauve, G.; McCullough, R. D., High field-effect mobilities for diblock copolymers of poly(3-hexylthiophene) and poly(methyl acrylate). *Adv Mater* **2007,** *19* (14), 1822-+.

19. Sauve, G.; Zhang, R.; Jia, S. J.; Kowalewski, T.; McCullough, R. D., Synthesis, mobility, and conductivity of well-defined regioregular poly(3-hexylthiophene) and diblock copolymers of regioregular poly(3-hexylthiophene). *P Soc Photo-Opt Ins* **2006,** *6336*, U164-U172.

20. Moon, H. C.; Bae, D.; Kim, J. K., Self-Assembly of Poly(3-dodecylthiophene)-block-poly(methyl methacrylate) Copolymers Driven by Competition between Microphase Separation and Crystallization. *Macromolecules* **2012,** *45* (12), 5201-5207.

21. Lim, H.; Chao, C. Y.; Su, W. F., Modulating Crystallinity of Poly(3-hexylthiophene) via Microphase Separation of Poly(3-hexylthiophene)-Polyisoprene Block Copolymers. *Macromolecules* **2015,** *48* (10), 3269-3281.

22. Lim, H.; Ho, C. C.; Wu, S. J.; Tsai, H. C.; Su, W. F.; Chao, C. Y., A poly(3-hexylthiophene) block copolymer with macroscopically aligned hierarchical nanostructure induced by mechanical rubbing. *Chem Commun* **2013,** *49* (80), 9146-9148.

23. Iovu, M. C.; Jeffries-El, M.; Zhang, R.; Kowalewski, T.; Mccullough, R. D., Conducting block copolymer nanowires containing regioregular poly(3-hexylthiophene) and polystyrene. *J Macromol Sci A* **2006,** *43* (12), 1991-2000.

24. Iovu, M. C.; Zhang, R.; Cooper, J. R.; Smilgies, D. M.; Javier, A. E.; Sheina, E. E.; Kowalewski, T.; McCullough, R. D., Conducting block copolymers of regioregular poly(3-hexylthiophene) and poly(methacrylates): Electronic materials with variable conductivities and degrees of interfibrillar order. *Macromol Rapid Comm* **2007,** *28* (17), 1816-1824.

25. Beckingham, B. S.; Ho, V.; Segalman, R. A., Formation of a Rigid Amorphous Fraction in Poly(3-(2 '-ethyl)hexylthiophene). *Acs Macro Lett* **2014,** *3* (7), 684-688.

26. Beckingham, B. S.; Ho, V.; Segalman, R. A., Melting Behavior of Poly(3-(2 '-ethyl)hexylthiophene). *Macromolecules* **2014,** *47* (23), 8305-8310.

27. Boudouris, B. W.; Ho, V.; Jimison, L. H.; Toney, M. F.; Salleo, A.; Segalman, R. A., Real-Time Observation of Poly(3-alkylthiophene) Crystallization and Correlation with Transient Optoelectronic Properties. *Macromolecules* **2011,** *44* (17), 6653-6658.

28. Ho, V.; Boudouris, B. W.; Segalman, R. A., Tuning Polythiophene Crystallization through Systematic Side Chain Functionalization. *Macromolecules* **2010,** *43* (19), 7895-7899.

29. Ho, V.; Boudouris, B. W.; McCulloch, B. L.; Shuttle, C. G.; Burkhardt, M.; Chabinyc, M. L.; Segalman, R. A., Poly(3-alkylthiophene) Diblock Copolymers with Ordered Microstructures and Continuous Semiconducting Pathways. *J Am Chem Soc* **2011,** *133* (24), 9270-9273.

30. Davidson, E. C.; Beckingham, B. S.; Ho, V.; Segalman, R. A., Confined Crystallization in Lamellae Forming Poly(3-(2 '-ethyl)hexylthiophene) (P3EHT) Block Copolymers. *J Polym Sci Pol Phys* **2016,** *54* (2), 205-215.

31. Martin, J.; Campoy-Quiles, M.; Nogales, A.; Garriga, M.; Alonso, M. I.; Goni, A. R.; Martin-Gonzalez, M., Poly(3-hexylthiophene) nanowires in porous alumina: internal structure under confinement. *Soft Matter* **2014,** *10* (18), 3335-3346.

32. Loo, Y. L.; Register, R. A.; Adamson, D. H., Polyethylene crystal orientation induced by block copolymer cylinders. *Macromolecules* **2000,** *33* (22), 8361-8366.

33. Quiram, D. J.; Register, R. A.; Marchand, G. R., Crystallization of asymmetric diblock copolymers from microphase-separated melts. *Macromolecules* **1997,** *30* (16), 4551-4558.

34. Quiram, D. J.; Register, R. A.; Marchand, G. R.; Adamson, D. H., Chain orientation in block copolymers exhibiting cylindrically confined crystallization. *Macromolecules* **1998,** *31* (15), 4891-4898.

35. Quiram, D. J.; Register, R. A.; Marchand, G. R.; Ryan, A. J., Dynamics of structure formation and crystallization in asymmetric diblock copolymers. *Macromolecules* **1997,** *30* (26), 8338-8343.

36. Loo, Y. L.; Register, R. A.; Ryan, A. J.; Dee, G. T., Polymer crystallization confined in one, two, or three dimensions. *Macromolecules* **2001,** *34* (26), 8968-8977.

37. Hamley, I. W.; Fairclough, J. P. A.; Bates, F. S.; Ryan, A. J., Crystallization thermodynamics and kinetics in semicrystalline diblock copolymers. *Polymer* **1998,** *39* (6-7), 1429-1437.

38. Michell, R. M.; Muller, A. J., Confined crystallization of polymeric materials. *Progress in Polymer Science* **2016,** *54-55*, 183-213.

39. Chen, H. L.; Hsiao, S. C.; Lin, T. L.; Yamauchi, K.; Hasegawa, H.; Hashimoto, T., Microdomain-tailored crystallization kinetics of block copolymers. *Macromolecules* **2001,** *34* (4), 671-674.

40. Chen, H. L.; Wu, J. C.; Lin, T. L.; Lin, J. S., Crystallization kinetics in microphase-separated poly(ethylene oxide)-block-poly(1.,4-butadiene). *Macromolecules* **2001,** *34* (20), 6936-6944.

41. Balsamo, V.; Paolini, Y.; Ronca, G.; Muller, A. J., Crystallization of the polyethylene block in polystyrene-b-polyethylene-b-polycaprolactone triblock copolymers, 1 - Self-nucleation behavior. *Macromol Chem Phys* **2000,** *201* (18), 2711-2720.

42. Bryant, W. M. D.; Pierce, R. H. H.; Lindegren, C. R.; Roberts, R., Nucleation and Growth of Crystallites in High Polymers - Formation of Spherulites. *J Polym Sci* **1955,** *16* (82), 131-142.

43. Liu, J. H.; Arif, M.; Zou, J. H.; Khondaker, S. I.; Zhai, L., Controlling Poly(3-hexylthiophene) Crystal Dimension: Nanowhiskers and Nanoribbons. *Macromolecules* **2009,** *42* (24), 9390-9393.

44. Brunacci, A.; Pedemonte, E.; Turturro, A., Determination of the Equation-of-State Parameters of Poly(Methyl Acrylate). *Polymer* **1992,** *33* (20), 4428-4431.

45. Richardson, M. J.; Savill, N. G., Volumetric Properties of Polystyrene - Influence of Temperature, Molecular-Weight and Thermal-Treatment. *Polymer* **1977,** *18* (1), 3-9.

46. Lee, H. H.; Register, R. A.; Hajduk, D. A.; Gruner, S. M., Orientation of triblock copolymers in planar extension. *Polym Eng Sci* **1996,** *36* (10), 1414-1424.

47. Huang, T. C.; Toraya, H.; Blanton, T. N.; Wu, Y., X-Ray-Powder Diffraction Analysis of Silver Behenate, a Possible Low-Angle Diffraction Standard. *J Appl Crystallogr* **1993,** *26*, 180-184.

48. Ilavsky, J., Nika: software for two-dimensional data reduction. *J Appl Crystallogr* **2012,** *45*, 324-328.

49. Zhang, W. L.; Gomez, E. D.; Milner, S. T., Predicting Chain Dimensions of Semiflexible Polymers from Dihedral Potentials. *Macromolecules* **2014,** *47* (18), 6453-6461.

50. McCulloch, B.; Ho, V.; Hoarfrost, M.; Stanley, C.; Do, C.; Heller, W. T.; Segalman, R. A., Polymer Chain Shape of Poly(3-alkylthiophenes) in Solution Using Small-Angle Neutron Scattering. *Macromolecules* **2013,** *46* (5), 1899-1907.

51. Fetters, L. J.; Lohse, D. J.; Graessley, W. W., Chain dimensions and entanglement spacings in dense macromolecular systems. *J Polym Sci Pol Phys* **1999,** *37* (10), 1023-1033.

52. Bates, F. S.; Fredrickson, G. H., Conformational Asymmetry and Polymer-Polymer Thermodynamics. *Macromolecules* **1994,** *27* (4), 1065-1067.

53. Almdal, K.; Hillmyer, M. A.; Bates, F. S., Influence of conformational asymmetry on polymer-polymer interactions: An entropic or enthalpic effect? *Macromolecules* **2002,** *35* (20), 7685-7691.

54. Matsen, M. W.; Bates, F. S., Conformationally asymmetric block copolymers. *J Polym Sci Pol Phys* **1997,** *35* (6), 945-952.

55. Bates, F. S.; Schulz, M. F.; Rosedale, J. H.; Almdal, K., Correlation of Binary Polyolefin Phase-Behavior with Statistical Segment Length Asymmetry. *Macromolecules* **1992,** *25* (20), 5547-5550.

56. Bates, F. S.; Schulz, M. F.; Khandpur, A. K.; Forster, S.; Rosedale, J. H.; Almdal, K.; Mortensen, K., Fluctuations, Conformational Asymmetry and Block-Copolymer Phase-Behavior. *Faraday Discuss* **1994,** *98*, 7-18.

57. Olsen, B. D.; Segalman, R. A., Self-assembly of rod-coil block copolymers. *Mat Sci Eng R* **2008,** *62* (2), 37-66.

58. Olsen, B. D.; Shah, M.; Ganesan, V.; Segalman, R. A., Universalization of the phase diagram for a model rod-coil diblock copolymer. *Macromolecules* **2008,** *41* (18), 6809-6817.

59. Loo, Y. L.; Register, R. A.; Ryan, A. J., Modes of crystallization in block copolymer microdomains: Breakout, templated, and confined. *Macromolecules* **2002,** *35* (6), 2365-2374.

60. Loo, Y. L.; Register, R. A.; Adamson, D. H., Direct imaging of polyethylene crystallites within block copolymer microdomains. *J Polym Sci Pol Phys* **2000,** *38* (19), 2564-2570.

61. Sirringhaus, H.; Brown, P. J.; Friend, R. H.; Nielsen, M. M.; Bechgaard, K.; Langeveld-Voss, B. M. W.; Spiering, A. J. H.; Janssen, R. A. J.; Meijer, E. W.; Herwig, P.; de Leeuw, D. M., Two-dimensional charge transport in self-organized, high-mobility conjugated polymers. *Nature* **1999,** *401* (6754), 685-688.

Chapter 4. Thermal Control of Confined Crystallization within P3EHT Block Copolymer Microdomains

The local, nanoscale organization of crystallites in conjugated polymers is often critical to determining the charge transport properties of the system. Block copolymer geometries, which offer controlled nanostructures with tethering of chains at interfaces, are an ideal platform to study the local organization of conjugated polymer crystallites. The model conjugated polymer poly(3-(2′-ethyl)hexylthiophene) (P3EHT) features a depressed melting temperature relative to the widely studied poly(3-hexylthiophene) (P3HT), which allows it to robustly form microphase separated domains that confine the subsequent P3EHT crystallites. Importantly, P3EHT crystallization in confinement is coupled to a rubbery second block via interfacial tethering, mechanical properties, and chain stretching. Here, the impact of thermal processing on the diblock copolymer structure is examined to elucidate the key driving forces controlling the final coupled diblock copolymer and crystalline structures. Surprisingly, the diblock copolymer domain size is significantly impacted by the temperature at which the conjugated domain is crystallized. Decreasing amounts of domain extension are observed with increasing crystallization temperatures. This temperature-dependent domain structure appears to be correlated with the crystallization processes; these processes are inferred from precise changes in the lamellar structure across melting. By carefully tracking the changes in domain structure across melting, this work identifies three distinct melting regimes. We suggest a structural model of the conjugated block melting processes consisting of (I) excluded-chain relaxation followed by (II) chain inter-digitation during melt-recrystallization, and finally (III) complete melting that is independent of the initial crystallization conditions. These results suggest that P3EHT crystallization processes associated with temperature-dependent chain diffusion and nucleation are primarily responsible for the unexpected temperature dependent crystallization behavior. They also emphasize that, contrary to common assumptions, less perfect conjugated polymer crystals may actually be associated with a poorly interdigitated structure. Furthermore, this work demonstrates the utility of leveraging a diblock copolymer structure with a rubbery second block in order to precisely track changes in the crystallite structure.

4.1 Introduction

Conjugated polymers have been utilized in applications including photovoltaics, light emitting diodes, and field effect transistors.[1-3] Importantly, the performance of these devices depend upon the charge transport properties of the constituent polymer, which in turn varies with the material's crystallinity.[4-11] Block copolymers containing crystalline conjugated blocks are of interest for incorporating both nanopatterning and conjugated polymers into a single material; furthermore, confinement of conjugated polymers within block copolymer microdomains provides an opportunity to study conjugated polymer crystallization in highly-defined geometries with tethered chains at the boundaries. These structures are a versatile platform for crystallization studies; diblock copolymers allow variable control over molecular weight, interfacial curvature, interfacial area, and coupled chain dynamics to understand the relative forces driving and controlling the polymer crystallization.

Achieving controlled confined crystallization of conjugated polymers within block copolymer microdomains requires a system which meets several basic criteria, and also achieves a critical balance of relevant forces. First, it is essential that the diblock copolymer system has a T_{ODT} greater than the melting temperature of the component conjugated polymer.[12] Meeting this criteria alone is challenging given that conjugated polymers generally have extremely high melting temperatures (in excess of 200°C). These high melting temperatures makes it challenging to access microphase-separated melts from which confined crystallites can develop. Because of these high melting temperatures, many attempts at incorporating conjugated polymers within microphase separated diblock copolymers have resulted in crystallization-driven self-assembly. Even in those cases where a microphase-separated melt is accessible, the driving force for crystallization may still be large enough relative to the forces maintaining microphase separation to result in breakout crystallization, destroying the microdomain structure. These criteria in a conjugated polymer containing system may be satisfied by leveraging a poly(3-alkylthiophene) with a modified side-chain, poly(3-(2′-ethyl)hexylthiophene) (P3EHT). The modified side-chain depresses the melting temperature to only ~80°C, permitting the robust formation of microphase-separated P3EHT microdomains which may subsequently crystallize.[13, 14]

Beyond simply achieving confined crystallization, identifying the relative driving forces that contribute to the final domain and crystalline structure is important for developing a deeper understanding of conjugated polymer crystallinity and for identifying critical design and processing parameters controlling these hierarchical block copolymers. Prior work on lamellar P3EHT-*b*-PMA found that the unique properties of conjugated polymers upon crystallization – in particular the preference for adopting an extended chain configuration – places constraints on the conditions required for crystallization. In particular, the stiff nature of the P3EHT chains during crystallization induces the orientation of the resulting crystallites such that chains orient perpendicular to the microdomain interface. Furthermore, achieving fully extended crystals with this orientation appears to be essential to crystallization; the diblock copolymers with P3EHT confined in a glassy polystyrene (PS) matrix microphase separate but suppress crystallization.[15] The morphology and perfection of conjugated crystallites are highly impacted by thermal history; therefore, modifying the thermal processing of the diblock copolymer is expected to moderate the driving forces controlling the final crystalline and domain structure of the conjugated-*b*-amorphous polymer. Prior work on both P3EHT homopolymer and on P3EHT-*b*-PMA found that P3EHT crystalline perfection can be manipulated through the system's isothermal crystallization temperature; decreasing the degree of undercooling resulted in more highly perfect crystallites.[15, 16] Conventional wisdom attributes this increased perfection to changes in ordering along the monomer-monomer (chain) direction, where improvements in crystallinity directly correspond to improved chain extension.[17-19] Comparisons to P3EHT homopolymer led to the conclusion that, in both P3EHT homopolymer and in lamellar diblock copolymers, these improvements in crystallinity instead corresponded primarily to improvements in order along the π-stacking order direction.[15, 16] Therefore, it is expected that improvements in confined P3EHT crystallite quality will not affect the overall domain spacing if changes in crystalline perfection are truly restricted to the π-stacking order direction; otherwise, domains are

expected to be larger with increasing crystallization temperature if crystallite perfection is associated with improved P3EHT monomer-monomer ordering.

Importantly, the bias of conjugated polymers towards forming extended-chain crystallites is not the only factor expected to influence the self-assembly and crystallinity of conjugated-*b*-amorphous materials. The kinetics of the crystallization process itself are also highly temperature dependent. At small degrees of undercooling, chain diffusion processes are typically fast relative to nucleation processes, causing crystallization to be nucleation limited; at lower temperatures, crystallites may readily form stable nuclei, but crystallization may be limited by the timescales required for chains to diffuse and add to growing crystallites. Diffusion versus nucleation limited regimes are expected to induce distinct features on crystallite morphology and chain organization. Recent isothermal crystallization kinetics studies of P3EHT homopolymer indicates that the transition from diffusion limited to nucleation limited regimes occurs at T_c = ~60°C (the transition is, as expected, molecular weight dependent).[20] Understanding the impact of thermal processing conditions over these limiting regimes is expected to have significant impact on controlling the final crystalline and domain structure. It is important to note that, in confinement, the transition from diffusion to nucleation limited regimes is expected to shift to higher temperatures given that interfacial chain tethering limits chain diffusion.

Furthermore, the amorphous block is expected to intrinsically play a significant role in the resulting diblock copolymer structure. As P3EHT forms extended-chain crystallites and the P3EHT microdomain extends, the PMA domain is forced to also expand, stretching the PMA chains. Essentially, the conformation of the crystalline polymer directly impacts the effective area per chain at the diblock copolymer interface, which in turn modulates the degree of chain stretching induced in the amorphous block.[21, 22] Importantly, theory predicts that a fold in the P3EHT chains forming the crystallites is capable of relieving this penalty. Furthermore, crystallite reorientation as a function of temperature in some flexible crystalline-*b*-amorphous systems has also been observed, and hypothesized to be due to moderation of amorphous block stretching. Thus, it is expected that the amorphous block stretching penalty is potentially a significant temperature-sensitive structural driving force in the system.[23, 24]

Interestingly, other systems of conjugated polymers have displayed surprising changes in domain structure with temperature, suggesting that there are some universal processes in the structure formation and resolution in these materials that are still not well-understood. For example, the model rod-coil system DEH-PPV-*b*-PI displays a show shrinkage with increasing temperature that cannot be easily attributed to a change in liquid crystalline phase or other packing considerations. PPV is sufficiently stiff to fully inhibit chain folding at the molecular weights used in this study, indicating that other mechanisms – perhaps present in conjugated diblock copolymers – driving these structural transitions are at play.[25]

This work examines the response of P3EHT-*b*-PMA self-assembly and crystallization to changing thermal processing conditions in order to identify the key forces at play in controlling the final domain and crystalline structure. The amorphous block deformability is critical to achieving P3EHT crystallization; importantly for this study, it also allows changes in the domain structure of the diblock copolymer as a whole to reflect chain reorganization in the P3EHT

block. Here, the P3EHT-*b*-PMA domain structure is examined both as a function of isothermal crystallization temperature and across the melting process to understand the interplay between crystallization and domain structure. P3EHT-*b*-PMA domains expand the most at the lowest crystallization temperatures, contradictory to our expectations that the more perfect crystallites formed at high temperatures correspond to the most extended chain crystallites. We examine several possibilities for this behavior, and suggest a driving mechanism associated with crystallites featuring excluded crystallization and poorly interdigitated chains developing at low crystallization temperatures. Furthermore, this work both provides unique insight into the processes of achieving improved crystalline perfection in conjugated polymers, as well as demonstrates the utility of block copolymer architectures to access unique features of conjugated polymer crystallization that would be difficult to access via other means.

4.2 Experimental

4.2.1 Synthesis

Reagents and solvents were used as received from Sigma Aldrich. P3EHT monomer was synthesized as previously described.[13] P3EHT and PMA were synthesized via ethynyl-terminated GRIM and ATRP followed by azide substitution, respectively.[13, 15] P3EHT-*b*-PMA was synthesized via coupling of component blocks by azide-alkyne click chemistry as previously described.[15] P3EHT and PMA without end functionalization were synthesized via acid-terminated GRIM and by ATRP without an azide substitution, respectively. Preparation of blends is discussed in the Appendix.

4.2.2 Molecular Characterization

Gel permeation chromatography (GPC) to determine molecular weights and dispersity relative to PS standards was performed on a Waters instrument using Agilent PLgel 5μm MiniMIX-D columns. The mobile phase was THF at 35°C with a flow rate of 0.3 mL/min. ^{1}H NMR spectra were collected on a Varian VNMRS 600 MHz spectrometer using deuterated chloroform (Cambridge) as the solvent with ~1 weight % polymer. Reported molecular weights are by end group analysis. Volume fractions are calculated using densities from gas pycnometry and literature as previously described.[15] Molecular characterization of P3EHT-*b*-PMA 11.1k/6.0k is previously reported.[15] H-terminated P3EHT homopolymer has a dispersity of 1.15 and a molecular weight of 11.3k by ^{1}H-NMR. PMA homopolymer has a dispersity of 1.13 and molecular weight of 5.0k by ^{1}H-NMR. Characteristics are in Table 4.1.

4.2.3 Differential Scanning Calorimetry

Samples for DSC were prepared by hermetically sealing between 1-10 mg of material inside TZero aluminum pans. Thermal processing is performed offline due to the long time scales associated with crystallization. Before each experiment, samples are heated to 150°C offline and held for ten minutes to clear thermal history. Isothermal crystallization of blends are performed for one week in temperature controlled ovens. Annealed samples are first crystallized at room temperature for a week, and then annealed in temperature controlled ovens overnight.

Table 4.1 Molecular characteristics of polymers used for study of thermal effects

Polymer	Dispersity (*Đ*)	^{1}H NMR Molecular weight
P3EHT-*b*-PMA	1.14	11.1k/6.0k
P3EHT	1.15	11.3k
PMA	1.13	5.0k

DSC traces on heating were collected on a TA Q2000 calorimeter by heating from -20˚C to 150˚C at 10˚C/min.

4.2.4 Small and Wide-Angle X-ray Scattering

Isotropic samples for X-ray scattering were prepared by melt-pressing into 1 mm thick aluminum washers at 150°C. Samples were isothermally crystallized for one week within temperature-controlled ovens prior to data collection. Annealed samples were first crystallized at room temperature for one week, and then annealed in temperature controlled ovens overnight. X-ray scattering collected upon melting was performed on a controlled heat stage at beamline 7.3.3 at the Advanced Light Source; data was collected with 2°C temperature resolution, and a five minute wait time was used to allow the temperature of each sample to stabilize and equilibrate. SAXS 2-D patterns were collected at the Advanced Light Source (ALS) beamline 7.3.3 and at the Stanford Synchrotron Radiation Laboratory (SSRL) beamline 1-5. Silver behenate (AgBe) was used to calibrate scattering patterns.[26] Scattering data was reduced using the Nika package for Igor,[27] and plotted against the momentum transfer vector $q = (4\pi/\lambda) \sin \theta$.

4.3 Results and Discussion

A P3EHT-*b*-PMA block copolymer was leveraged to study the detailed coupling between P3EHT crystallization and diblock copolymer domain structure as a function of thermal history. Furthermore, blends of P3EHT-*b*-PMA with PMA and P3EHT homopolymer probe the impact of PMA chain stretching and P3EHT decoupling respectively on structure formation. While previous work has identified the P3EHT preference for extended chain crystals as critical for achieving crystallinity in confinement and driving the final domain structure, this study examines the detailed interactions moderating this structure.[15] The goal is to understand how the constituent forces interact to control the resulting crystallinity and domain structure. In particular, temperature-dependent driving factors are expected to include changes in crystalline perfection, stretching of the coupled amorphous block induced by crystallization, and temperature-dependent chain diffusion and nucleation effects. Therefore, the roles of temperature in moderating these interactions is examined by tracking the domain structure as a function of crystallization temperature and as a detailed function of temperature during melting. Investigating the thermal responsive behavior of P3EHT-*b*-PMA domains reveals that, surprisingly, the final domain size is largest at large degrees of undercooling; higher crystallization temperatures result in more compact domains. Correlating these shifts to changes in the crystallinity as measured by DSC and WAXS challenges some of the assumed mechanisms of how improvements in order proceed in confinement, while clarifying the mechanism of melt-recrystallization. In particular, this work suggests that the primary changes in domain structure with thermal processing are connected to crystallization processes. Furthermore, over the regimes studied here, PMA chain stretching upon crystallization does not appear to be capable of inducing P3EHT chain folding according to a classical model, reinforcing the conclusion that extended chain crystallization is a key driver of structure.

4.3.1 Impact of Thermal History on the Final Crystallization-Templated Domain Structure

In developing block copolymers with confined conjugated polymer crystallization, it is important to understand the interactions between domain structure and crystallization.

Importantly, many of the relevant forces and dynamics at play are temperature dependent. Notably, chain diffusion kinetics improve as a function of temperature while nucleation processes become less favored with increasing temperature. Furthermore, the penalty of stretching PMA chains also increases as a function of temperature. Here, crystallinity is particularly highly coupled to the PMA chain stretching due to the observed orientation of P3EHT chains perpendicular to the P3EHT-*b*-PMA interface (Figure 4.1a); in principle, an equilibrium degree of chain folding in crystallites could be coupled to the degree of PMA chain stretching. In this work, the P3EHT-*b*-PMA system is an excellent system to examine the roles of these highly coupled interactions due to the deformability of the rubbery PMA. While increasing crystallization temperatures leads to improved crystalline perfection (Figure 4.1b), we did not expect a change in domain size. This expectation rested on prior work on the diblock copolymer and homopolymer, which indicated that improvements in crystallinity with isothermal crystallization temperature lay mainly in the π-stacking direction.[15, 16] If there were any change to be seen, an increase in domain size was expected with crystallization temperature due to more extended chains. Increased crystallization temperatures and improved crystalline perfection are often assumed to correspond to increasing degrees of chain extension by analogy to the well-understood processes of lamellar thickening in traditional flexible polymers.[18, 19, 28-33] Here, to probe these relationships, the domain structure across a family of diblock copolymers was measured as a function of isothermal crystallization temperature. The measurements definitively found that the final structure is indeed significantly moderated by the isothermal crystallization temperature – samples showed a variation in final structure size of as much as 10% which is determined purely by a combination of the crystallization conditions and thermal history across this family of lamellar samples (Figure 4.1c). Surprisingly, however, the materials show the opposite trend to the expected one: the largest domains, and thus greatest degree of expansion, is observed at low crystallization temperatures, while the least is observed at high temperatures. This observation directly challenged our assumptions of several of the fundamental processes and crystallite structuring occurring in these materials.

Several possibilities present themselves to explain this unexpected behavior. Notably, P3EHT crystallization to form fully-extended chains imposes a stretching penalty upon the coupled PMA block that increases as a function of temperature (Figure 4.2a).[21, 22] The system can relieve this stretching penalty by either changing the orientation of crystallites relative to the interface, or by inducing folding within the P3EHT chain. Both of these responses create new energetic penalties P3EHT chains will have to bend near the interface for a change in orientation, or along the chain length for folding, which are significant bending penalties within conjugated polymers. If crystallites tilt or reorient with chains parallel to domains as a function of temperature, this would effectively increase the area per chain at each interface, therefore reducing the penalty of stretching the amorphous PMA block (Figure 4.2b). However, our previous work examined the relative orientation of crystallites confined within lamellar diblock copolymers via SAXS/WAXS of aligned lamellae both as a function of T_c and during the melting process.[15] Regardless of the conditions, the orientation found is constant, and is only consistent with crystalline P3EHT chains oriented perpendicular to the domain interfaces. Thus, the observed decreased domain spacing with increased T_c cannot be attributed to a balance between chain orientation and chain stretching penalties.

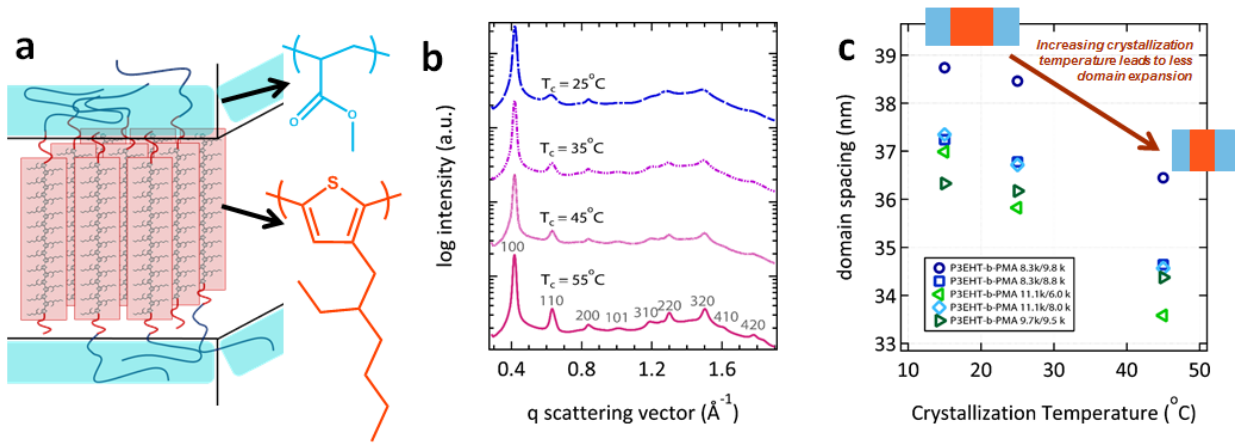

Figure 4.1 Illustration of P3EHT-*b*-PMA diblock and impact of crystallization temperature on domain structure

(a) Cartoon of crystalline P3EHT-*b*-PMA diblock copolymers containing rubbery poly(methyl acrylate) (PMA) and conjugated poly(3-(2'-ethyl)hexylthiophene (P3EHT) components with P3EHT chains perpendicular to the domain interfaces. (b) The most compact final structure is also the structure with the highest quality crystallites via WAXS (c) P3EHT-*b*-PMA diblock copolymers display the most expansion upon crystallization at lower temperatures measured via SAXS.

Alternatively, with increasing temperature, a chain-stretching penalty could induce folding of the associated crystallizable block (Figure 4.2b). To study this, the normalized P3EHT domain size (relative to the P3EHT contour length) is found as a function of crystallization temperature (Figure 4.2c) using the constituent volume fractions. These results show that as the crystallization temperature increases, the P3EHT domain size (normalized to the M_n P3EHT contour length) decreases roughly linearly from 1.10 to slightly less than 1.00. These results emphasize that, as the crystallization temperature increases, the P3EHT certainly does not chain fold by a traditional model. By a traditional model, we would expect a series of normalized P3EHT domain size of $d_{P3EHT}/L_{c,P3EHT}$ = 1.0, 0.5, 0.33, 0.25, etc corresponding to 0, 1, 2, 3, etc. folds per chain with increasing domain temperature. Thus, if P3EHT is folding in confinement it must instead be associated with only partial folding or folding only near the edges of P3EHT domains (as depicted in Figure 4.2b). Furthermore, the fact that at low temperatures the P3EHT domain size is considerably longer than the P3EHT contour length indicates that chains may not be fully interdigitated (as opposed to merely fully extended). At high T_c, the d_{P3EHT} is slightly larger than the (M_n-based) contour length of the P3EHT. Potentially, this could reflect local chain folding at the edges of crystallites; alternatively, this could be an effect from the P3EHT block's small but finite dispersity.

4.3.2 Coupling of Domain and Thermal Transitions Upon Melting

While in crystalline homopolymers, polymer crystals cannot achieve an equilibrium structure, in principle they are able to do so in block copolymer structures by achieving an equilibrium degree of chain folding.[21, 22] However, this does not necessarily mean that the resulting structure will actually be in equilibrium. In particular, polymer crystallization is a highly hierarchical process that is also dependent upon nucleation and chain diffusion effects to achieve crystallinity; ultimately, this can result in secondary nucleation and other effects. To more deeply understand the details of how P3EHT crystallization is coupled to the resulting domain structure, and to help deconvolute the relevant forces, a detailed investigation of the relationship between domain structure and crystallinity upon melting as a function of crystallization temperature (T_c = 25°C, 35°C, 45°C, and 55°C) was performed. The domain size of the P3EHT-*b*-PMA structure was measured as a function of increasing temperature with high temperature resolution in-situ SAXS (Figure 4.5). Melting clearly falls into three regimes, identifiable via shifts in d-spacing as identified by SAXS (Figure 4.3a); the onsets of these shifts correlate well with the onsets of melting peaks identified from differential scanning calorimetry (Figure 4.3b).

The first, broad low-temperature regime results in a large impact on domain structure, especially in diblock copolymers crystallized at low temperatures. Interestingly, upon tracking the domain spacing through this transition using SAXS, the materials display a very broad, slow change spread over a wide temperature window. Notably, the onset of the initial domain shrinkage by SAXS agrees well with the onset of this initial peak as melted by DSC. Peaks as measured by DSC show slightly later onsets and extend over a smaller temperature window than the transitions by SAXS, which is likely an impact of the significantly faster rates in the DSC. For low temperature crystallization, this initial relaxation corresponds to several nanometers of

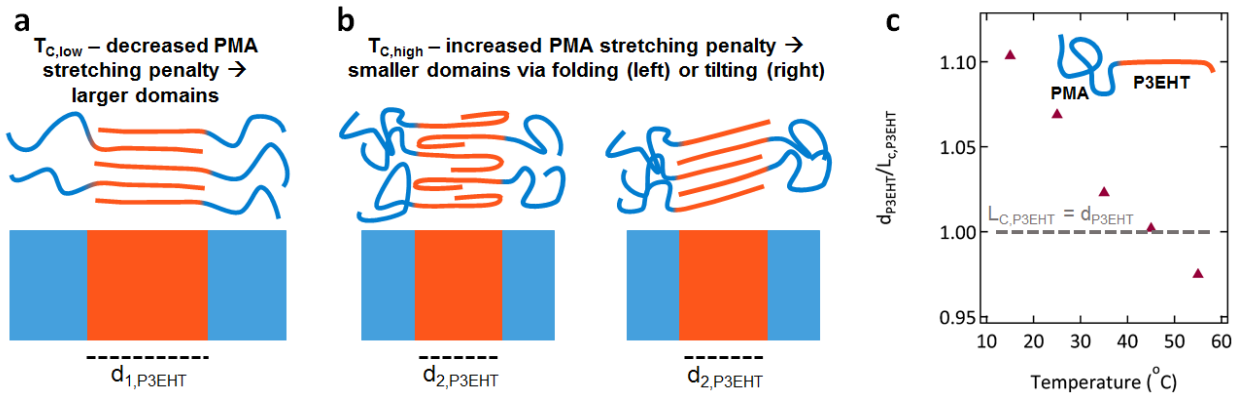

Figure 4.2 P3EHT domain size as a function of crystallization temperature

(a) Fully extended P3EHT chains induce a stretching penalty in coupled PMA chains, which is decreased at lower temperatures and could allow for larger domains. (b) As this penalty increases with temperature, it could induce folding (left) or tilting (right) in P3EHT chains, causing smaller overall domain size. (c) P3EHT domain size as a function of T_c is inconsistent with a model of integer chain folding. At low T_c, P3EHT domain sizes are ~10% larger than the P3EHT contour length.

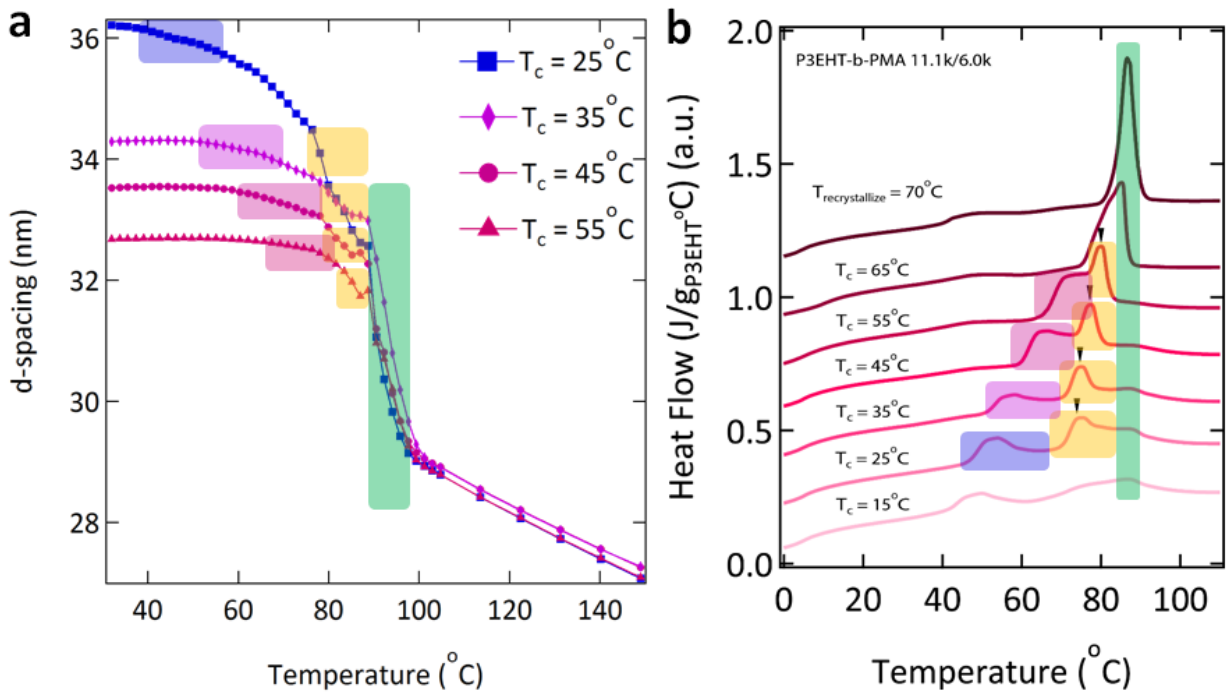

Figure 4.3 Domain and thermal transitions of diblock on heating as a function of T_c

Domain spacing of P3EHT-*b*-PMA during melting, and correlation of domain features to melting features by DSC (a) Onset of initial domain shrinkage during melting as well as final melting show excellent agreement with (b) initial and final features by DSC.

the total difference in domain spacing observed as a function of temperature; for high temperature crystallized samples, it is merely on the order of half a nanometer. This significantly informs our model of the internal structure of the crystallites within the domains and their formation as a function of temperature. This low-melting region must correspond to an ordered region at the edges of the domains; across this low melting peak, these regions disorder and chains relax, resulting in a net shrinkage of the domains (Figure 4.4). At low T_c, a much larger shrinkage is observed over this low-temperature regions. This implies that low T_c causes much more P3EHT to participate in these excluded regions. For T_c of 45°C and greater, these melting features clearly begin to overlap; the regions highlighted in Figure 4.3 are intended as a guide to the eye. Correspondingly, with increasing T_c, this transition has an increasingly minimal impact on domain structure, implying that fewer chains are excluded from the central crystallites with higher T_c.

In order to better understand the nature of the low-melting peak, as well as to investigate improved methods for developing highly perfect crystallites, a P3EHT-*b*-PMA that was initially crystallized at 25°C was subsequently annealed overnight at 70°C. This reveals that the material does not melt-recrystallize on the timescales of the DSC scan as it shows only a single peak on melting (Figure 4.3b), and that post-processing annealing can achieve higher degrees of perfection than manipulating the confined crystallites via varying the degree of undercooling alone. Furthermore, despite ageing this sample at room temperature for two days after annealing prior to running the DSC, the broad low-melting peak observed at temperatures just below the melt-recrystallization peak has vanished; only a weak peak at ~40°C remains. Thus, we conclude that the low-melting region actually corresponds to secondary crystallization of material excluded from crystallites at the center of domains. We hypothesize that in the analogous homopolymer these regions merely constitutes the rigid amorphous fraction,[34] and that here the tethering to the block copolymer interface and relative mobility of the PMA enhances the local ordering such that these regions are truly crystalline. Interestingly, the origin of these excluded regions may be related to the balance between diffusion-limited and nucleation-limited crystallization. Recent work examining isothermal crystallization kinetics of P3EHT homopolymer have found that below 65°C, crystallization is limited by diffusion (i.e., P3EHT readily forms many nuclei, but slow chain diffusion makes the growth of crystallites challenging).[20] If indeed this is also the limitation in diblock copolymers, nucleation may create crystallites at the centers of domains that do not optimally interdigitate chains; additional growth and chain extension results in significant material excluded from the central crystallites but permits for subsequent ordering of that material. The T_c dependent variability in exclusion is attributed to decreasing diffusion limitations on crystallization with higher temperature; over the examined range, diffusion limitations are expected to dominate over nucleation limitations.[20] Further, this model by which parts of chains are excluded from the center of the crystallite as a function of temperature is a satisfactory explanation for the observation that the measured P3EHT domain sizes are actually slightly more than the M_n-based P3EHT contour length for large degrees of undercooling (Figure 4.2c).

Furthermore, the second melting regime provides additional insight into the melt-recrystallization mechanism in these materials. From domain-spacing as a function of melting as

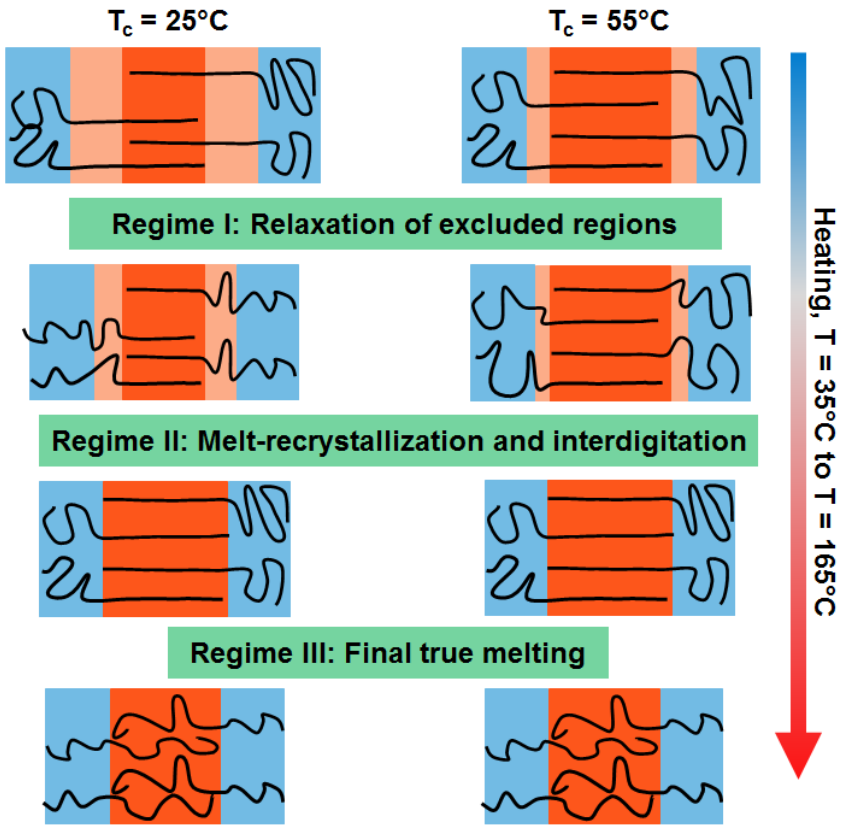

Figure 4.4 Illustration of suggested melting mechanism

Cartoon of suggested melting mechanism across the three regimes. Green labels correspond to transitions between figures. The initial state (top of figure) depends on T_c, which then influences the melting behavior until reaching a common domain and crystalline conformation at the beginning of regime III.

tracked by SAXS, the transition from the first regime to the second is identified as the inflection point in curvature as a function of temperature. It is important to note that the rate of temperature change in the SAXS (2°C temperature resolution with 5 minute sample equilibration times at each step) was very slow relative to the DSC (10°C/minute). Upon the onset of the second melting peak/second melting regime, samples showed a sudden decrease in domain spacing. The onset of this second melting regime – measured both by DSC and by the change in curvature of the SAXS domain melting – shifts to higher temperatures with T_c. The SAXS measurements track the response of the coupled domain and crystallite structure with heating across this entire second regime, showing that eventually the measurements begin to restabilize. Interestingly, the domain structures begin to converge at the end of the second melt-recrystallization regime. However, these measurements are surprising in several respects. First, while these are consistent with the initial degree of crystallite perfection being manipulated by T_c, it was surprising to find that the domain size apparently shrinks across melt-recrystallization. Importantly, we previously found that while order along the alkyl chain stacking direction did not change significantly during melt-recrystallization, significant improvements in order along the π-stacking direction were observed.[16] Furthermore, we found that the evidence did not support a model describing additional chain extension with improvements in crystallinity.[16] However, the further decrease in domain size during melting which is simultaneous with an improvement in crystalline order was surprising, as we did not expect to observe chain-folding during melt-recrystallization. This model is, however, consistent with this regime overcoming diffusion limitations and permitting local melting followed by allowing the previously excluded chains to interdigitate and recrystallize into highly perfect crystals (Figure 4.4). This model does result in more of the material along the length of the chain participating in the crystallite after melt-recrystallization, although it is not due to a change in the degree of chain folding. Importantly, identifying these changes in crystallite structure as a function of temperature – and attributing the different regimes to the component processes – would be extremely challenging in the homopolymer via standard techniques. That we can discern these processes in our system demonstrates the utility of manipulating diblock copolymer morphologies to improve our understanding of the constituent processes within conjugated diblock copolymer materials.

Finally, the last component melting regime corresponds to the equilibrium melting of the crystallite in the diblock copolymer. The convergence of the final melting temperature is difficult to probe via DSC alone, as at the faster melting rates, diffusion limitations prevent some of the melt-recrystallization process. However, by slow melting, domain structure as measured via SAXS clearly shows that all samples finally melt – corresponding to a significant loss of extension – at the same temperature and nearly the same domain size. These measurements provide additional support that these materials initially form imperfectly crystalline materials which then are improved via the melt-recrystallization process; furthermore, it emphasizes that the final melting is independent of thermal history, and may correspond to an equilibrium-controlled temperature and domain size.

This study of the coupling between crystallite and domain structure reveals a number of key ideas. First, by studying this detailed coupling, this work has been able to elucidate a more intricate mechanism for how material is excluded from the primary crystallites during initial

crystallization to form ordered regions; further, it shows how after melting of these adjacent excluded regions, this material is incorporated into the primary crystallites during the melt-recrystallization process, leading to an apparent shrinkage of the domains as interdigitation occurs. Observing this coupling is only possible due to this system design with a rubbery matrix that allows deformation in response to P3EHT crystallization. Further, it illustrates how to achieve highly crystalline materials in confinement, and demonstrates that clearly understanding the crystallization dynamics – in particular, diffusion and nucleation limitation – are helpful during system design and processing. Finally, it is important to emphasize that the crystallization as a function of T_c observed here is clearly a diffusion-limited, highly non-equilibrium effect. Not only is it clear the perturbations of the lamellar structure observed is a result of both primary and secondary crystallization processes, which are intrinsically non-equilibrium, but also are clearly impacted by diffusion-controlled kinetics during crystallization. Furthermore, the diblock copolymer is clearly path dependent; a structure will not return to a given domain structure without melting and repeating isothermal crystallization. For example, a material that is crystallized at 25°C, allowed to melt-recrystallize at 70°C, and then returned to 25°C will maintain the domain and crystallite structure of the recrystallized material, emphasizing that this is the more stable state.

4.4 Conclusions

Here, the relationships between diblock copolymer structure, crystallization, and thermal processing are investigated. The P3EHT-*b*-PMA system is an ideal model system with which to investigate this coupling due to the deformable nature of the PMA block; the tethering between P3EHT and PMA chains at the interface means that changes in P3EHT crystallite packing also directly impact the PMA structure. Furthermore, changes in the P3EHT crystalline structure are manifested as changes in the overall domain structure, allowing the overall diblock copolymer to behave as a highly sensitive probe to changes along the chain direction of the crystalline structure. Surprisingly, this work finds that the overall domain size (and thus the along-chain crystallite dimensions) are inversely proportional to temperature; higher T_c result in more compact domains. This result directly contradicts previous assumptions that in conjugated polymers, improvements in crystallite order/perfection are directly comparable to the lamellar thickening processes observed in flexible crystalline polymers, where with increasing isothermal crystallization temperature (or over the course of a melt-recrystallization process), chains become less folded and more extended. Here, by tracking the P3EHT domain size as a function of processing conditions, we found that chain folding that follows an integer number of folds definitively does not occur; local folding near the edges of domains remains a possibility. By studying the detailed melting behavior of these materials via differential scanning calorimetry, we find three distinct melting regimes from which we suggest a model of crystallinity in confinement. We suggest that regions are excluded from the primary crystallite as a function of crystallization temperature; the first melting regime corresponds to relaxation of excluded components of chains; the second (melt-recrystallization) regime corresponds to interdigitation and incorporation of these chains within the main crystallite. This melt-recrystallization enables simultaneous improvements in order along the π-stacking directions. The final melting regimes corresponds to melting of these crystallites which, after melt-recrystallization, are structurally

independent of their prior thermal history. This work demonstrates that leveraging a block copolymer containing conjugated components is a useful system for investigating the structural details of crystallinity. Finally, this work suggests that unique crystallization processes associated with conjugated polymers can result in unusual temperature-dependent behavior, and suggests processing rules for achieving highly crystalline materials in confinement.

4.5 Appendix

4.5.1 Tracking the Temperature Dependence of Domain Structure Upon Melting

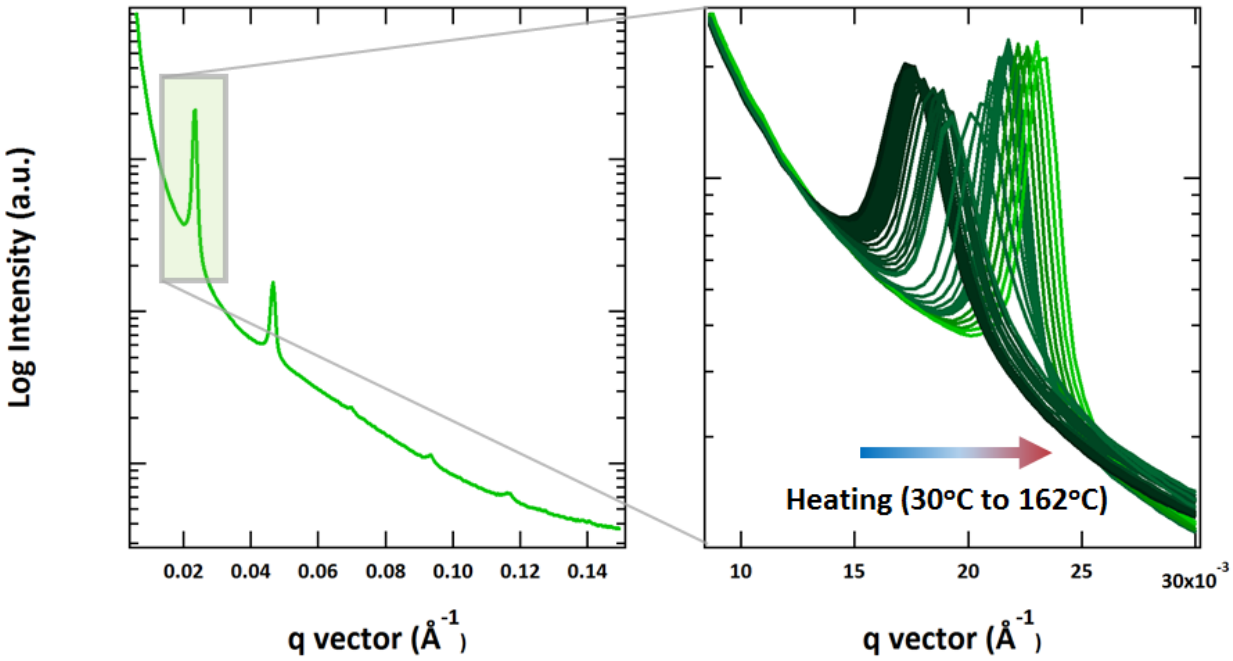

Figure 4.5 Tracking of temperature-dependent domain structure via SAXs

Temperature dependence of domain structure is tracked via SAXS by following the position of the primary peak as a function of temperature.

4.5.2 Blends of P3EHT-*b*-PMA with PMA and P3EHT Homopolymers

Blends were prepared by measuring out the desired diblock copolymer and homopolymer for each final composition on a balance precise to 0.01 mg. Blends were then dissolved in THF to completely mix sample, cast into Teflon boats, and dried under vacuum at 50°C for 24 hours to remove solvent. Dried materials were melted at 150°C for ten minutes before creating SAXS/WAXS or DSC samples in order to remove thermal history and solvent processing effects. Table 4.2 describes the blend compositions for both PMA and P3EHT swollen diblock copolymers.

In P3EHT-*b*-PMA, the primary driving force for the crystallization temperature dependent domain behavior appears to be nonequilibrium effects attributed to the diffusion limited crystallization kinetics. However, PMA chain stretching is potentially still a contributor to driving changes in structure. To directly test the impact of selective chain stretching on the confined crystallization, blends of PMA in P3EHT-*b*-PMA were created. A low molecular weight PMA was synthesized to selectively swell the PMA block. Furthermore, the domain spacing with blended PMA were plotted against the expected domain spacing for PMA that does not evenly well (forms a 'dry brush' as opposed to a 'wet brush') (Figure 4.7). Blending PMA increases the amount of stretching tethered PMA experiences for a given interfacial area (Figure 4.8a). Thus, blending in PMA homopolymer increases the driving force for P3EHT decrease the interfacial area per chain for a given crystalline state. Here, we examine the normalized P3EHT domain spacing crystallized at both 25°C and at 55°C as a function of blended PMA content. Furthermore, P3EHT crystallites tethered to a PMA block with blended PMA homopolymer are expected to be more folded/less thermally stable than P3EHT in the neat diblock copolymer. This is expected to lead to a depression in the ultimate (regime III) melting temperature with increasing PMA content.

Interestingly, blending PMA homopolymer into the constituent diblock copolymer does appear to result in a decrease in normalized P3EHT domain size (Figure 4.8b). These results indicate that even in the pure diblock copolymer, the PMA block is influencing the development of the final domain structure. Furthermore, at the final melting temperature of the system, increasing the PMA blend content is not influencing the degree of lateral crystalline order (order in the π-π and the alkyl chain stacking directions). By DSC of blended P3EHT-*b*-PMA recrystallized at 75°C, the system shows minimal perturbation of melting temperature until reaching high fractions of free PMA homopolymer (Figure 4.8c). These results indicate that while PMA chain stretching participates in driving the P3EHT structure during crystallization, it seems to have a minimal impact on the final, thermal-history independent structure before melting.

Blends with P3EHT were also created to selectively test the impact of decoupling P3EHT chain crystallization from interfacial tethering. Interestingly, P3EHT-*b*-PMA shows significant extension upon crystallization across all P3EHT containing blends (Figure 4.9a). This indicates that, even at high degrees of P3EHT that are not interfacially tethered, P3EHT chains remain oriented relative to the interface. Even at very high volume fractions of P3EHT, blends retained a lamellar nanostructure. The normalized P3EHT domain spacing increases dramatically with

Table 4.2 Blend compositions of PMA and P3EHT swollen diblock copolymers

Polymer	$\varphi_{P3EHT,\ crystalline}$	% of free PMA	% of free P3EHT
P3EHT-*b*-PMA	0.64	0	–
P3EHT-*b*-PMA + PMA_8	0.62	8%	–
P3EHT-*b*-PMA + PMA_{20}	0.59	20%	–
P3EHT-*b*-PMA, PMA_{37}	0.53	37%	–
P3EHT-*b*-PMA, PMA_{50}	0.47	50%	–
P3EHT-*b*-PMA, $P3EHT_8$	0.66	–	8%
P3EHT-*b*-PMA, $P3EHT_{19}$	0.69	–	19%
P3EHT-*b*-PMA, $P3EHT_{38}$	0.74	–	38%
P3EHT-*b*-PMA, $P3EHT_{44}$	0.76	–	44%
P3EHT-*b*-PMA, $P3EHT_{50}$	0.78	–	50%

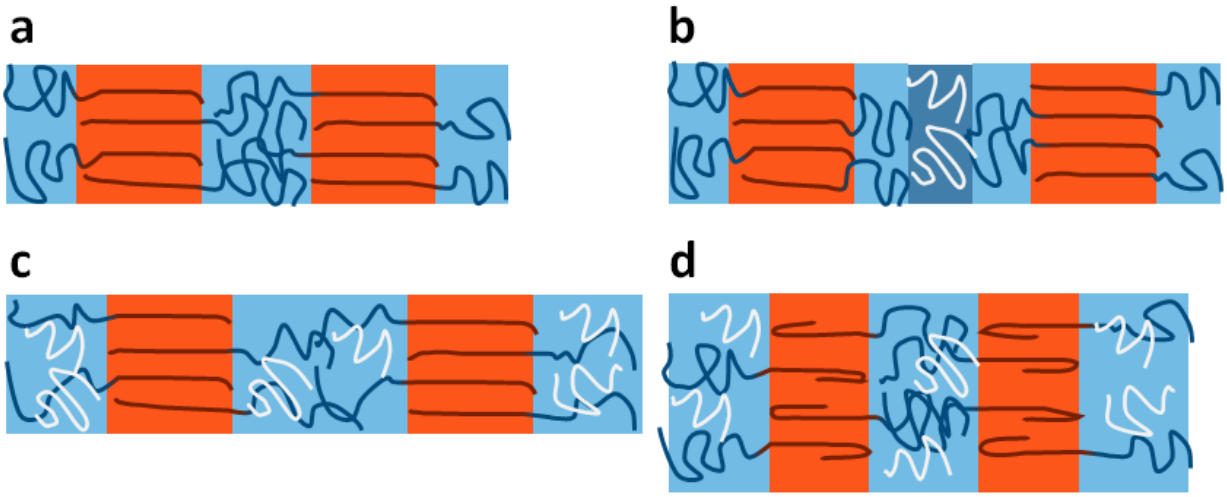

Figure 4.6 Cartoons of potential impact of PMA on P3EHT-*b*-PMA domain structure

Cartoon showing the potential impacts of PMA homopolymer swelling on P3EHT crystalline structure, and dependence on brush characteristics of the PMA. (a) Shows neat P3EHT-*b*-PMA with fully extended P3EHT chains, (b) displays that if PMA homopolymer does not swell the PMA chains, but rather segregates to the center of the PMA domains, while the entire domain spacing will increase, it will not impact the P3EHT structure (c) shows that if PMA homopolymer is added and evenly swells the PMA domains, if the P3EHT is unperturbed, the PMA chains in the diblock copolymer will be stretched (d) emphasizes the alternative to (c) in which PMA chain stretching is relieved by folding of P3EHT.

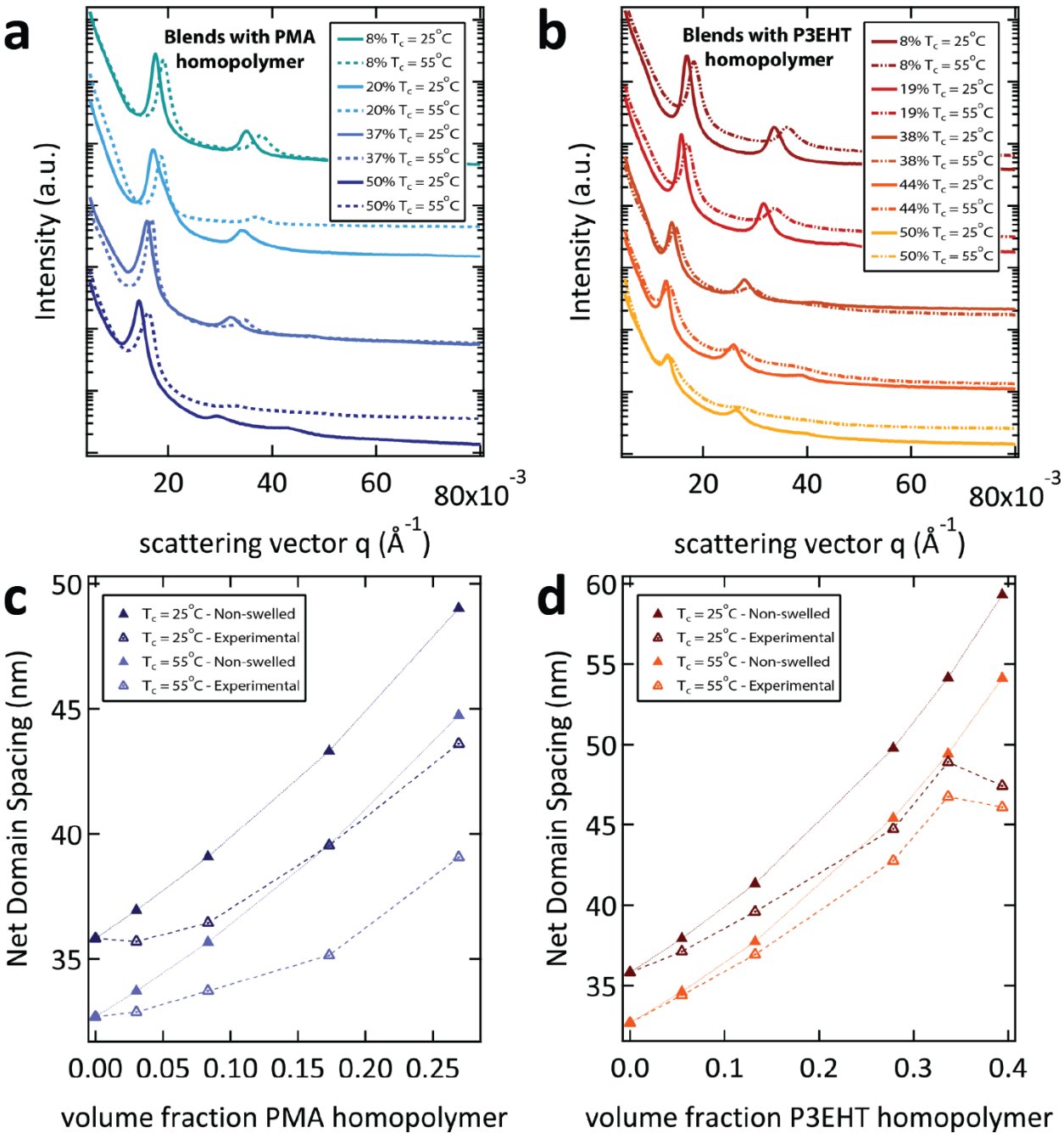

Figure 4.7 Actual domain spacing versus theoretical dry brush case for blends

(a, b) SAXS traces from P3EHT-*b*-PMA blends with PMA and P3EHT respectively (c,d) Changes with T_c across PMA and P3EHT blend compositions, actual domain sizes versus expected domain sizes if blended homopolymer forms a dry brush. Actual domain sizes are significantly smaller than that expected for the dry brush case, emphasizing that constituent homopolymers do in fact swell the associated blocks.

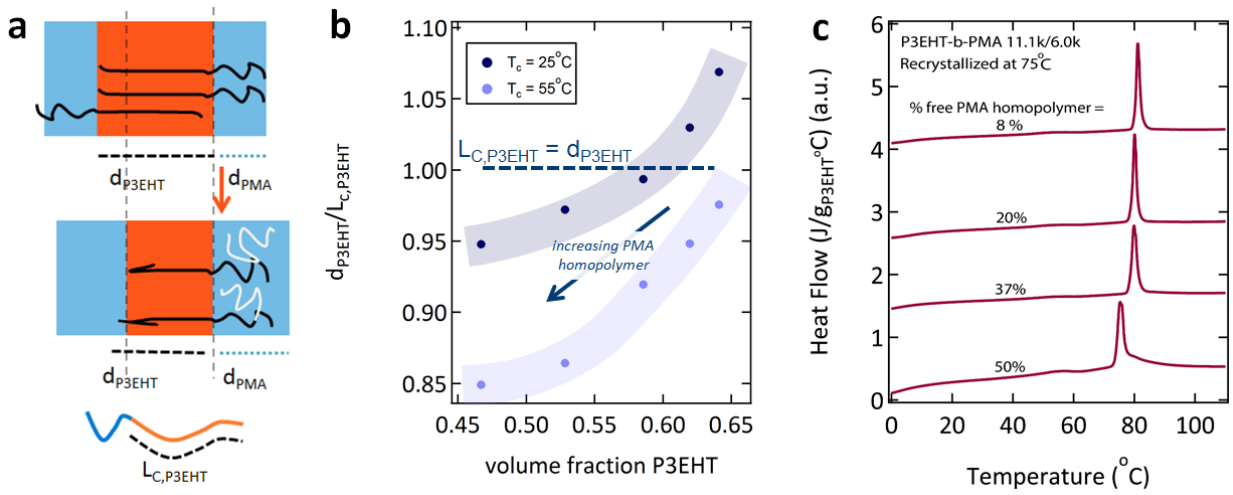

Figure 4.8 Impact of blending PMA homopolymer into P3EHT-*b*-PMA diblocks

(a) Blending PMA homopolymer to selectively swell the PMA domain decreases the domain size of the P3EHT for both high- and low-temperature crystallization. (b) Cartoon of how blending PMA homopolymer may impact PMA chain stretching and P3EHT chain conformation in crystallites. (c) DSC of P3EHT-*b*-PMA that has been selectively swelled with PMA was initially crystallized at 25°C and then recrystallized at 75°C.

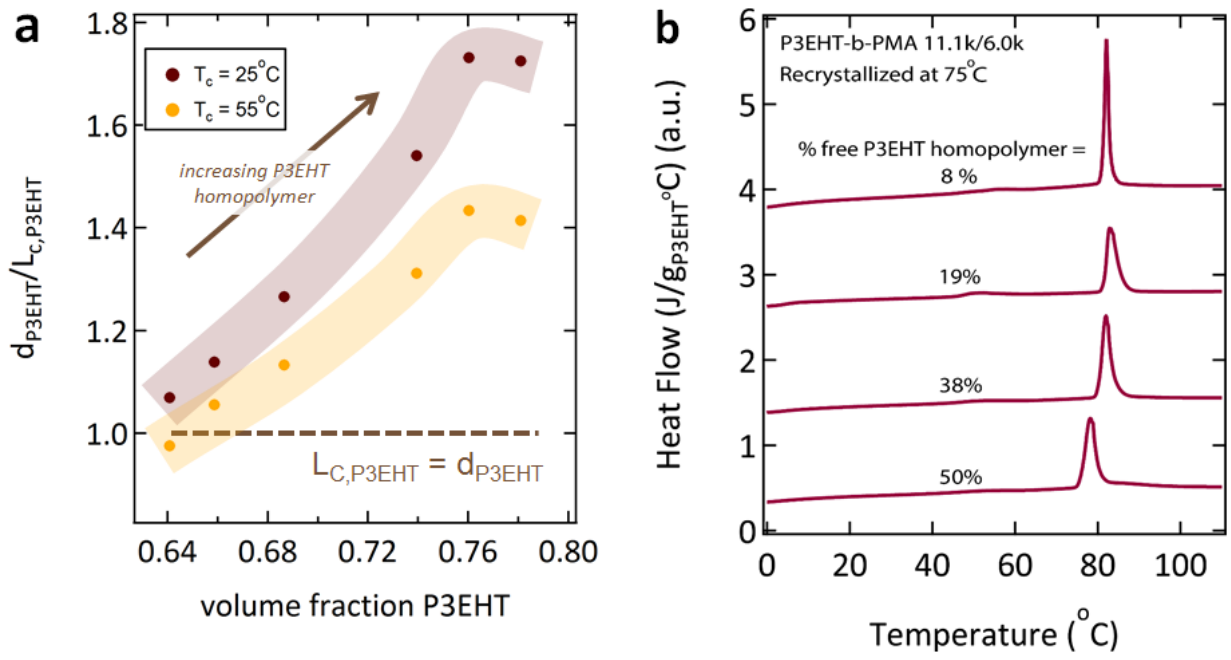

Figure 4.9 Behavior of P3EHT-*b*-PMA blended with P3EHT homopolymer

(a) P3EHT blends show an increase in normalized P3EHT domain size as the P3EHT fraction is increased, corresponding to swelling of the P3EHT domain. Increased extension at low temperature crystallization emphasizes the net orientation perpendicular to domain interfaces induced on crystallites even at high homopolymer compositions. Volume fractions correspond to up to 50% free P3EHT homopolymer (b) Blends with P3EHT results in minimal change in P3EHT melting temperature.

P3EHT content, indicating that P3EHT swells the domain. Instead of simply fully extending and decreasing the area occupied per PMA chain, the P3EHT forms crystallites that are not fully interdigitated, perhaps due to kinetic limitations similar to the neat diblock copolymer. Melting temperature is again not significantly impacted for annealed crystallites (Figure 4.9b).

4.6 Acknowledgements

We gratefully acknowledge support from the NSF-DMR Polymers Program through grant no. 1206296. User facilities were used at both the Advanced Light Source and the Stanford Synchrotron Radiation Light Source, supported by the Director, Office of Science, Office of Basic Energy Sciences, of the U.S. Department of Energy under Contracts No DE-AC02-05CH11231 and DE-AC02-76SF00515. We also gratefully acknowledge use of the UCSB MRL Shared Experimental Facilities supported by the MRSEC Program of the NSF under Award No. DMR 1121053; a member of the NSF-funded Materials Research Facilities Network.

4.7 References

1. Salleo, A., Charge transport in polymeric transistors. Mater Today 2007, 10 (3), 38-45.

2. Sirringhaus, H.; Tessler, N.; Friend, R. H., Integrated optoelectronic devices based on conjugated polymers. Science 1998, 280 (5370), 1741-1744.

3. Thompson, B. C.; Frechet, J. M. J., Organic photovoltaics - Polymer-fullerene composite solar cells. Angew Chem Int Edit 2008, 47 (1), 58-77.

4. Himmelberger, S.; Dacuna, J.; Rivnay, J.; Jimison, L. H.; McCarthy-Ward, T.; Heeney, M.; McCulloch, I.; Toney, M. F.; Salleo, A., Effects of Confinement on Microstructure and Charge Transport in High Performance Semicrystalline Polymer Semiconductors. Adv Funct Mater 2013, 23 (16), 2091-2098.

5. Himmelberger, S.; Duong, D. T.; Northrup, J. E.; Rivnay, J.; Koch, F. P. V.; Beckingham, B. S.; Stingelin, N.; Segalman, R. A.; Mannsfeld, S. C. B.; Salleo, A., Role of Side-Chain Branching on Thin-Film Structure and Electronic Properties of Polythiophenes. Adv Funct Mater 2015, 25 (17), 2616-2624.

6. Jimison, L. H.; Himmelberger, S.; Duong, D. T.; Rivnay, J.; Toney, M. F.; Salleo, A., Vertical Confinement and Interface Effects on the Microstructure and Charge Transport of P3HT Thin Films. J Polym Sci Pol Phys 2013, 51 (7), 611-620.

7. Tseng, H. R.; Phan, H.; Luo, C.; Wang, M.; Perez, L. A.; Patel, S. N.; Ying, L.; Kramer, E. J.; Nguyen, T. Q.; Bazan, G. C.; Heeger, A. J., High-Mobility Field-Effect Transistors Fabricated with Macroscopic Aligned Semiconducting Polymers. Adv Mater 2014, 26 (19), 2993-2998.

8. Snyder, C. R.; Kline, R. J.; DeLongchamp, D. M.; Nieuwendaal, R. C.; Richter, L. J.; Heeney, M.; McCulloch, I., Classification of Semiconducting Polymeric Mesophases to Optimize Device Postprocessing. J Polym Sci Pol Phys 2015, 53 (23), 1641-1653.

9. Kline, R. J.; McGehee, M. D.; Kadnikova, E. N.; Liu, J. S.; Frechet, J. M. J.; Toney, M. F., Dependence of regioregular poly(3-hexylthiophene) film morphology and field-effect mobility on molecular weight. Macromolecules 2005, 38 (8), 3312-3319.

10. DeLongchamp, D. M.; Kline, R. J.; Jung, Y.; Lin, E. K.; Fischer, D. A.; Gundlach, D. J.; Cotts, S. K.; Moad, A. J.; Richter, L. J.; Toney, M. F.; Heeney, M.; McCulloch, I., Molecular basis of mesophase ordering in a thiophene-based copolymer. Macromolecules 2008, 41 (15), 5709-5715.

11. Kline, R. J.; McGehee, M. D., Morphology and Charge Transport in Conjugated Polymers. Journal of Macromolecular Science, Part C 2006, 46 (1), 27-45.

12. Loo, Y. L.; Register, R. A.; Ryan, A. J., Modes of crystallization in block copolymer microdomains: Breakout, templated, and confined. Macromolecules 2002, 35 (6), 2365-2374.

13. Ho, V.; Boudouris, B. W.; Segalman, R. A., Tuning Polythiophene Crystallization through Systematic Side Chain Functionalization. Macromolecules 2010, 43 (19), 7895-7899.

14. Ho, V.; Boudouris, B. W.; McCulloch, B. L.; Shuttle, C. G.; Burkhardt, M.; Chabinyc, M. L.; Segalman, R. A., Poly(3-alkylthiophene) Diblock Copolymers with Ordered Microstructures and Continuous Semiconducting Pathways. J Am Chem Soc 2011, 133 (24), 9270-9273.

15. Davidson, E. C.; Beckingham, B. S.; Ho, V.; Segalman, R. A., Confined Crystallization in Lamellae Forming Poly(3-(2 '-ethyl)hexylthiophene) (P3EHT) Block Copolymers. J Polym Sci Pol Phys 2016, 54 (2), 205-215.

16. Beckingham, B. S.; Ho, V.; Segalman, R. A., Melting Behavior of Poly(3-(2 '-ethyl)hexylthiophene). Macromolecules 2014, 47 (23), 8305-8310.

17. Snyder, C. R.; Henry, J. S.; DeLongchamp, D. M., Effect of Regioregularity on the Semicrystalline Structure of Poly(3-hexylthiophene). Macromolecules 2011, 44 (18), 7088-7091.

18. Nieuwendaal, R. C.; Snyder, C. R.; DeLongchamp, D. M., Measuring Order in Regioregular Poly(3-hexylthiophene) with Solid-State C-13 CPMAS NMR. Acs Macro Lett 2014, 3 (2), 130-135.

19. Snyder, C. R.; Nieuwendaal, R. C.; DeLongchamp, D. M.; Luscombe, C. K.; Sista, P.; Boyd, S. D., Quantifying Crystallinity in High Molar Mass Poly(3-hexylthiophene). Macromolecules 2014, 47 (12), 3942-3950.

20. Yu, L., Davidson, E.D., Andersson, M.R., Segalman, R.A., Muller, C., Isothermal Crystallization Kinetics and Time-Temperature-Transformation of a Polythiophene Derivative. In Preparation 2016.

21. Whitmore, M. D.; Noolandi, J., Theory of Crystallizable Block Copolymers. Makromol Chem-M Symp 1988, 16, 235-249.

22. Douzinas, K. C.; Cohen, R. E.; Halasa, A. F., Evaluation of Domain Spacing Scaling Laws for Semicrystalline Diblock Copolymers. Macromolecules 1991, 24 (15), 4457-4459.

23. Chen, H. L.; Hsiao, S. C.; Lin, T. L.; Yamauchi, K.; Hasegawa, H.; Hashimoto, T., Microdomain-tailored crystallization kinetics of block copolymers. Macromolecules 2001, 34 (4), 671-674.

24. Zhu, L.; Chen, Y.; Zhang, A. Q.; Calhoun, B. H.; Chun, M. S.; Quirk, R. P.; Cheng, S. Z. D.; Hsiao, B. S.; Yeh, F. J.; Hashimoto, T., Phase structures and morphologies determined by competitions among self-organization, crystallization, and vitrification in a disordered poly(ethylene oxide)-b-polystyrene diblock copolymer. Phys Rev B 1999, 60 (14), 10022-10031.

25. Olsen, B. D.; Segalman, R. A., Structure and thermodynamics of weakly segregated rod-coil block copolymers. Macromolecules 2005, 38 (24), 10127-10137.

26. Huang, T. C.; Toraya, H.; Blanton, T. N.; Wu, Y., X-Ray-Powder Diffraction Analysis of Silver Behenate, a Possible Low-Angle Diffraction Standard. J Appl Crystallogr 1993, 26, 180-184.

27. Ilavsky, J., Nika: software for two-dimensional data reduction. J Appl Crystallogr 2012, 45, 324-328.

28. Hoffman, J. D.; Lauritzen, J. I., Crystallization of Bulk Polymers with Chain Folding - Theory of Growth of Lamellar Spherulites. J Res Nat Bur Stand 1961, A 65 (4), 297-+.

29. Lauritzen, J. I.; Hoffman, J. D., Extension of Theory of Growth of Chain-Folded Polymer Crystals to Large Undercoolings. J Appl Phys 1973, 44 (10), 4340-4352.

30. Hoffman, J. D.; Weeks, J. J., Melting Process and Equilibrium Melting Temperature of Polychlorotrifluoroethylene. J Res Nbs a Phys Ch 1962, 66 (Jan-F), 13-+.

31. Hoffman, J. D.; Weeks, J. J., X-Ray Study of Isothermal Thickening of Lamellae in Bulk Polyethylene at Crystallization Temperature. J Chem Phys 1965, 42 (12), 4301-&.

32. Koch, F. P. V.; Heeney, M.; Smith, P., Thermal and Structural Characteristics of Oligo(3-hexylthiophene)s (3HT)(n), n=4-36. J Am Chem Soc 2013, 135 (37), 13699-13709.

33. Marsh, H. S.; Reid, O. G.; Barnes, G.; Heeney, M.; Stingelin, N.; Rumbles, G., Control of Polythiophene Film Microstructure and Charge Carrier Dynamics Through Crystallization Temperature. J Polym Sci Pol Phys 2014, 52 (10), 700-707.

34. Beckingham, B. S.; Ho, V.; Segalman, R. A., Formation of a Rigid Amorphous Fraction in Poly(3-(2 '-ethyl)hexylthiophene). Acs Macro Lett 2014, 3 (7), 684-688.

Chapter 5. Conclusion and Future Outlook

This dissertation leverages the model conjugated polymer P3EHT to examine the interplay between conjugated polymer crystallization and the structure of the diblock polymer itself. We show here that a balance of parameters is important for both (1) templating a block copolymer morphology in the melt and then (2) allowing crystallization in that morphology to proceed under controlled conditions. Importantly, a number of parameters are key for accomplishing the resulting crystallinity. In the melt, the molecular characteristics and conformational asymmetry are critical, in addition to the asymmetry in polymer backbone shape observed in liquid crystalline rod-coil block copolymers. The range of morphologies achievable in the melt directly determines the morphologies accessible following crystallization. The focus of this dissertation has been not on that phase behavior, but on the interplay between conjugated polymer crystallization and the microphase separated nanostructures. In particular, crystallization is capable of deforming or even destroying nanostructures, even once the criteria to establish those nanostructures in the melt have been achieved. Equally importantly, block copolymers tether their paired conjugated polymers at the interfaces, and template the sizes of the domains. Given that polymers must structurally rearrange in order to crystallize, this tethering and confinement could be expected to either help or hinder the resulting structure; in this work, we find that the coupled chains appear to slow crystallization kinetics primarily through slowing the diffusion dynamics at the interface. Also, the final structure is dependent on the properties of the conjugated polymer itself: how stiff is it in the melt relative to the crystalline state? How strong are the bending penalties upon crystallization? What is the temperature dependence of nucleation and chain diffusion required for crystal growth? How strong are these forces relative to stretching penalties in the amorphous block? The utility of this dissertation lies in its ability to identify and exploit a model system that elucidates some of the key characteristics of thermally-processed conjugated polymers, and to leverage this model system to discover the unusual behavior of conjugated polymer diblocks, which is necessary to understand for the design of future systems.

A first critical parameter to consider in these systems is the role of conformational asymmetry and chain shape in determining the available melt phases of these semiflexible-flexible diblock materials. While P3EHT is stiff relative to most flexible polymers, with a persistence length of 3 nm in solution, it is by no means well-described as a rod. However, we see here that lamellar morphologies are preferred in the melt over an extremely wide phase window. Furthermore, this phase space is biased towards lamellar morphologies when P3EHT (the stiffer block) is the majority component – even at extremely high P3EHT volume fractions due to blending in P3EHT. While accessing curved domains of the majority component is surely possible, it is expected to be fundamentally challenging to find the correct composition to achieve this for most conjugated diblock systems, especially as new high performing donor-acceptor materials with increasingly stiff backbones are incorporated. Improved modeling and predictions for the existence and volume fraction for windows of existence of these phases would aid the process of finding them, as would the development of highly controlled synthetic methods over conjugated polymer molecular weight and chain-end reactivity. Fundamental studies which examine the impact of backbone stiffness versus χN on self-assembly is

challenging to decouple in the conjugated systems; leveraging a highly controlled model system such as polypeptoids, in which individual monomers with defined chirality can be controlled to create chemically identical yet conformationally distinct chains is a promising avenue to take. Ultimately, it would be excellent to decouple the impacts of chain shape (the continuum from rod to coil) from chain stiffness (variation in persistence length for a chain described by a given shape) on the resulting self-assembly; the ratio of chain persistence length to contour length is useful for defining the degree to which a chain is semiflexible, while the ratio of persistence lengths between the two blocks describes their relative stiffness. While extremes in this biaxial phase space have been explored, many real systems lie in the intermediary space, which has not been explicitly and experimentally explored.

The associated challenge lies in the interaction between conjugated polymer crystallization and the associated nanostructure. This work has shown that the drive to create extended-chain crystallites has a significant impact on the system's ability to crystallize, in addition to an impact on the resulting structure. We have seen that a mobile second block during crystallization is essential to allow crystallization. Thus far, we have accomplished this via the incorporation of a rubbery second block, but in principle a plasticizing agent selective for the amorphous block could improve its mobility during crystallization and then be removed to allow for the desired final mechanical properties in addition to excellent crystallinity. This is also interesting in light of ultimately creating conjugated-conjugated block copolymers; whichever phase crystallizes first may restrict the ability of the second block to achieve an ideal morphology. Importantly, the studies in this dissertation have found that the conditions under which the material is crystallized are critically important for controlling the final morphology. For example, by identifying the limitations on the crystallites (for example, temperatures over which diffusion versus nucleation dominates self-assembly), it is possible to pre-emptively identify conditions which will optimize the final crystallites. Moreover, as these conditions appear to be a function of morphology, in cylindrically (or spherically) confined domains, it is possible to optimize crystallinity by choice of thermal pathway; for example, by first seeding crystallization with a very large degree of undercooling, and then annealing the resulting crystallites at high temperatures to high quality crystallites.

A further challenge is to extend the structural studies performed here to the transport properties of the system through the conjugated phase. In the P3EHT-*b*-PMA system, we observed significant changes in the domain and crystalline structure as a function of thermal processing, however, the relatively low baseline mobility of the system made it challenging to probe the impact of these structural changes on charge transport. Designing a system that accomplishes the rules required for an accessible melt phase and confined crystallization, yet with higher baseline mobilities, would enable a series of fascinating studies of how charge mobility varies with crystallinity. Importantly, in P3EHT-*b*-PMA – and we expect for other conjugated diblocks as well – the crystalline chains orient with the chains perpendicular to the diblock interface. In a crystalline homopolymer, it is challenging to completely decouple crystallite size and perfection from the impact of tie chains; conjugated diblocks confined within lamellar diblocks compared to the homopolymer are an ideal model system for such a decoupling study.

An additional potential challenge lies in the induced orientation of P3EHT chains within the diblocks. Given that the crystallites appear to have an extremely strong preference to crystallize perpendicular to the domain interfaces, this has important implications for the charge transport of these systems. The fastest transport direction in conjugated polymers is along the chain backbone, which in these geometries is oriented such that tie chains between crystallites along the chain backbone are strongly disfavored in confinement. If long range high mobilities are desired in nanostructured diblock systems, we expect that these would be optimized by somehow inducing percolation along the chain backbone; in other words, creating a conjugated polymer structure such that charge can move mostly along the chain backbone and then move between chains at aggregation sites near the chain ends. An initial concept would be that including a blended amount of homopolymer might accomplish this, however in Chapter 4 we see that blending P3EHT homopolymer into the diblock seems to still result in chains oriented perpendicular to the domain interfaces. Developing design strategies for this in the diblock system will be a significant challenge.

Importantly, this work highlights the promise of using conjugated polymer containing diblocks to study fundamental crystallization phenomena. Well-ordered diblocks can be, as shown here, an especially sensitive probe to small changes in domain sizing measured via small-angle X-ray scattering over in-situ studies, which indicate specific mechanisms at play within the domains. Capturing these changes in crystallite form factor along a specific orientation direction via techniques such as electron microscopy or AFM would be incredibly difficult for the resolution we are able to resolve. Further, while electron microscopy and AFM would be sensitive to density and mechanical properties, respectively, the coupled domain studies specifically examine chain extension effects. Here, this has allowed us to directly understand the chain conformation in confinement, as well as gain mechanistic insight into how improvements in crystalline perfection occur in P3EHT. In combination with techniques such as AFM or TEM, building the diblocks can be an excellent tool to probe the crystalline structure, particularly for clarifying changes in order along the chain direction as a function of processing and boundary conditions.

An important and associated question is in just how good of a model system P3EHT is for the crystallization of new high mobility conjugated polymers. Some of the new generation, high-mobility conjugated donor-acceptor polymers feature extremely stiff polymers and never fully dissolve in solvent regardless of temperature. Furthermore, the crystallization of these homopolymers is incredibly different from the poly(3-alkylthiophene)s; while π-stacking continues to be an important feature, fibrillar crystallites often feature chains oriented with their long axis aligned parallel to the chain axis. Future conjugated block copolymer studies should incorporate these next generation materials. While the high melting temperatures of these materials will require careful molecular design to accomplish confined crystallization, including these materials will answer important questions about how these stiffer polymers with apparently different modes of crystallization will behave in confinement and interact with the overall domain structure. Interestingly, while new backbone percolated materials appear to require lower degrees of crystallinity (and instead rely on local aggregation) for excellent performance, in block copolymer confinement the induced orientation may fundamentally change the physics to

be optimized. By preventing tie chains between crystallites, interchain transfer is expected to be significantly more limiting in diblock confinement regardless of the conjugated polymer used; therefore large, perfect crystals are expected to be essential for enabling long-range charge transport. The implications of this might be that the optimal materials and optimal crystallization behavior of conjugated polymers in a homopolymer versus in a block copolymer will diverge.

Overall, we have made significant advances in our ability to not only create highly controlled nanostructures including conjugated polymer components, but also to confine conjugated polymer crystallization within those nanostructured domains. By considering the balance of χN and conjugated polymer melting temperature, it is possible to design a polymer that crystallizes in confinement from an ordered melt. From the chain shape and conformational asymmetry of the system, a desired nanostructure in the ordered melt can be achieved, which templates the crystallinity. The relative chain stiffness in the melt versus after crystallization can be used to design for a second block that permits the growth of extended-chain crystallites – enabling highly crystalline material. The more similar these relative chain stiffnesses are, and the less change in density the conjugated polymer undergoes during crystallization, the less the polymer will need a mobile amorphous block to accommodate crystallization. Finally, through knowledge of diffusion and nucleation limitations in the conjugated block, a thermal pathway to optimize the desired final state can be developed. We see that conjugated polymers bring several additional requirements to the parameter set used to describe confined crystallization in typical flexible polymers; in particular, these are driven by the relatively extended-chain conformation preferred by the conjugated polymers. Here, the P3EHT containing block copolymer behavior highlights a number of these interactions, and the degree to which they are dominant in the self-assembly is expected to vary based on the molecular characteristics of the particular conjugated polymer.